LOW CYCLE CORROSION FATIGUE AND CORROSION FATIGUE CRACK PROPAGATION OF HIGH STRENGTH 7000-TYPE ALUMINUM ALLOYS

Approved:

Dr. Edgar A. Starke, Jr.
Chairman

Dr. Miroslav Marek

Dr. Ervin E. Underwood

Date approved by Chairman: May 17, 1978

LOW CYCLE CORROSION FATIGUE AND CORROSION FATIGUE CRACK PROPAGATION OF HIGH STRENGTH 7000-TYPE ALUMINUM ALLOYS

A THESIS

Presented to

The Faculty and Graduate Division

by

Fu-Shiong Lin

In Partial Fulfillment

of the Requirements for the Degree

Doctor of Philosophy

in the School of Chemical Engineering

Georgia Institute of Technology

May, 1978

TABLE OF CONTENTS

TABLE OF CONTENTS (Concluded)

ACKNOWLEDGMENTS

The author wishes to express his sincere appreciation to his thesis advisor, Dr. Edgar A. Starke, Jr., for his patient and good guidance during the investigation period. He also wishes to thank Dr. M. Marek and Dr. E. E. Underwood for their helpful suggestions in reviews of this work. He would also like to thank Dr. R. F. Hochman and Dr. J. T. Berry for participating on the oral examining committee and their suggestions in this work.

The author would like to thank the Alcoa Technical Center for preparing the alloys used in this research and for the numberous discussions with Dr. T. H. B. Sanders, Jr. The author also thanks Mr. E. J. Coyne, Jr., Mr. J. G. Rinker and Mr. R. E. Sanders, Jr. for their reviews of his thesis.

The author would like to thank Mr. Charles Blackwood and Mr. Danny Averette for their preparation of samples. He also thanks Dr. B. R. Livesay for his permission to use his machine shop.

The author would like to thank his parents and brothers, especially for his wife, daughter and son for their encouragement.

The financial support of the Air Force of Scientific Research under Grant No. 74-2615B and Grant No. 78-3471 is greatly appreciated.

LIST OF ILLUSTRATIONS

LIST OF ILLUSTRATIONS (Continued)

LIST OF ILLUSTRATIONS (Continued)

LIST OF ILLUSTRATIONS (Continued)

LIST OF ILLUSTRATIONS (Continued)

LIST OF ILLUSTRATIONS (Continued)

LIST OF TABLES

NOMENCLATURE

a	crack length
A	Paris coefficient
B	breadth of sample
C	Coffin-Manson exponent
COD	crack opening displacement at maximum load
da	change in crack length
dN	change in number of cycles
E	modulus of elasticity
H	height of specimen
k'	cyclic strain hardening coefficient
K	stress intensity level
K_I	stress intensity level for mode I loading
m	Paris exponent
n	monotonic strain hardening exponent
n'	cyclic strain hardening exponent
N_f	number of cycles for failure
W	width of sample
Y	stress intensity calibration factor
$\Delta\varepsilon_p$	change in plastic strain
ΔK	stress intensity range
$\Delta\sigma$	change in applied stress
ε_f	monotonic fracture strain

NOMENCLATURE (Continued)

ε_f'	fatigue ductility coefficient
ε_y'	cyclic yield strain
ρ'	microstructural parameter
σ_{ys}	monotonic yield strength
σ'_{ys}	cyclic yield strength
P	applied load
q	parabolic averaging exponent

SUMMARY

I. LOW CYCLE CORROSION FATIGUE

Four Al-6Zn-2Mg-xCu alloys with almost identical microstructures were chosen to investigate the effect of copper content on the low cycle corrosion fatigue behavior. Nominal copper contents were 0.01, 1.0, 1.6 and 2.1% Cu. Three different environments were employed: dry air, distilled water, and a 3.5% NaCl solution. The two alloys with 1.6 and 2.1% Cu were chosen for studying the effect of degree of recrystallization (DR) on the low cycle corrosion fatigue properties in these environments. Each was processed to produce two different DR.

The cyclic strain resistance of 7000-type aluminum alloys generally increases with increasing copper content from 0.01 to 2.1%, regardless of the test environment; furthermore this trend is more pronounced for tests conducted in distilled water or in a 3.5% NaCl solution. This improvement is attributed to the increased homogeneity of slip as copper content increases. Ample evidence obtained from the results of supplemental experiments strongly supports this interpretation. For the 1.6 and 2.1% Cu alloys, the cyclic strain resistance is inversely related to the magnitude of the DR regardless of the test environment, with the 2.1% Cu alloy exhibiting less sensitivity to a change in DR. This phenomenon is due to a more uniform cyclic deformation of an alloy with low DR

than with high DR. The small effect observed for the 2.1% Cu alloy is due to a smaller difference in the homogeneity of deformation between the alloy with low DR and with high DR.

The distinct break point observed in the Coffin-Manson plots at high plastic strain amplitudes (> 1.2%) is interpreted as a change in fracture mode from a brittle-like fatigue fracture at low plastic strain amplitudes to a ductile fracture and/or an increase of the density and intensity of slip bands at high plastic strain amplitudes and/or the considerably smaller values of tensile ductility of the alloy than its fatigue ductility coefficient. The mechanisms for cyclic softening described in this study are possibly associated with the combined actions of slip-band softening and grain boundary cracking. The cyclic strain hardening exponents increase with increasing copper content as does the cyclic strain resistance of the alloys.

The environmental sensitivity of these alloys decreases considerably as the Cu content increases from 0.01 to 1.0%. As copper content further increases from 1.0 to 2.1%, the sensitivity to environmental effects continues to decrease, but not so markedly. The high environmental sensitivity of the low copper content alloys is attributed to the fact that the localized slip bands considerably intensify the metal-environment interactions. It is suggested that the low cycle corrosion fatigue of these alloys tested in distilled water is primarily due to a hydrogen embrittlement phenomenon. For tests conducted in a 3.5% NaCl solution, hydrogen embrittlement

still plays an important role but the preferential dissolution and/or adsorption process may also have a detrimental effect.

II. CORROSION FATIGUE CRACK PROPAGATION

Four Al-6Zn-2Mg-xCu alloys with almost identical grain structures were chosen to investigate the effect of copper content on the fatigue crack propagation (FCP) resistance in the presence of dry air, distilled water and a 3.5% NaCl solution. Each alloy, processed to produce two different degrees of recrystallization, was chosen to study the effect of the microstructural feature on the FCP resistance in these environments.

The fatigue crack growth rates (FCGR) for the four different copper content alloys, tested in dry air, generally decrease with decreasing copper content over the range of ΔK values studied. This is attributed, for the low copper content alloys, to the planar slip in the plastic zone ahead of a growing crack resulting in a large amount of a zig-zag crack and the crack branching. For tests conducted in corrosive environments, however, the FCGR decreases with increasing copper content, especially for $\Delta K > 7.5$ MPam$^{\frac{1}{2}}$. This is due to a large degree of homogeneous deformation for the high copper content alloys, resulting in a significant decrease of the metal-environment interactions. The frequency of the occurrence of a zig-zag crack and the crack branching is dependent upon the alloy chemistry, the magnitude of ΔK values and the test environment.

Although the degree of recrystallization studied here has only a minor effect on the FCP resistance, the results seem to indicate that the effect is dependent upon the slip mode, the magnitude of DR, the recrystallized grain size, the presence of insoluble particles, the subgrain size and the test environment. The subgrain and grain boundaries may play some role in the FCP process since the crack path is generally along the subgrain boundaries in the unrecrystallized grains and the orientation of the fatigue fracture surface changes at grain boundaries.

The cyclic strain hardening exponent, n', emerges as the single index most closely related to the LCF and FCP resistance for these three environments studied. The reasons that the sequence of the LCF resistance is not consistent with that of the FCP resistance are probably related to the occurrence of a large amount of a zig-zag crack and the crack branching for the low copper content alloys tested in dry air and the considerable difference in the amount of material involved in the reversed plastic deformation process between the LCF and FCP samples. The predicted crack growth rates, using the equation derived by Chakrabortty, are acceptably close to the experimental data for all alloys tested in various environments.

The environmental sensitivity to the FCGR does reduce with increasing copper content in these 7000-type aluminum alloys. Considerable changes are found as the copper content increases from 0.01 to 1.6%, but only slight changes are observed as copper further increases from 1.6 to 2.1%. A remarkable difference in the

FCGR is observed when tests were conducted in dry air and in distilled water, while an insignificant difference was found between distilled water and a 3.5% NaCl solution. On the basis of these results, it is suggested that the corrosion fatigue of aluminum alloys exposed in distilled water or a 3.5% NaCl solution is primarily due to a hydrogen embrittlement phenomenon.

PART I

LOW CYCLE CORROSION FATIGUE OF HIGH STRENGTH 7000-TYPE ALUMINUM ALLOYS

CHAPTER I

INTRODUCTION

It has long been recognized that the fatigue properties of metals are markedly affected by corrosive environments and consequently, it is well known that most structural alloys fail by corrosion fatigue since they are exposed to an environment while undergoing cyclic loading. It is apparent that the consideration of corrosion fatigue characteristics associated with the intended service environment is a primary factor in evaluating and selecting materials to resist fatigue cracking. Fatigue life of structural alloys may be considered to consist of fatigue crack initiation and fatigue crack propagation. As a fatigue crack is initiated, the subcritical crack grows to a certain length, the stress intensity factor at the crack tip reaches a critical value, and finally, the fracture becomes unstable, thus terminating the life of the structure. For fail-safe and safe-life design philosophies, the corrosion fatigue behavior of materials is employed to predict the useful life of the structure before catastrophic failure. This research program emphasizes the corrosion fatigue behavior of 7000-type aluminum alloys important to the aircraft industry.

Intensive studies have been performed by a number of investigators with the aim of improving fatigue properties of high-strength aluminum alloys. Conventional studies of such variables as

alloy chemistry[1,2], aging treatment[3-6], grain structure[7] and inclusion contents[8,9], or thermomechanical processing[10-12] have achieved some improvements in fatigue resistance and led to a general agreement on some points. However, there are still numerous inconsistencies among these investigations. Large discrepancies may result from the failure to characterize some microstructural parmeters such as grain size, inclusions, degree of recrystallization, etc. Although the effects of these parameters on fatigue properties have not been completely established, it is believed that they do have an influence.

This research is designed to sort out the contribution of various microstructural parameters on the corrosion fatigue behavior of high strength 7000-type alloys. Four Al-6Zn-2Mg-xCu type aluminum alloys with almost identical microstructures were chosen to study the effect of copper content on fatigue properties. Each alloy was also processed to produce different DR in order to investigate the effect of that microstructural feature on fatigue behavior. PART I deals with the effect of copper content and DR on the low cycle corrosion fatigue behavior in the presence of dry air, distilled water and a 3.5% NaCl solution. PART II deals with the effect of these two parameters on the corrosion fatigue crack growth in these environments.

CHAPTER II

REVIEW OF THE LITERATURE

The Nature and Morphology of Precipitates

Aluminum alloys of the 7000-series are precipitation-hardenable. The mechanical behavior of these alloys can be related to the nature and morphology of precipitates. The sequence of precipitation in Al-Zn-Mg alloys at aging temperatures below 150°C has generally been accepted[13] as:

Super-saturated solid solution → Spherical G.P. zones → η' → η ($MgZn_2$)

where η' is a hexagonal transition precipitate formed as thin platelets on {111} matrix planes and η is an equilibrium phase. The G.P. zones and η' precipitates are the most effective strengthening agents because they are coherent or partially coherent to the matrix. Grain boundary precipitate free zones (PFZ) and grain boundary precipitates have always been observed and their features strongly depend on quenching rate and aging temperature. The characteristics of these precipitation phenomena have been found to profoundly affect the mechanical properties and resistance to stress corrosion cracking[14].

The addition of copper to an Al-Zn-Mg alloy revealed that copper did participate in the super-saturated solid solution → G.P. zones → η' precipitation processes as indicated by an increased

temperature range of zone stability and by a sharp change of solution potential[15,16]. Higher copper contents offered greater precipitation hardening. Baba[17], using electrical resistivity measurements, found that copper additions to an Al-Zn-Mg alloy increased the maximum change in resistivity during aging at 90° C. He concluded that the number of G.P. zones was increased by the copper addition. This conclusion is also confirmed by the findings of Sanders and Starke[4], who used an X-ray small angle scattering technique and showed that for a copper-containing Al-Zn-Mg alloy, the number of nuclei for G.P. zone formation increased and resulted in a higher volume fraction of G.P. zones. They also indicated that the transition from G.P. zone to η' occurred earlier for the copper-containing alloy aged at a temperature of 120°C. The addition of copper was thought to stimulate precipitation throughout the grains, resulting in a significant reduction of the PFZ width. This would reduce the potential difference between the grain and the free boundary, and accordingly, reduce intergranular fracture and improve stress corrosion cracking resistance.

The strengthening mechanisms of the precipitation hardening aluminum alloys have been discussed in detail[18,19]. For aging conditions which produce peak hardness, coherent and partially coherent precipitates (G.P. zones and η' phases) may be penetrated and sheared by the moving dislocations. As a result, the deformation is very inhomogeneous and slip bands are observed[4,5]. In contrast, incoherent precipitates (η phases) and intermetallic compounds are not penetrated by the dislocations but are looped as

described by Orowan[20]. The dislocation looping of incoherent particles will result in a more homogeneous deformation.

Characteristics of Low Cycle Fatigue

Low cycle fatigue (LCF) is generally defined to be the failure of materials under cyclic loading in less than 10^5 cycles, and is usually carried out in the reversed strain control mode. The empirical relationship between the plastic strain range and the cycles to failure has been reported by Manson[21] and Coffin[22] and is given by:

$$\frac{\Delta\varepsilon_p}{2} = \varepsilon_f'(2N_f)^{-C} \qquad (1.1)$$

where $\frac{\Delta\varepsilon_p}{2}$ is the plastic strain amplitude, N_f is the number of cycles to failure. ε_f' is the fatigue ductility coefficient, and C is the fatigue ductility exponent. Equation 1.1 is generally referred to as the Coffin-Manson low cycle fatigue equation. Plastic strain amplitude versus reversal cycles to failure can adequately be represented by a straight line on log-log coordinates for most materials investigated, and the slope of the straight line, C, is variable and normally ranges between about -0.5 and -0.7. The value of the fatigue ductility coefficient, ε'_f, in this plot is the plastic strain intercept at $4N_f = 1$[22] or $2N_f = 1$[23]. These two parameters C and ε'_f are considered to represent the fatigue ductility properties of a metal. Using typical experimental values for the constants, it is apparent that a metal with a high intercept and a shallow slope, i.e. a large value of ε'_f and a small value of C,

will have the best resistance to cyclic strains. However, a break in the curve of the $\frac{\Delta\varepsilon_p}{2}$ vs $2N_f$ relationship has been found in several materials[4,24,25] and has been explained either by a change from the intergranular to transgranular cracking, by a change from localized slip bands to homogeneous deformation, or by a change in deformation processes as a function of the plastic strain amplitude.

Other important information is obtained from the low cycle fatigue tests by plotting cyclic stress amplitude versus number of cycles. These curves define the cyclic hardening and/or softening behavior. This technique has been employed to study the cyclic stress-strain response of materials. In general, the curves show that rapid hardening or softening occurs in the first few percent of life. After the transient stage, a steady state or saturation condition is normally obtained prior to complete fracture. A metal will display softening or hardening, depending on its initial condition[26]. For the case of precipitation hardenable aluminum alloys, the mechanisms of cyclic hardening are analagous to those of static tensile tests[18,19]. For example, in the case of coherent precipitates, the following parameters make contributions: chemical contribution, interface dislocations, coherency strain, difference in the elastic moduli and creation of new surface area. On the other hand, cyclic hardening in an alloy with incoherent particles must be attributed to the fact that dislocations moving in the matrix form prismatic loops and geometrically necessary dislocations. In addition, the operation of a large number of slip systems leads to many dislocation intersections. Cyclic softening is sometimes found in

aluminum alloys, and it is generally ascribed to either precipitate re-solution[27], aging inhomogeneities[28], or disordering[34]. There is one additional and important piece of information to be derived from the low cycle fatigue tests. If a plot is made of different plastic strain amplitudes, $\frac{\Delta\varepsilon_p}{2}$, versus the corresponding saturated flow stress, σ_s, this curve is called the cyclic stress-strain curve and represents the equilibrium fatigue behavior of a given material. The slope of the curve is called the cyclic strain-hardening exponent, n'. The parameter, C, has been related to n'. Morrow[29] has shown through an energy argument that this relation can be written as

$$C = -\frac{1}{1+5n'} \tag{1.2}$$

Thus, it is obvious from this relationship that the best single index of the change in finite life fatigue resistance induced by alloying is the cyclic strain hardening exponent, n'. It is of interest to note that in order to increase the plastic strain resistance, it is best to increase n'.

Fatigue Crack Initiation and Propagation

The fatigue failure of a smooth specimen is commonly divided into (i) the crack initiation period and (ii) the crack growth period. The latter can be separated into two different stages[30] based on the change in crack morphology. Stage I cracks propagate along the crystallographic plane of maximum shear stress, changing direction with orientation at grain boundaries. Stage II cracks, on the other hand, propagate in a direction approximately

perpendicular to the maximum tensile stress. Thus, the stage II crack grows in a regular manner, often advancing a certain distance in each stress cycle in a way that produces distinctive striations on the fracture surface. The critical crack length for the change of crack propagation mode (stage I to II) depends on the magnitude of loading and the plastic deformation mode.

Fatigue crack nucleation in smooth specimens has been found to be associated with persistent slip bands (PSB's) which may occur on the surface of samples and exhibit irregular intrusions and/or extrusions within the bands[31]. Explanations for the formation of intrusions and extrusions are random-walk mechanisms or slip-ratcheting mechanisms. The first model suggests that the notch-peak geometry develops as a result of random, irreversible displacements on the primary glide plane. The second model suggests that specific motion of dislocations is repeated cycle after cycle to produce either an extrusion or intrusion, depending on the sign of the screw dislocation. In materials with low stacking fault energy (SFE) which have planar slip, random-walk nucleation is likely. Rapid nucleation of cracks by the slip-ratcheting mechanism requires easy cross-slip and hence is favored for the high SFE materials. The amount of work on slip-band cracking perhaps over-emphasizes the frequency of its incidence, since there are many cases in which fatigue cracks nucleate at other sites. These include grain boundaries, twin-matrix interfaces, second phase particles, and, in precipitation-hardenable materials, soft regions produced by strain localization.

Stage I crack growth is just a continuation process to extend crack initiation on a slip band. In unnotched specimens the fraction of life spent in growing stage I cracks will depend upon the magnitude of cyclic load, specimen geometry, microstructure and slip mode. The transition from stage I to stage II growth has been attributed to the progressive decrease of the shear-stress/normal-stress ratio acting on a crack growing from a free surface into the interior of a specimen. Slip-controlled processes thus become more difficult and mechanisms controlled by tensile stress are favored[32]. It is found that the transition is profoundly affected by the SFE of a material, and stage I fractures are often featureless except for damage arising from rubbing of the mating surfaces[33]. Two models have been proposed for stage I crack extension[31]. The plastic blunting model is applicable to metals with high SFE in which slip bands are broad and contain a cell structure. Cross-slip is easy in these materials and blunting of the crack tip is possible. Another is the unslipping model which is applicable to planar slip mode materials for which the SFE is low, slip bands are very narrow, and local cross-slip is improbable.

Stage II crack growth is along a direction normal to the maximum principal tensile stress. The fracture surfaces of stage II crack growth are characterized by the appearance of fatigue striations, which become visible as soon as the crack starts to deviate from the crystallographic path. These features have proved

to be of considerable diagnostic use in investigating service failure. The detail of stage II crack growth will be discussed in PART II of this thesis.

The Effects of Microstructure on LCF

The principal requirement for fatigue resistance is to increase the ability of the alloy to deform by homogeneous slip rather than by slip concentration in narrow bands. Homogeneous deformation of precipitation hardenable alloys not only requires a homogeneous microstructure, but also requires stable precipitate phases to prevent localized softening due to dislocation shearing. With regard to this idea, several LCF experiments[4-6] have been conducted in both inert and corrosive environments in this laboratory. The results are very consistent with this idea, i.e., the cyclic strain resistance of 7000-type aluminum alloys increases with increasing aging time at a given aging temperature. This is attributed to a change in deformation mode from localized slip bands to uniform deformation. A similar finding was reported by Calabrese and Laird[34] for the case of an Al-4% Cu alloy. If it is aged to produce the ordered precipitates penetrable by dislocations, cyclic softening occurs which is explained by a disordering mechanism. This eventually leads to the development of weak sites for crack initiation and stage I crack growth. On the other hand, impenetrable precipitates are much more effective in homogenizing the slip and crack nucleation takes place at grain boundaries.

In aluminum alloys there are always some insoluble particles (inclusions) and dispersoid particles existing in the matrix due to the presence of the impurity elements Fe and Si as well as the grain refining elements Zr, Cr or Mn. The effect of these particles on fatigue properties is still not resolved. For example, in two investigations[9,36], crack initiation takes place at such sites, and the effect of inclusions on crack propagation is significant, particularly at short lives. This may be attributed to the fact that particle/matrix interfaces are probably weak and provide suitable sites for crack initiation. In another investigation[37], a commercial 2024 alloy showed much longer fatigue life than a pure 2024 alloy. The evidence from observation of microstructural changes due to cyclic loading implied that this improvement is ascribed to the change of deformation features from slip bands to homogeneous slip. A study of these references emphasizes that the effect of second phase particles on fatigue properties is not dependent solely upon the particles. The effect is thought to be significantly associated with volume fraction of particles and their distributions, individual particle or particle clusters, the aging condition of aluminum alloys, and the stress amplitude of the fatigue loading.

The effects of grain size and boundary on fatigue properties are still in dispute[32,38,39]. In general, the grain size effect on fatigue life is dependent upon the magnitude of stacking fault energy, which determines the ability of cross-slip, and eventually controls the dislocation substructure developed by fatigue deformation. In spite of this fact, the low cycle fatigue properties

of pure aluminum are improved as grain size decreases[38]. This is possible due to a fact that large grain sizes permit even greater discontinuity in strain from grain to grain, thereby increasing the tendency for fold formation and early nucleation of cracks[40].

The Effect of Environment on Fatigue Properties

The fatigue life of aluminum alloys is significantly decreased in the presence of various environments[6,41-44] such as atmospheric air, water and a 3.5% NaCl solution. Many results have revealed that the principal corrosion agent in the atmosphere is moisture. Fatigue crack propagation rates of aluminum alloys are also dramatically increased by these environments[45-50]. Data from two investigations[47,48] implied that oxygen appeared to accelerate crack propagation rates to a certain extent at the low stress intensity range, but the crack propagation rate was the same as in the inert environment at the high stress intensity range. In another investigation[46], however, oxygen did not accelerate the crack propagation rates over the stress intensity range tested. The effects of hydrogen on fatigue properties have been studied by Bradshaw and Wheeler[49] and by Wei[46]. Both studies indicated that hydrogen has no accelerating effect on crack propagation.

The fatigue process in the absence of corrosion is not completely understood although progress in this area has been great in recent years. It is not surprising that the corrosion fatigue process remains elusive, however, several mechanisms have been proposed to explain the shorter fatigue life and higher fatigue

crack growth rates in corrosive environments. The marked effect of water vapor as compared to that of oxygen on fatigue behavior of aluminum alloys suggests that some form of hydrogen embrittlement is responsible for the loss in fatigue properties when moisture is present[41,45-48]. This assumption is strengthened by the observation that hydrogen is evolved from slip bands or propagating cracks in a moisture-containing or liquid environment[41], and by the finding that crack propagation is controlled by the thermally activated processes with apparent activation energies that depend strongly on the crack-tip stress-intensity parameter[46]. Recently, some investigators[68] have suggested that the low diffusivity of hydrogen is counter-balanced by the fact that hydrogen atoms need only be present in the alloy free surface for crack initiation and in the plastic zone of growing cracks for propagation. They postulate that the mechanism involves the production of hydrogen atoms at clean surfaces exposed by slip or at the crack tip, and the diffusion of hydrogen atoms into the metal.

It is generally agreed that corrosion fatigue in aqueous solutions is an electrochemical process. A preferential dissolution mechanism has been proposed[51-54] which suggests that preferential local dissolution of metal at emerging slip steps accelerates the extrusion-intrusion phenomenon, and accordingly results in premature crack nucleation and initial growth. Crack propagation is further accelerated by the corrosion created notch at the specimen surface and by preferential dissolution at the base of the growing crack. Stubbington[44] observed brittle striations on aluminum alloys

fatigued in a corrosive environment, and proposed that they might be the result of lowering the surface energy by ion adsorption. This mechanism was confirmed by Pelloux[54,55] who applied reversed current (cathodic to anodic) to the fatigue samples, and observed an instantaneous change in the type of fracture (ductile to brittle striations). These results indicate that the controlling factor in corrosion fatigue may be an adsorption process which lowers surface energy and changes the fracture mode. Alternatively, several investigators[56-59] suggest that a wet oxide layer has lower stiffness than a dry one, and the stiffness of the oxide layer determines the image forces on dislocations and the ease with which they can escape from the matrix to contribute to the formation of extrusion-intrusion and to slip-plane decohesion. Although several important mechanisms of corrosion fatigue are described above, the exact mechanism of this phenomenon remains elusive.

CHAPTER III

EXPERIMENTAL PROCEDURES

Alloys

Four 7000-type aluminum alloys with the same Zn and Mg contents but with different copper contents were chosen for this investigation. The chemical compositions of the alloys, which were in plate form 7.5 mm thick, are shown in Table 1.1. All alloys were solutionized, stretched 1.5%, and aged 24 hours at a temperature of 120°C. They were prepared at the Alcoa Technical Center, Pa.

Each alloy was produced with different DR by rolling them at different temperatures, but with the same percentage of reduction. The maximum DR was obtained by rolling the plates at lower temperatures and at a higher percentage of reduction than those of low DR. The manufacturing processes are described as follows: The 2.2 inch thick plates of all alloys were rolled to 0.75 inch thick using identical procedures. That is, the 2.2 inch thick plates were homogenized at a temperature of 480°C for 12 hours, air cooled to 400°C, and then rolled by six passes. The percentage of reduction for each pass was 18.2, 11.1, 12.5, 14.3, 16.7 and 25.0%, respectively, and the plates were re-heated to 400°C between passes. Four different DR for each alloy were prepared by the following procedures:

Table 1.1 Chemical Composition (Weight Percent) of the Four Aluminum Alloys.

Alloy	Cu	Zn	Mg	Zr	Ti	Fe	Si	Al
0.01 Cu	0.01	6.41	2.08	0.11	0.02	0.05	0.05	bal.
1.0 Cu	0.98	6.10	2.20	0.12	0.02	0.05	0.05	bal.
1.6 Cu	1.56	6.07	2.24	0.12	0.02	0.05	0.06	bal.
2.1 Cu	2.11	5.97	2.11	0.12	0.02	0.07	0.06	bal.

No. 1: The 0.75 inch thick plates were rolled to 0.25 inch in two passes, the percentage of reduction for each pass being 40.0 and 44.4% respectively. The plates were re-heated to 400°C before rolling for each pass.

No. 2: The same as No. 1 except for a pre-heat temperature of 370°C.

No. 3: The same as No. 1 except for a pre-heat temperature of 340°C.

No. 4: The 0.75 inch thick plates were pre-heated at a temperature of 260°C, and then rolled to the final thickness of 0.25 inch (66.7% reduction).

Microstructural Examination

Optical microscopy was used to determine the DR after etching the specimens. The unrecrystallized grains would be identified as the dark areas as shown in Fig. 1.1. The method employed for determination of DR was the point counting analysis described by Hilliard[60]. Because the DR varies significantly with distance from the plate surfaces, the magnitude of DR for the entire plate was determined by averaging measurements taken at various depths through the plate thickness. Both L-S (longitudinal-short transverse) and T-S (long transverse-short transverse) sections were used for the determination.

In order to observe crack initiation on the LCF samples, some samples were removed after a certain number of cycles prior

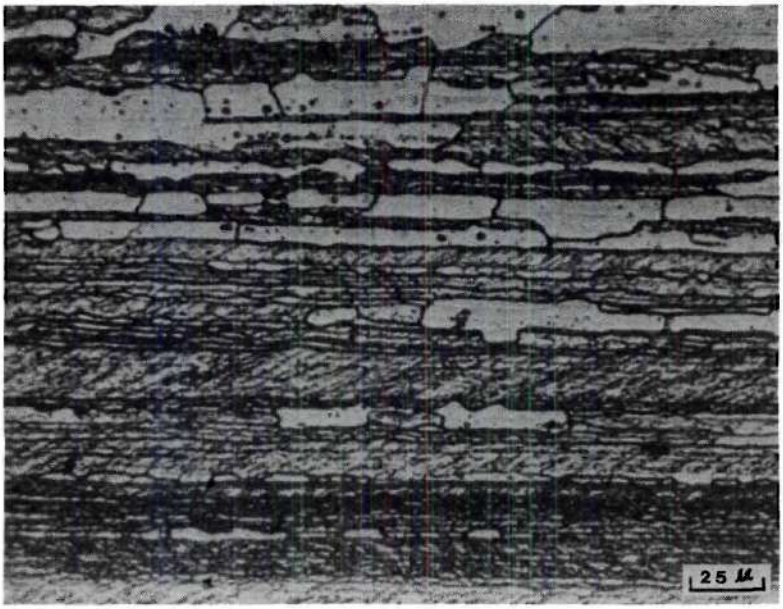

Figure 1.1. An over-etched specimen to determine DR. The dark areas represented the unrecrystallized grains. 1.0% Cu alloy, HNO_3 etch.

to complete failure. The surface of the sample was subsequently examined by optical microscopy.

The subgrain sizes of various aluminum alloys were determined by transmission electron microscopy (TEM). Thin foils were systematically cut from different depths in the plate in L-S sections. The subgrain size was measured in the longitudinal direction and expressed as the nearest integral number of microns. These data permitted a diagram to be plotted of subgrain size versus the probability of its occurrence (%). In order to observe the change of microstructure due to cyclic loading, thin foils were cut from the LCF test samples, 1-3 mm below the fracture surface. Thin foils were prepared by a dimpling technique, using a 25% HNO_3-methonal solution. The foils were examined in a JEOL, JEM-100C electron microscope operating at 100 KV.

Low Cycle Fatigue Tests

Four alloys with almost identical microstructure, having different copper content, were chosen for studying the effect of copper content on the LCF properties. Both 1.6 and 2.1% Cu alloys with two different DR were chosen for investigating the effect of DR on the LCF behavior since they showed the largest difference in DR of the four alloys. The test samples were machined with the tensile axes perpendicular to the rolling direction of the plate. The samples were cylindrical with a gage section approximately 5.0 mm long by 3.0 mm diameter. The specimens were hand-polished with 320, 600 grit emergy paper, then with polishing cloths

impregnated with 6 μm and 1 μm diamond paste. Some of the samples were electropolished for surface observations after the tests.

Push, pull LCF tests were performed on an Instron Testing Machine. The strain was measured with a 10 mm Instron Extensometer clamped to struts rigidly fixed to the grip. A Wood's metal reservoir was used to insure proper alignment of the sample with respect to the loading axis. A cross head speed of 2 mm/min. was used for all tests. The tests were conducted in dry air (3 ppm max. H_2O content), distilled water and a 3.5% NaCl solution. A soft cup 2 inches in diameter was sealed to the sample which was completely submerged in the solution during the low cycle corrosion fatigue test. The solution was not changed during the test. Data obtained from the tests were plotted on log-log coordinates of $\frac{\Delta\varepsilon_p}{2}$ and $2N_f$, cyclic stress amplitude vs number of cycles and logarithmic cyclic stress-strain curve.

CHAPTER IV

EXPERIMENTAL RESULTS AND DISCUSSION

Microstructural Evaluation

Results obtained for the DR and the monotonic mechanical properties for the four different copper content alloys are presented in Table 1.2. The four alloys employed for investigating the effect of copper content on the LCF behavior have similar DR. On the other hand, both the 1.6 and 2.1% Cu alloys, which showed a large difference in DR, were used for studying the effect of that parameter on the LCF behavior. An example of the microstructure for the 0.01% Cu alloy is shown in the optical micrograph of Fig. 1.2. Part A shows some subgrains and the directional, high angle grain boundaries as revealed by an HNO_3 etch. Part B shows another area in which subgrains are completely revealed. The unrecrystallized, large grains (about 1100 μm) for the four alloys at these DR (3, 3, 5 and 6%) are essentially identical because they were rolled under the same schedule. The microstructure of alloys with higher DR was also studied. The typical examples of microstructures for the 2.1% Cu alloy are shown in Fig. 1.3, pictures A and B, for different sections of a plate. As is apparent in these pictures, the dark areas contain unrecrystallized grains while the white areas are composed of

Table 1.2. Degree of Recrystallization of the Four Aluminum Alloys and Their Monotonic Mechanical Properties.

Alloy	DR L-S Section	DR T-S Section	Yield Strength (MPa)	Tensile Strength (MPa)	Elongation (%)	Ductility (%)	n
0.01 Cu	3	3	482.2	551.7	14.0	31.2	0.028
1.0 Cu	3	3	522.3	588.0	17.1	32.5	0.031
1.6 Cu	5	5	529.2	613.5	17.9	32.5	0.033
1.6 Cu	30	28	528.2	614.7	18.7	33.1	0.030
2.1 Cu	6	5	545.9	613.5	17.1	36.4	0.032
2.1 Cu	45	47	533.1	615.4	17.3	35.3	0.033

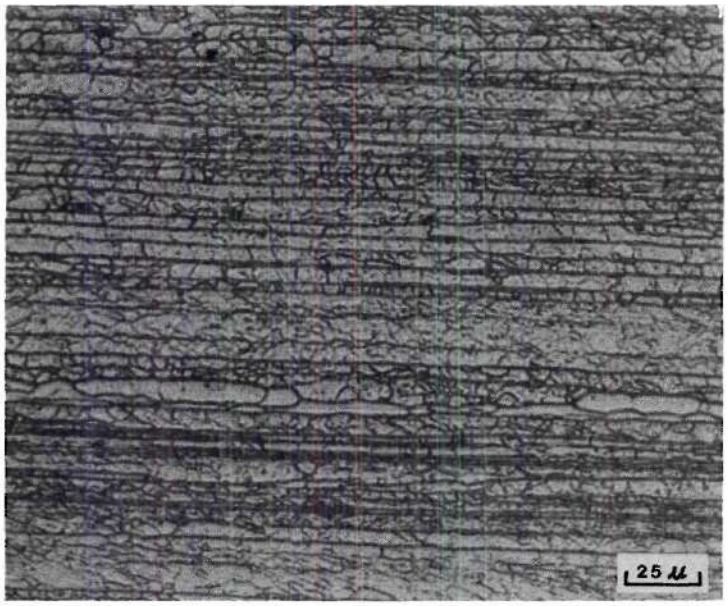

(A)

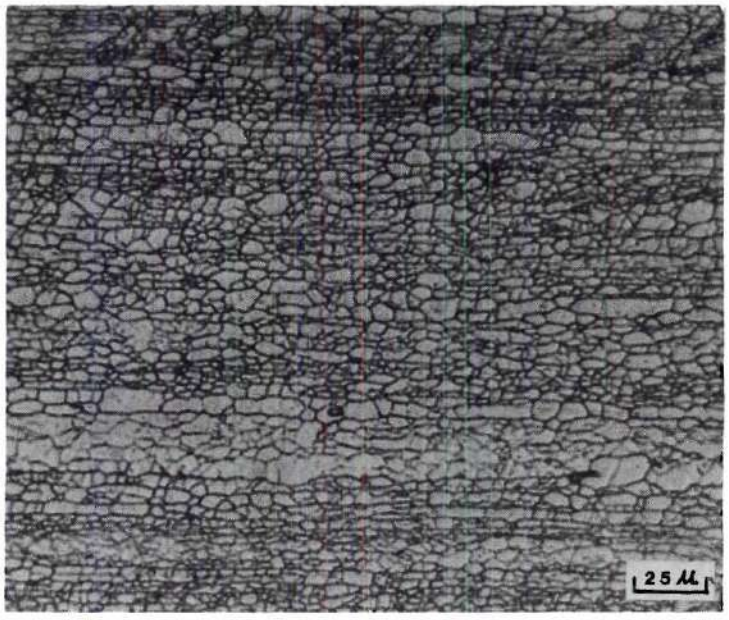

(B)

Figure 1.2. Microstructure of the 0.01% Cu alloy with 3% DR, L-S section. (A) subgrains and the directional, high angle grain boundaries; (B) subgrains only. HNO_3 etch.

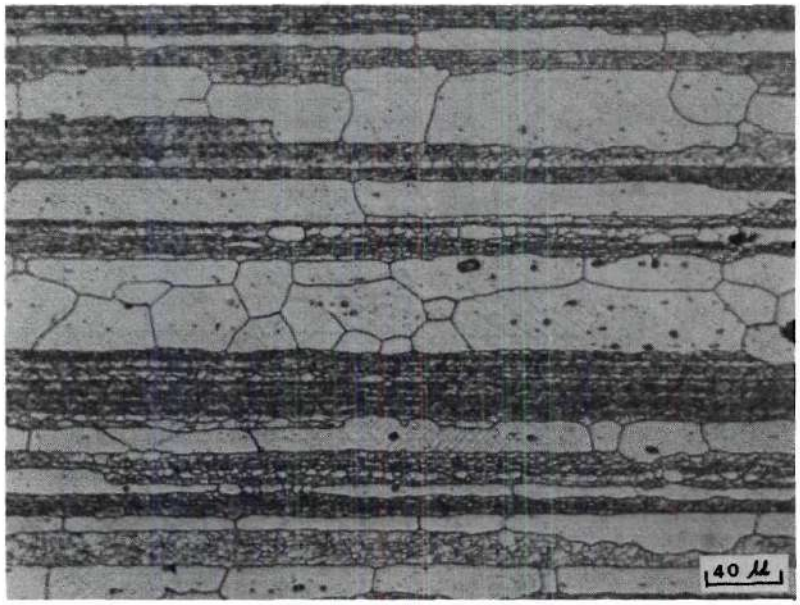

(A)

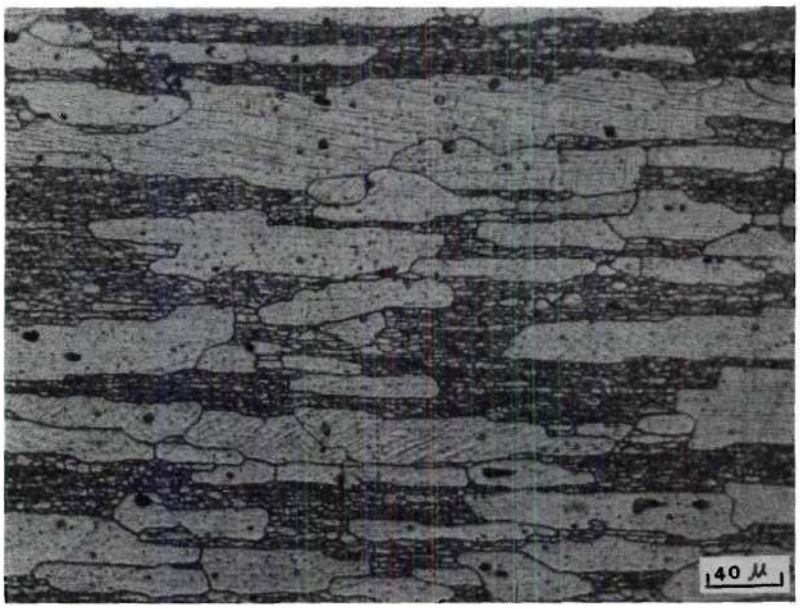

(B)

Figure 1.3. Microstructure of the 2.1% Cu alloy with 45% DR, (A) L-S section, and (B) T-S section. HNO_3 etch.

recrystallized grains. The recrystallized grain size varied from 10 μm to 370 μm; hence, the determination of an average grain size was not attempted.

The subgrain size in the unrecrystallized grains of all alloys was determined by TEM. It was found that subgrain size varies not only from one unrecrystallized grain to another, but also within the same unrecrystallized grain. Consequently, the subgrain size was plotted statistically against the probability of its occurrence, to express the size distribution of subgrain sizes. The results are shown in Fig. 1.4. In diagram A, for the four alloys with low DR, note that the 0.01, 1.6 and 2.1% Cu alloys exhibit similar distribution curves, but the 1.0% Cu alloy contains a larger percentage of small subgrains. For example, the 1.0% Cu alloy contains 20% of 3 μm subgrains, while the others contain only about 10% of this size. It is important to note that the four curves overlap. The small change in the spread of subgrain size (maximum difference is about 10% between 1.0 and 2.1% Cu alloys at the subgrain sizes of 3 μm or 6 μm) is not likely to significantly affect the LCF behavior. The subgrain size distribution in the unrecrystallized grains for the 1.6 and 2.1% Cu alloys with high DR was also determined and is given in diagrams B and C, Fig. 1.4. It is obvious from these diagrams that the spread in subgrain size is remarkably different between an alloy with low DR and the same alloy with high DR. Interpretation of why subgrain size in the unrecrystallized grains for an alloy with high DR is smaller than that for the same alloy with low DR can be based on two well-established facts[61]: One is that the initial subgrain size due to hot rolling is strictly dependent upon the

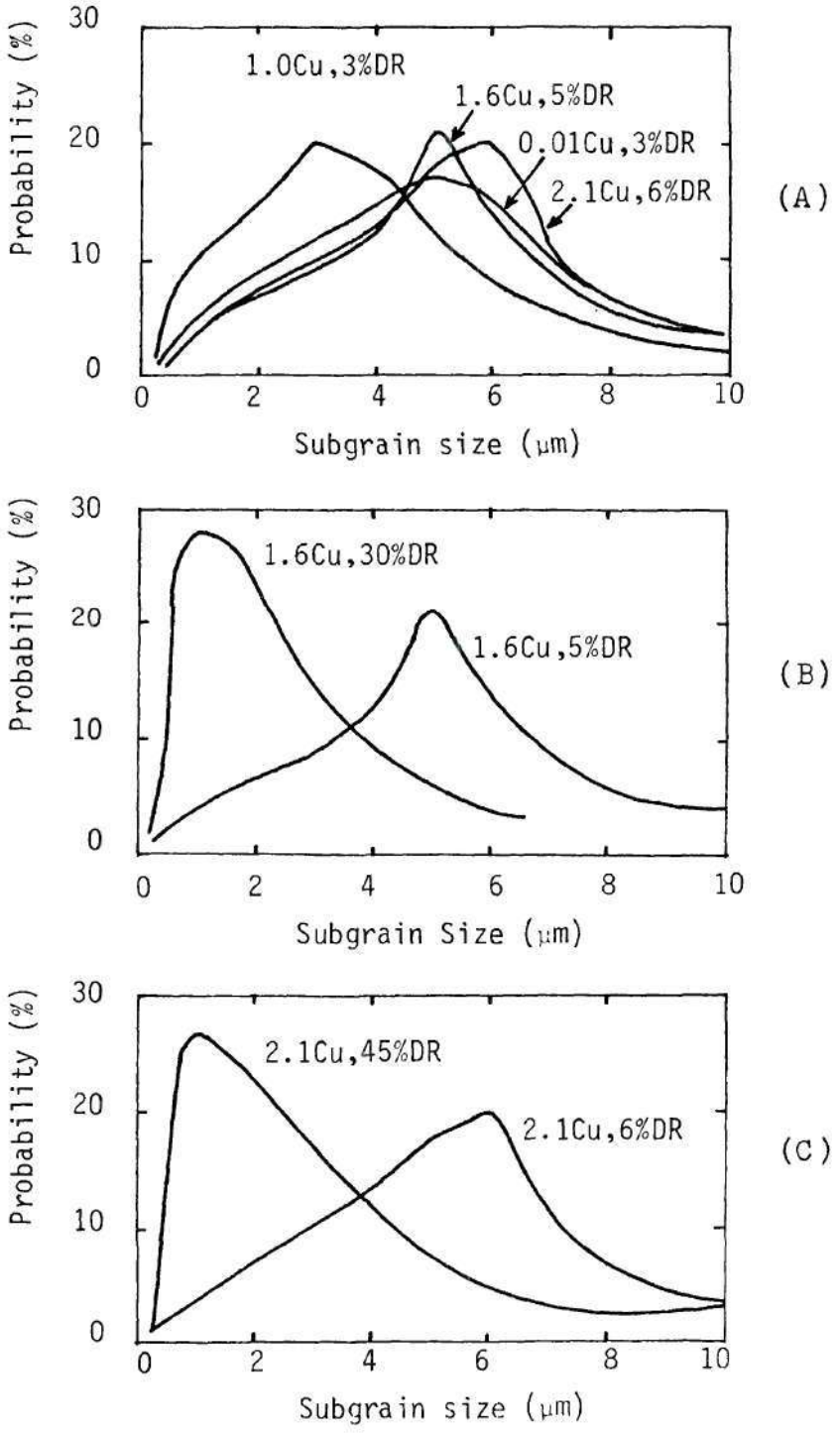

Figure 1.4. Subgrain size in the unrecrystallized grains vs statistical probability of its occurrence, (A) four alloys with low DR, (B) the 1.6% Cu alloy with low and high DR, and (C) the 2.1% Cu alloy with low and high DR.

magnitude of deformation--a higher magnitude of deformation produces smaller subgrains. Thus, an alloy with high DR contained smaller subgrains since it was hot rolled to a 22% greater reduction than the same alloy with low DR. The other is that the presence of very fine Al_3Zr particles in these alloys markedly descreases the movement of dislocations by pinning them, even during solutionizing at high temperature.

Using TEM, an extensive study was made to examine precipitation features on subgrain boundaries and on high angle grain boundaries of all the alloys. It is of interest to note that no significant difference in precipitation features was found between these two different boundaries for this aging treatment. The precipitation features are similar for the four alloys observed by TEM. An example of precipitation in a 2.1% Cu alloy is given in Fig. 1.5, where micrographs A and B show subgrain boundaries and a high angle grain boundary, respectively. Both subgrain and grain boundaries are decorated with precipitates.

Monotonic Mechanical Properties

These properties for the experimental materials are presented in Table 1.2. The yield strength, tensile strength, ductility and strain hardening exponents (n), in general, increase with increasing copper contents. This is especially true for the yield strength and ductility. This trend can be attributed to the fact that the addition of copper in Al-Zn-Mg alloys not only increases the volume fraction of strengthening precipitates[4,17], but also increases the

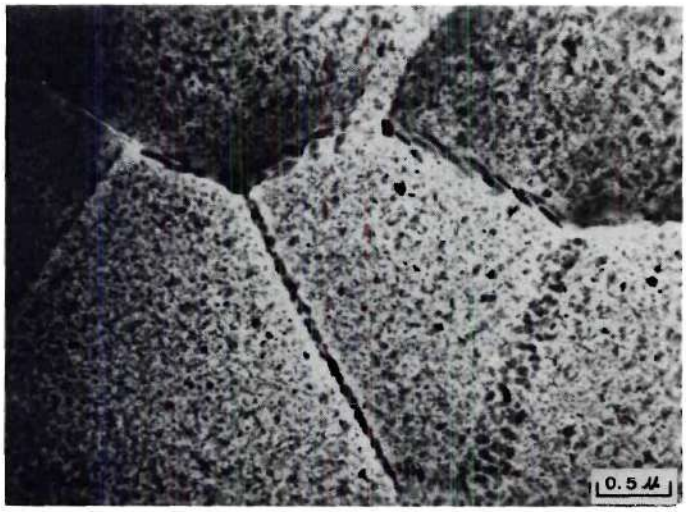

(A)

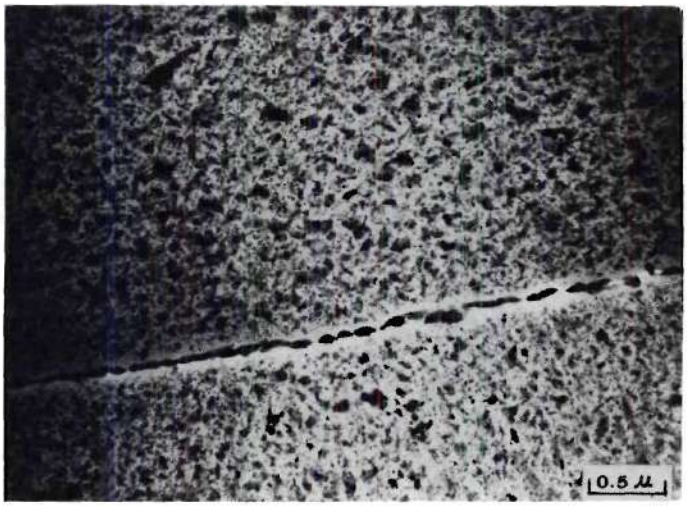

(B)

Figure 1.5. Transmission electron micrographs of precipitation features of the 2.1% Cu alloy, (A) subgrain boundaries, and (B) a high angle grain boundary.

number of partially coherent and incoherent precipitates[4]. It can also be seen from this table that the monotonic mechanical properties are not significantly affected by the changes of DR. This phenomenom is related to the fact that the monotonic mechanical properties of these precipitation hardenable alloys are strictly dependent upon the strengthening precipitates.

Effect of Copper Content on the LCF Behavior

The results of LCF tests are plotted on the basis of the Coffin-Manson equation and shown in Figures 1.6 and 1.7. Figure 1.6 reveals the effect of environment on the LCF behavior for the 0.01 and 1.0% Cu alloys with constant (3%) DR, while Figure 1.7 does the same for the 1.6 and 2.1% Cu alloys with variable DR. These results will be discussed later. For clearer comparisons of the effect of copper content on the LCF behavior in these alloys, the test data are grouped, on the basis of the magnitude of DR and the test enviroment, and shown in diagram A, B and C of Figure 1.8. The values of important parameters derived from these plots are presented in Table 1.3. Analyzing these plots, particularly their relative position and the slope of each curve, several important facts are obtained. The cyclic strain resistance of the 7000-type aluminum alloys generally increases with increasing copper content, regardless of the test environment. This trend becomes much more noticeable when the tests are conducted in distilled water or a 3.5% NaCl solution. The difference in cyclic strain resistance for the four alloys decreases at high plastic strain amplitudes, especially for

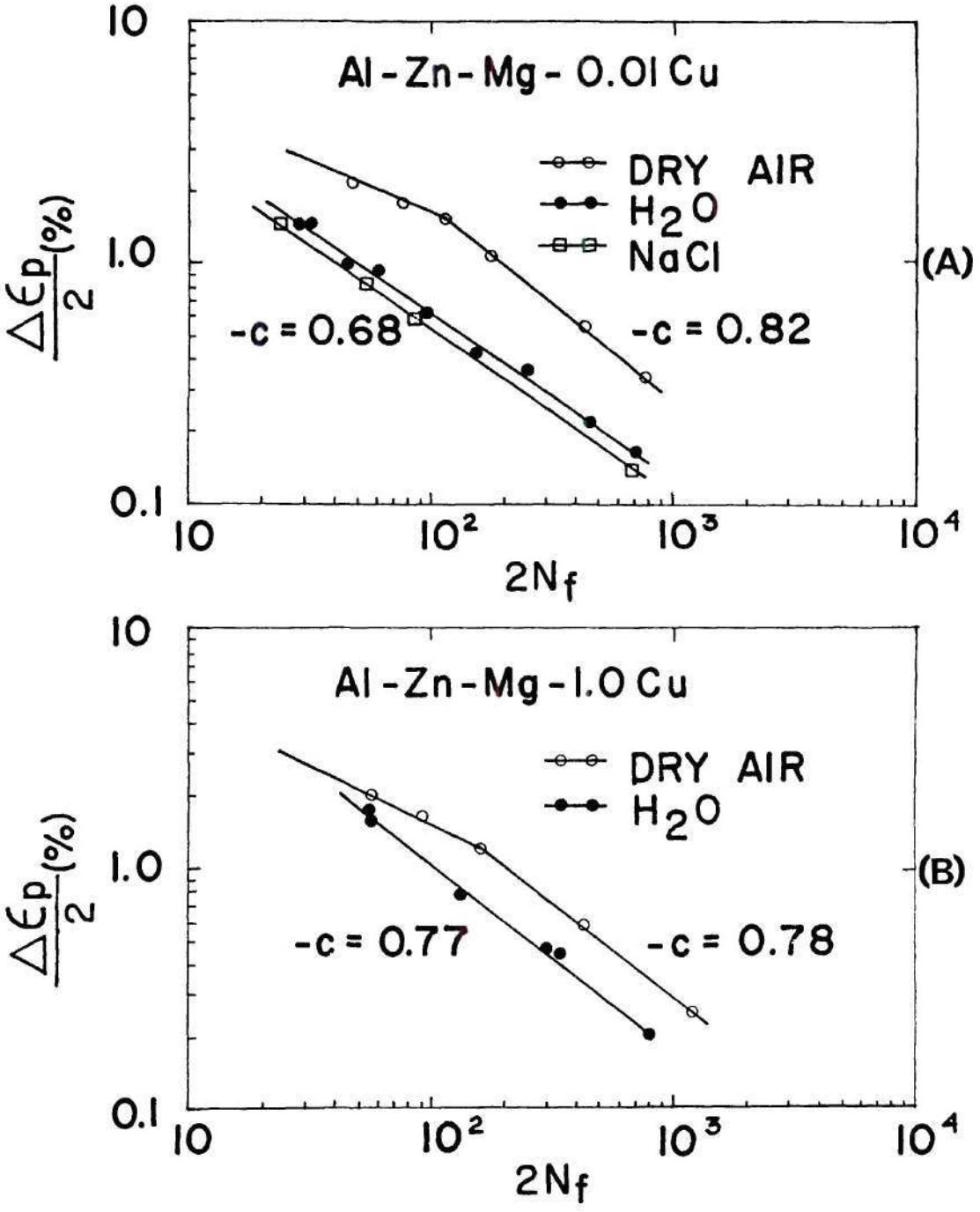

Figure 1.6. Effect of environments on the LCF behavior of (A) the 0.01% Cu alloy with 3% DR, and (B) the 1.0% Cu alloy with 3% DR.

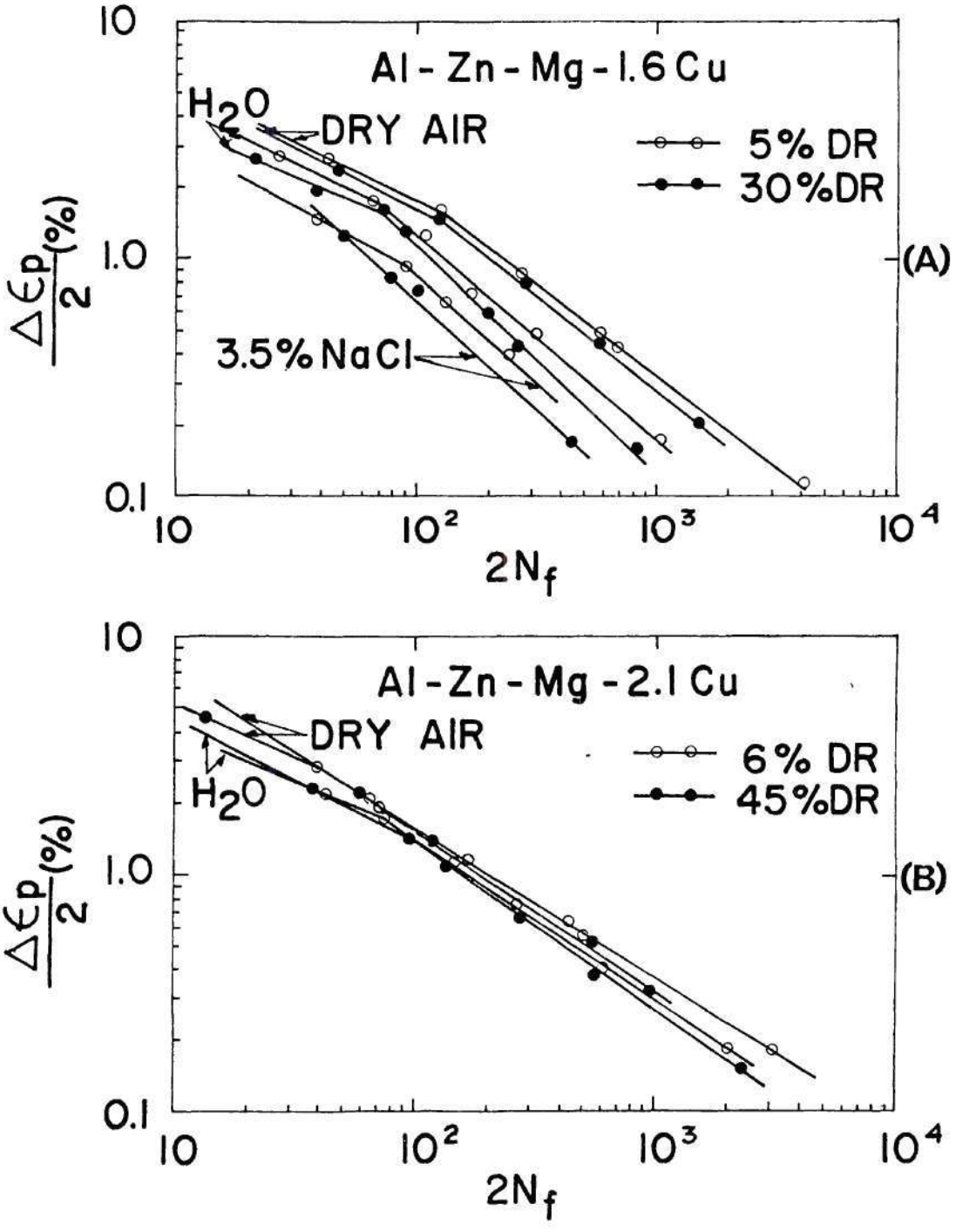

Figure 1.7. Effect of the DR on the LCF behavior tested in various environments, (A) the 1.6% Cu alloy, and (B) the 2.1% Cu alloy.

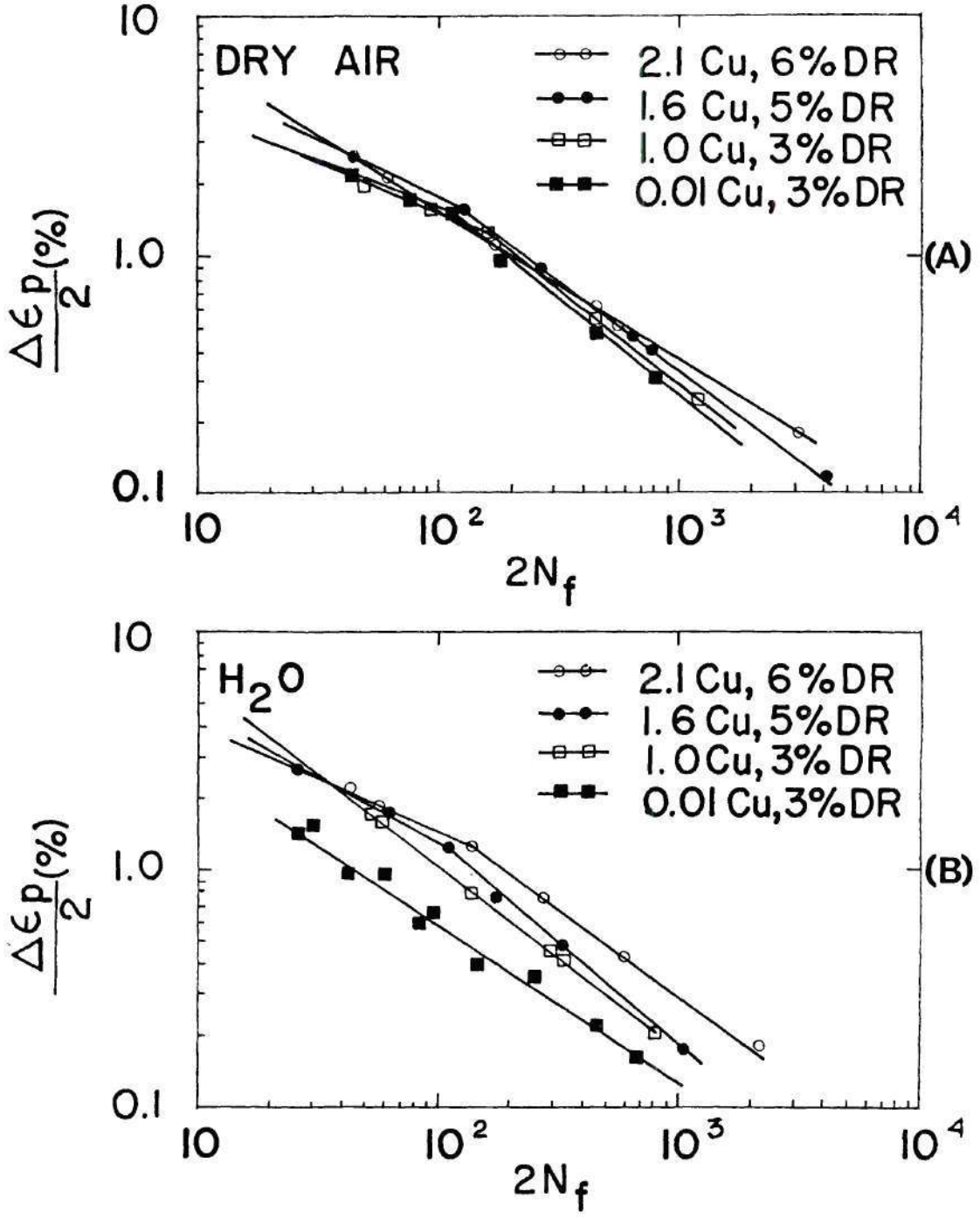

Figure 1.8. Effect of the copper content of 7000-type aluminum alloys on the LCF behavior, tests conducted in (A) dry air, (B) distilled water and (C) a 3.5% NaCl solution.

Continued

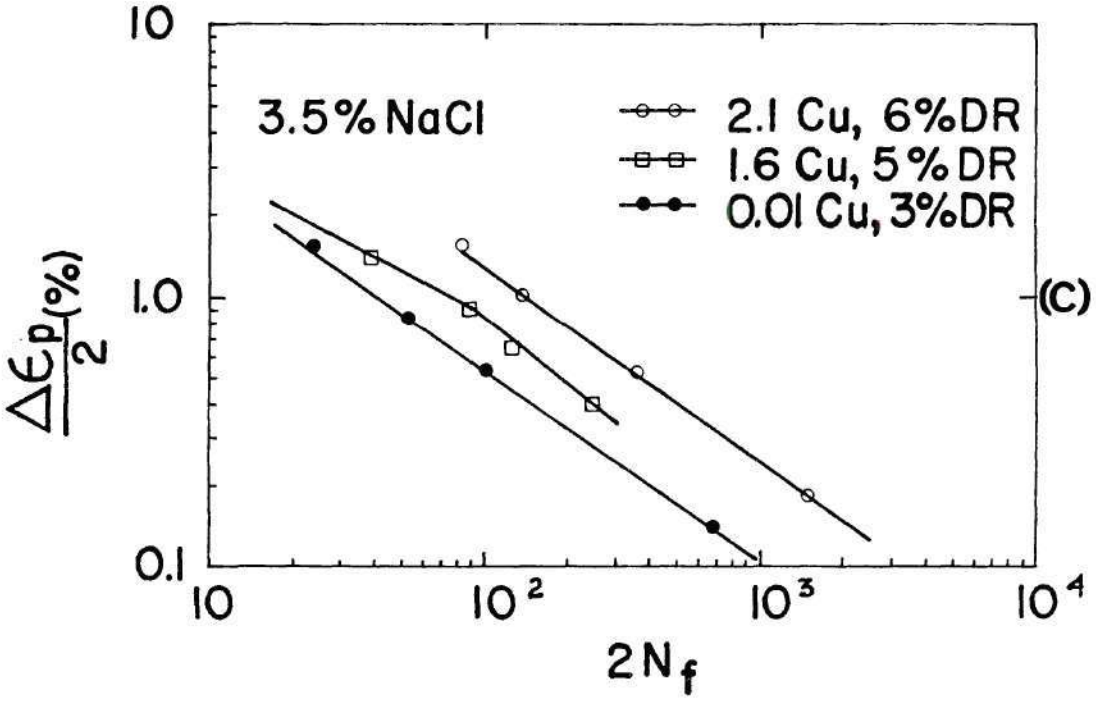
10
1.0
0.1
3.5% NaCl
2.1 Cu, 6%DR
1.6 Cu, 5% DR
0.01 Cu, 3%DR
(C)
$\frac{\Delta\epsilon_p(\%)}{2}$
10
10^2
10^3
10^4
$2N_f$

Table 1.3. The LCF Data Tests Conducted in Dry Air, Distilled Water and a 3.5% NaCl Solution.

Alloy	DR (%)	Dry Air			H_2O			3.5% NaCl		
		-C	$2N_f = 1$	n'	-C	$2N_f = 1$	n'	-C	$2N_f = 1$	n'
0.01 Cu	3	0.82 0.43	125 16	0.063	0.68	23	0.063	0.68	20	0.063
1.0 Cu	3	0.78 0.48	115	0.075	0.77	63	0.075	-	-	-
1.6 Cu	5	0.77 0.48	110 24	0.088	0.85 0.43	125 19	0.088	0.85 0.54	100 16	0.088
1.6 Cu	30	0.79 0.51	118 24	0.082	0.93 0.42	180 13	0.082	0.85	90	0.082
2.1 Cu	6	0.63	46	0.114	0.68 0.41	54 14	0.114	0.70	62	0.114
2.1 Cu	45	0.67 0.43	50 20	0.099	0.71 0.48	60 20	0.099	-	-	-

tests conducted in dry air. The occurrence of a break point in the Coffin-Manson plots is observed for most of alloys tested in the three environments.

As has been noted in the previous section, the alloys chosen for investigating the effect of copper content on the LCF behavior had almost identical microstructures, e.g., the percentage of DR, the unrecrystallized grain size and subgrain size. Therefore, the only significant parameter to affect the LCF properties appears to be the copper content. Copper atoms do participate in the precipitation processes[4,15-17], and thus change the character of precipitates; and as a result, they alter the type of interactions between precipitates and dislocations. A lot of supplemental results were obtained from these experiments such as: optical observation of slip traces on the surfaces of the LCF test samples, examination of slip features by TEM and measurement of the Bauschinger effect. All of these observations help to elucidate why the cyclic strain resistance of these alloys is directly related to the copper content.

The LCF test samples of the 0.01 and 2.1% Cu alloys were cyclically strained at a given plastic strain amplitude to a predetermined number of cycles prior to failure. Extensive studies were subsequently made to observe the slip traces on the surfaces of samples, but since the test samples were cylindrical, the field of view was limited. The slip band appearance was found to be profoundly affected by the presence of copper, as is apparent in Fig. 1.9. Picture A shows the sharp and planar slip band features of the 0.01% Cu alloy. The length of slip band is longer and the

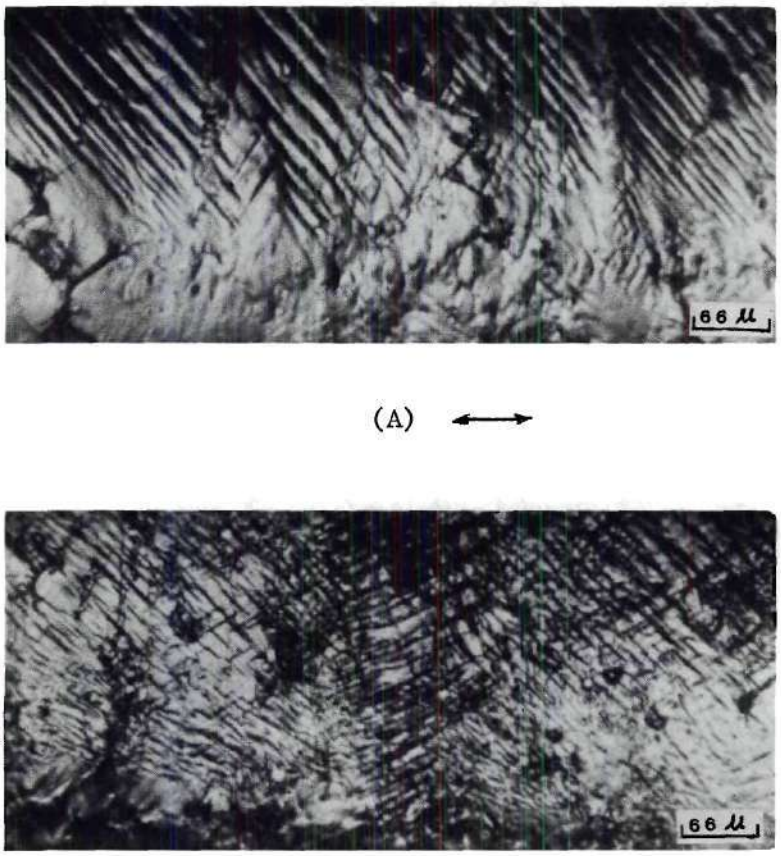

Figure 1.9. Observations of slip traces on the polished surfaces of the LCF samples tested in dry air for 80 cycles, (A) the 0.01% Cu alloy with 3% DR, $\Delta\varepsilon_p/2 = 0.72\%$, and (B) the 2.1% Cu alloy with 6% DR, $\Delta\varepsilon_p/2 = 0.76\%$. Arrow: direction of the loading axis.

height of slip step is higher, when compared with those of the 2.1% Cu alloy shown in picture B. In contrast to the low copper content alloy, slip bands with diffuse and wavy character were observed for the alloy with 2.1% Cu.

Evidence further supporting the correlation described above was also found by exhaustive TEM examination of thin foils cut from the LCF test samples. The overall appearance of cyclic deformation was similar for the low copper content alloys, i.e., predominantly uniform deformation despite the magnitude of the plastic strain. However, some localized slip bands were found in the alloys containing copper equal to and below 1.6%. On the other hand, it is important to note that no slip bands were observed in thin foils of the 2.1% Cu alloy, regardless of the magnitude of plastic strain and DR. Typical examples of slip band features for the 0.01 and 1.6% Cu alloys are displayed in Figs. 1.10 and 1.11. Fig. 1.10 shows the slip band features of samples (0.01% Cu alloy) cyclically strained at low and high plastic strain amplitudes. Note that the slip band features are quite different between plastic strain lower and higher than that for the occurrence of a break point in the Coffin-Manson plot. Micrograph A is representive of the slip band character of a sample cyclically strained at a value of $\frac{\Delta\varepsilon_p}{2}$ below the break point. The band was broad in appearance, and passed through subgrain boundaries but failed to penetrate the high angle grain boundary. The slip bands shown in micrographs B and C were obtained from a sample cyclically strained at a value of $\frac{\Delta\varepsilon_p}{2}$ above the break point. The appearance of these slip bands is sharp and

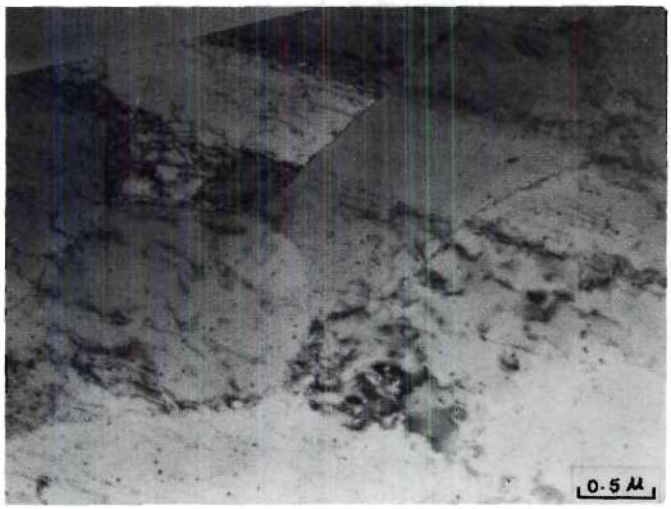

(A)

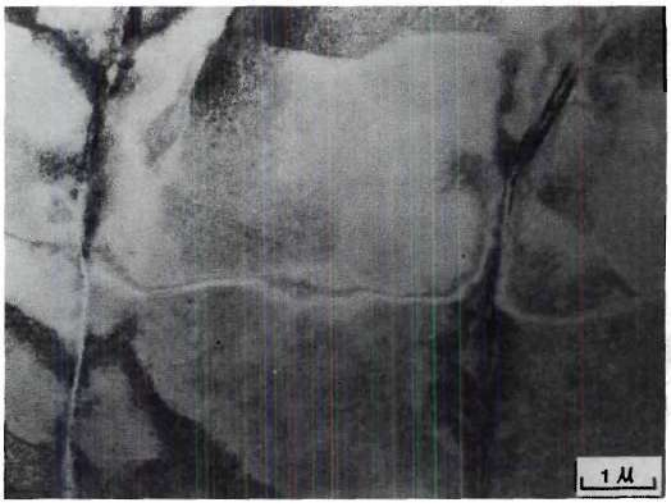

(B)

Figure 1.10. Transmission electron micrographs of the LCF samples for the 0.01% Cu alloy with 3% DR tested in dry air until failure, showing slip bands. (A) plastic strain amplitude below the break point, $\Delta\varepsilon_p/2 = 0.53\%$, $N_f = 215$ cycles, slip band is parallel to [011], (B) above the break point, $\Delta\varepsilon_p/2 = 2.2\%$, $N_f = 24$ cycles, and (C) at high mag., slip band is parallel to [101].

Continued

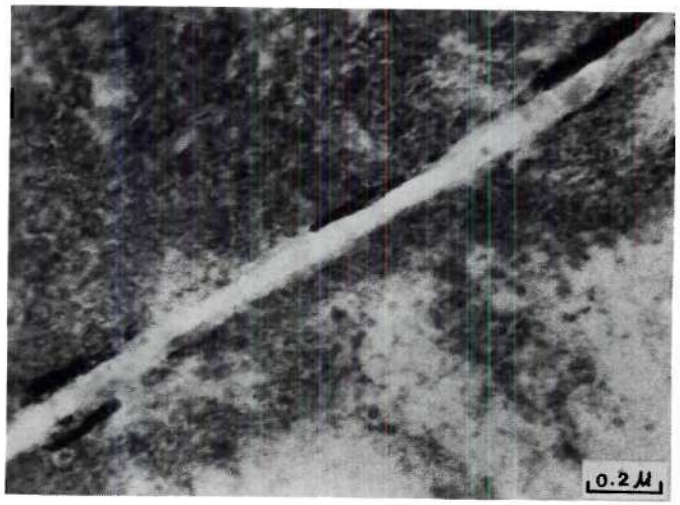

(C)

intense. They passed through the high angle grain boundaries. In addition, the frequency of occurrence of slip bands seems to increase as the magnitude of plastic strain increases, above the break point. The identical phenomena were also found for the 1.6% Cu alloy as shown in Fig. 1.11. These observations imply that dislocations easily shear coherent precipitates in the low copper content alloys resulting in planar slip. Planar slip may increase the reversibility of slip and thus improve the LCF resistance for some of the low SFE materials[35,38], however, in age-hardenable alloys, planar slip can cause softening on the slip bands[27,83] resulting in strain localization. This leads to an early crack initiation by slip band decohesion, especially for the corrosive environment, whereas localized strain concentration will intensify the metal-environment interactions resulting in a significantly detrimental effect. For the high copper content alloys such as 2.1% Cu, not only do dislocations shear coherent and partially coherent precipitates, but they also loop the more numerous incoherent precipitates. The latter deformation mechanism reduces the slip reversibility, but it produces a high degree of homogeneity of deformation. Optical observations of the surfaces of fatigue samples containing low copper contents also showed that cracks initiated on the slip bands and then propagated along these preferable paths, as shown in Fig. 1.12. Intensive grain boundary cracking was also observed.

On the basis of findings by Stoltz and Pelloux[62], aluminum alloys heat treated to contain easily shearable precipitates exhibited a small Bauschinger effect while alloys with nonshearable precipitates

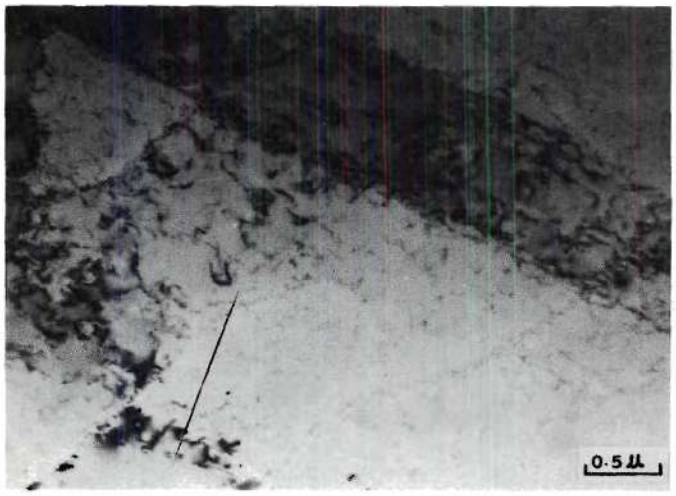

(A)

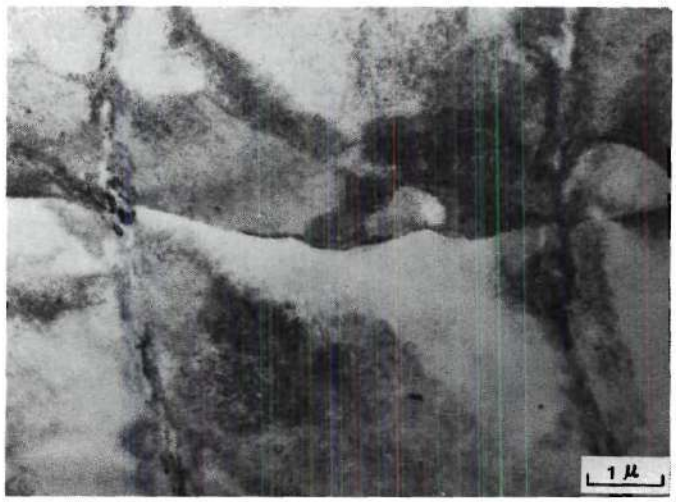

(B)

Figure 1.11. Transmission electron micrographs of the LCF samples for the 1.6% Cu alloy with 5% DR tested in dry air until failure, showing slip bands, (A) plastic strain amplitude below the break point, $\Delta\varepsilon_p/2 = 0.42\%$, $N_f = 355$ cycles, slip band is parallel to [101], and (B) above the break point, $\Delta\varepsilon_p/2 = 2.6\%$, $N_f = 22$ cycles.

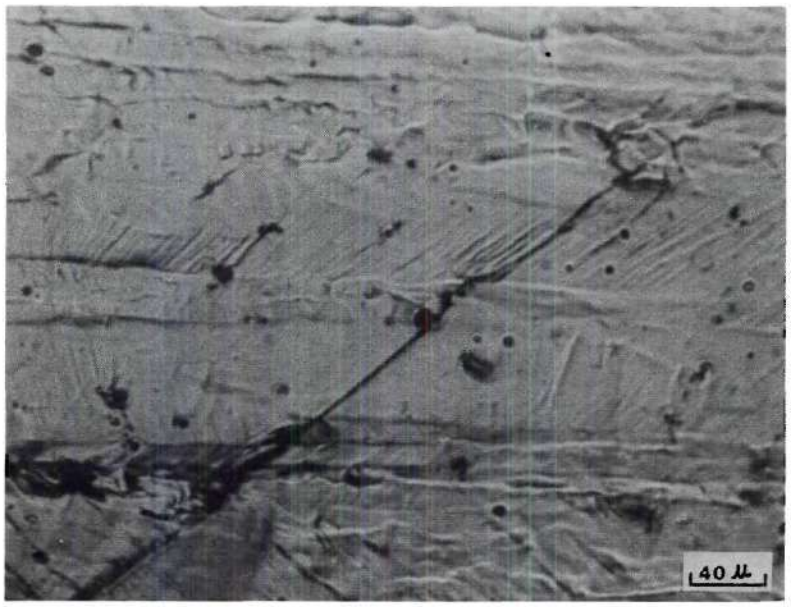

(A)

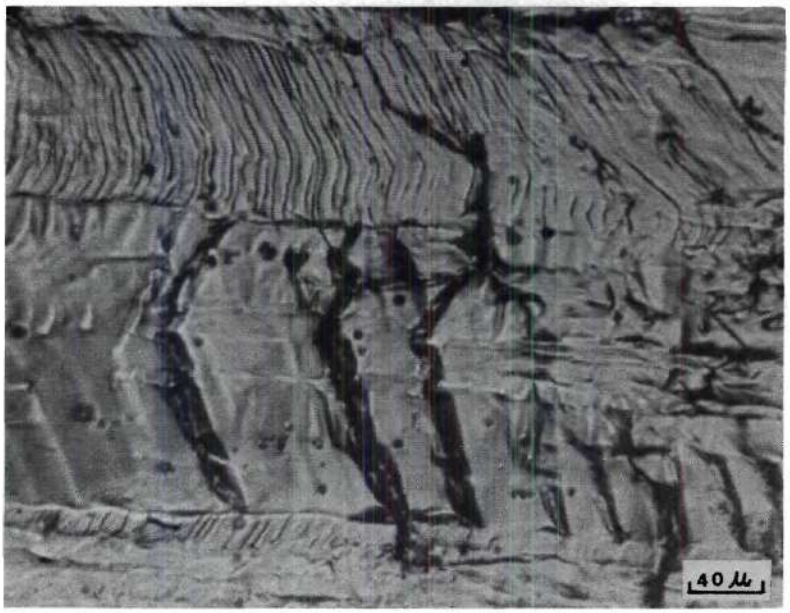

(B)

Figure 1.12. Observation of slip band cracks on the polished surfaces of the LCF samples tested in dry air before failure, (A) the 0.01% Cu alloy with 3% DR, $\Delta\varepsilon_p/2$ = 0.72% for 80 cycles, and (B) the 1.6% Cu alloy with 5% DR, $\Delta\varepsilon_p/2$ = 0.81% for 100 cycles.

showed a larger effect. Evidence of dislocation shearing of coherent precipitates for the low copper content alloys and dislocation looping of incoherent precipitates for the high copper content alloys can also be provided by a measurement of the Bauschinger effect for the aluminum alloys studied here. The effect of copper content in 7000-type aluminum alloys at this aging treatment (24 hours at 250°F) on the Bauschinger effect is shown in Fig. 1.13. It appears that the Bauschinger effect increases slightly as copper content changes from 0.01 to 1.6%, especially for a total strain smaller than 4.5%; whereas the effect increases tremendously for the 2.1% Cu alloy. It is also shown in this figure that the Bauschinger effect is probably dependent upon the type of precipitates. However, grain or subgrain boundaries play a small role for the present study, since the same alloy with different DR exhibited very similar values of the Bauschinger effect. These findings are consistent with the observation of deformation features in thin foils cut from the fatigue samples. The frequency of occurrence of slip bands appears to decrease as the copper content increases, and no slip bands were observed in thin foils of the alloy containing 2.1% Cu.

Ample evidence was obtained from the present experiments to conclude that the cyclic strain resistance of 7000-type aluminum alloys, aged at 250°F for 24 hours, increase with increasing copper content. Moreover this phenomenon must be due to the following facts. For the low copper content alloys, the presence of more easily shearable precipitates results in the occurrence of localized slip bands. This strain localization leads to an early crack

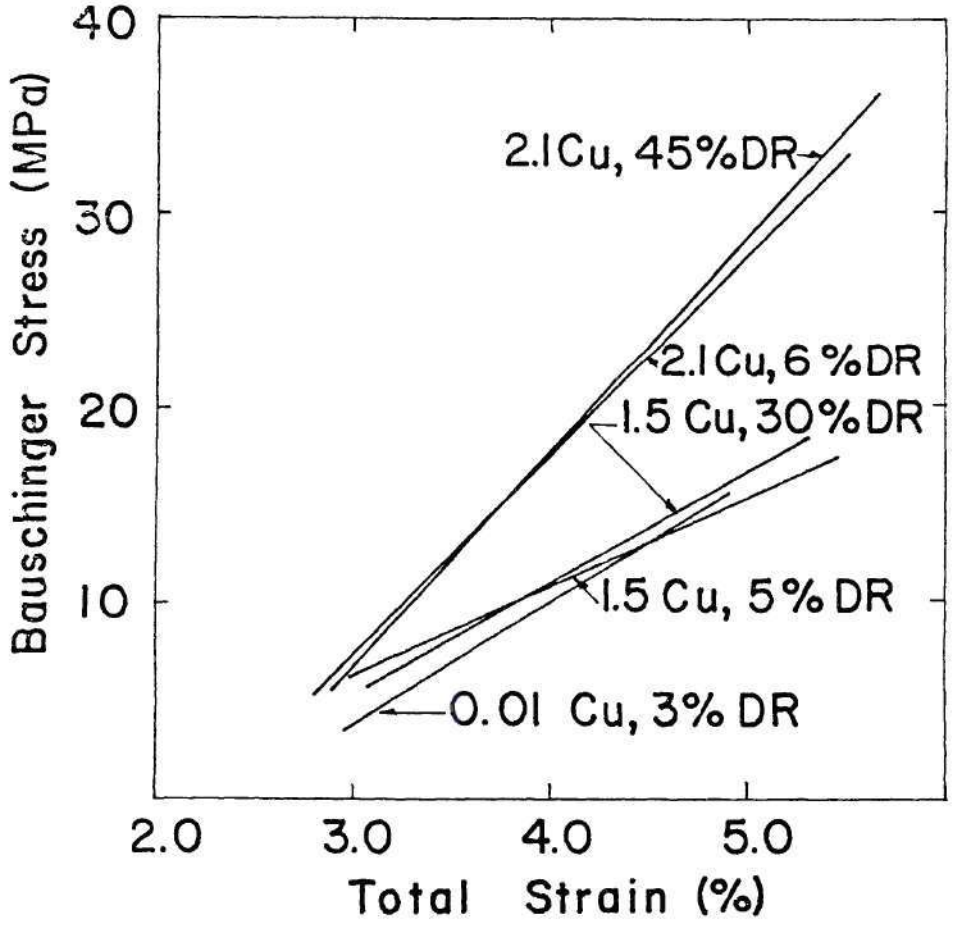

Figure 1.13. The effect of copper content in 7000-type aluminum alloys on the Bauschinger effect at the first half cycle.

initiation by slip band decohesion, and crack propagation is also easy along these preferable paths. For the high copper content alloys, which contain more partially coherent and incoherent precipitates, dislocation looping of incoherent precipitates results in a relatively more homogeneous deformation with resulting improvement in the fatigue resistance.

Effect of DR on the LCF Behavior

The effect of DR on the LCF behavior for the 1.6 and 2.1% Cu alloys is shown in Fig. 1.7, plotted as $\Delta\varepsilon_p/2$ vs $2N_f$. It is apparent from these curves that the cyclic strain resistance for both alloys is inversely related to the percentage of DR, regardless of the test environment. It is also important to note that for the 1.6% Cu alloy, the magnitude of the difference in cyclic strain resistance due to the difference in DR is larger than that for the 2.1% Cu alloy, even though the latter has a greater difference in DR. This trend becomes more noticeable when the tests are conducted in distilled water.

The alloys with lower DR exhibited higher cyclic strain resistance, which is attributed to the more uniform deformation. It is well known that subgrains or small grains can induce the activation of more slip systems due to the mutual influences of neighboring subgrains or small grains. This results in a larger degree of homogeneity of deformation. The mechanism was confirmed by the observation of slip traces in thin foils cut from the fatigue samples with different DR. For the 1.6% Cu alloy, the frequency of

occurrence of localized slip bands was greater in the large recrystallized grains than that in the unrecrystallized grains. An example of the appearance of slip bands in a large recrystallized grain is given in Fig. 1.14. It is interesting to note that a lot of fine slip was concentrated to form a large slip band. This is a typical slip band in the LCF samples, i.e. numerous fine slip joined together forming the notch-peak topography of the band (PSB). This explanation is fully supported by the results of optical observations, shown in Fig. 1.15, where the PSB's were more prevalent in the large recrystallized grains, although slip traces were also observed in the unrecrystallized grains. Moreover, the recrystallized grains in these samples were quite large (up to 370 μm) as described previously. Presumably, the large grain size increases localization of strain in the slip bands which results in a high stress concentrations at grain boundaries. This will result in early crack initiation by slip band decohesion, or by grain boundary cracking as exhibited in Fig. 1.12 and 1.15 respectively. Since no cell structures were observed for either alloy cyclically strained up to high plastic strain amplitudes, the magnitude of stress or strain concentration is thus dependent on the grain size. Another function of subgrain boundaries is to change the slip direction, as can be seen in micrograph A of Fig. 1.10. This leads to a decrease in the magnitude of localized stress and/or strain concentration. All of these factors result in a higher degree of homogeneity of deformation and a decrease in the magnitude of localized stress concentration, and thus improve the cyclic strain

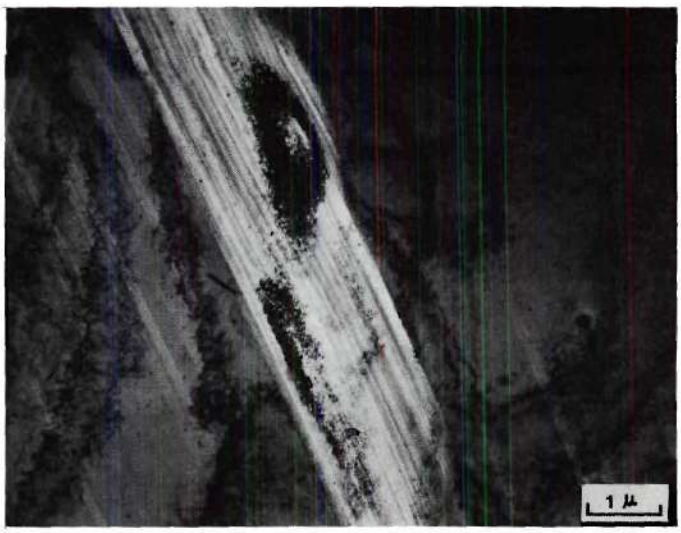

Figure 1.14. Transmission electron micrograph of the LCF sample for the 1.6% Cu alloy with 30% DR tested in dry air, showing a slip band in a large recrystallized grain, $\Delta\varepsilon_p/2 = 0.78\%$, $N_f = 144$ cycles, slip band orientation is parallel to $[0\bar{1}1]$.

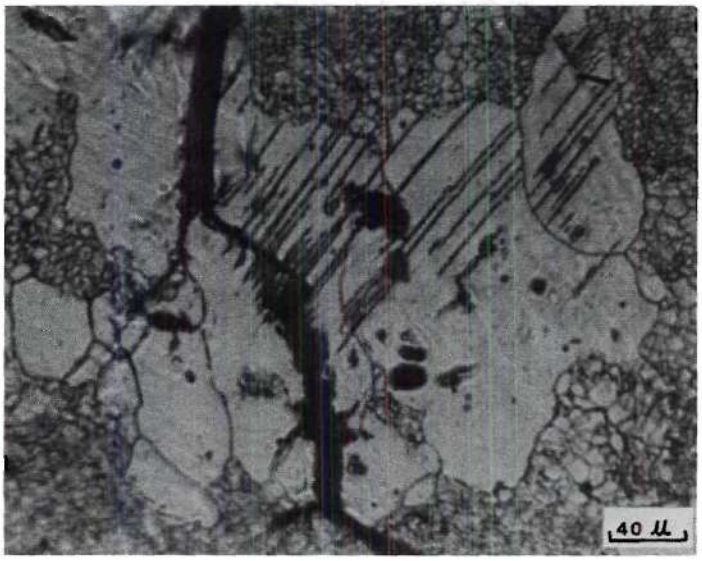

(A)

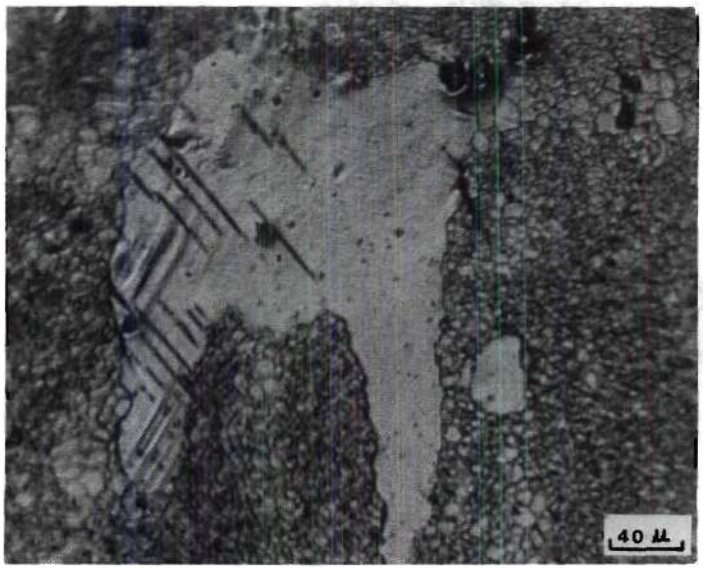

(B)

Figure 1.15. Observation of the polished surfaces of the LCF samples for the 1.6% Cu alloy with 30% DR tested in dry air for 60 cycles, (A) $\Delta\varepsilon_p/2 = 0.78\%$, showing PSB's and grain boundary cracking in the recrystallized grains, (B) $\Delta\varepsilon_p/2 = 0.67\%$, showing PSB's in the recrystallized grains. HNO_3 etch.

resistance for an alloy with low DR. The effect of DR on the LCF behavior, in this case, is not due to the difference in the spread of subgrain size since the alloy with high DR contains 10% more of the smaller subgrains. The effect of the difference in the spread of subgrain size on the LCF resistance, if any, is small and would be masked by the greater effect of the difference in DR.

The magnitude of the change in cyclic strain resistance of the 1.6% Cu alloy due to the difference in DR is greater than that for the 2.1% Cu alloy, especially for tests conducted in distilled water. This effect can be attributed to the greater difference in degree of homogeneity of deformation between the 1.6% Cu alloy with low DR and with high DR. Much of the information in the previous section indicated that a sharp change in deformation behavior was found between the 2.1% Cu alloy and the others (0.01, 1.0 and 1.6% Cu). The former alloy exhibited homogeneous cyclic deformation regardless of the magnitude of DR; thus, there was a smaller difference in degree of homogeneity of deformation due to the difference in DR, resulting in a smaller difference in the cyclic strain resistance. The effect of DR on the LCF behavior was not determined for the low copper content alloys (0.01 and 1.0% Cu) since they did not show much difference in DR for the processing used in this study. Nevertheless, it is reasonable to make a conclusion, based on the results for the 1.6 and 2.1% Cu alloys and the cyclic deformation characteristics for the four different copper alloys, that the effect of DR on the LCF resistance may be much more important for the low copper content alloys which exhibit more

planar slip for the aging condition used. This conclusion is in general agreement with the results of other studies[31,38], which indicated that the effect of grain size on the fatigue properties is dependent upon the slip mode.

The Discontinuity in the Coffin-Manson Plots

A distinct break in the Coffin-Manson plots was found at a value of plastic strain amplitude greater than 1.2% for most of the alloys, regardless of the test environment, as can be seen in Figs. 1.6 to 1.8. Similar findings for aluminum alloys have also been reported by other investigators[4,5,25]. Based on the data obtained from the present study combined with the results in the literature, one may predict that the occurrence of the break will be found in these plots since the fatigue ductility coefficient extrapolated to the low lives from the Coffin-Manson equation markedly exceeds the tensile ductility of materials. For example, the fatigue ductility coefficient for the 1.6% Cu alloy tested in dry air is 205% ($4N_f$ =1) or 110% ($2N_f$ = 1), which is much larger than the tensile ductility of 32% (see Table 1.2 and 1.3). The position of the break point and the magnitude of the slope change are found to be strongly dependent upon the values of ε'_f and -C before the break, i.e., depend on the cyclic deformation behavior. For instance, the 2.1% Cu alloy, which exhibits a more homogeneous deformation, has the break point at higher plastic strain amplitude and less slope change since it has lower values of ε'_f and -C before the break point than those of the other alloys.

The occurrence of a break at high plastic strain amplitudes has been explained by several investigators[4,5,24,25]. One suggestion is that the break is due to a change in the mode of crack propagation from intergranular to transgranular fracture as a function of plastic strain amplitude[24]. An extensive search was made here for any changes in the mode of crack propagation for samples tested at low and high plastic strain amplitudes. However, only transgranular fracture was observed by SEM, despite the magnitude of plastic strain, as can be seen from Fig. 1.16. For the low plastic strain amplitudes below the break point, the fatigue fracture surface exhibited pockets of striations and some areas with a flat featureless pattern, micrograph A in Fig. 1.16. The flat featureless regions may be associated with slip band decohesion resulting from strain localization. The overload region exhibited a dimple pattern indicative of ductile fracture. However, for the high plastic strain amplitudes above the break point, the fatigue fracture surface displayed only dimple rupture, i.e., monotonic fracture patterns, as shown in micrograph B, Fig. 1.16. The fatigue fracture surfaces of the other alloys were of a similar nature. Therefore, a change from intergranular to transgranular does not appear to be the reason for the break. However, on the basis of the changes in fracture surface appearance as a function of plastic strain amplitudes discussed above, this break may be, at least in part, associated with the changes of a brittle-like fatigue fracture at low plastic strain amplitudes to a ductile (monotonic type) fracture at high plastic strain amplitudes.

Another suggestion is that the break is due to a change from localized slip bands to homogeneous slip as a function of plastic

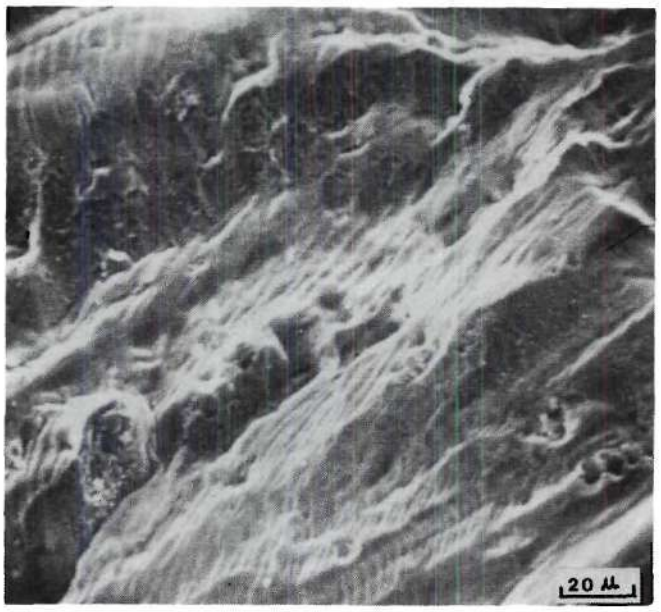

(A)

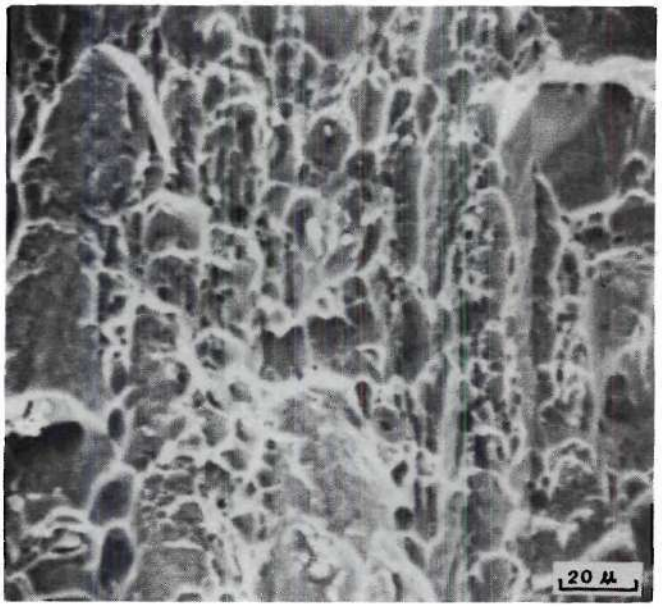

(B)

Figure 1.16. Scanning electron fractographs of the fatigue fracture surfaces for the 1.6% Cu alloy with 30% DR tested in dry air, (A) the plastic strain amplitude below the break point, $\Delta\varepsilon_p/2 = 0.11\%$, $N_f = 2090$ cycles. (B) above the break point, $\Delta\varepsilon_p/2 = 2.61\%$, $N_f = 22$ cycles.

strain amplitude[5,25]. Extensive TEM examination revealed that for the low copper content alloys (< 1.6% Cu) most grains deformed homogeneously over the total strain range studied. However, a few grains showed strain localization (as shown in Figures 1.10 and 1.11). The percentage of grains showing this inhomogeneous slip increased as the strain amplitude decreased. However, the cyclic deformation features were quite uniform for the 2.1% Cu alloy regardless of the magnitude of plastic strain. A change in the degree of homogeneity of deformation does not clearly explain the observed discontinuity in the Coffin-Manson curves.

Thirdly, the break may be due to a change in deformation processes as a function of plastic strain amplitude[4]. For the commercial-type alloys tested over the range of plastic strain amplitudes in this study, cell structures due to cyclic-loading were not found in thin foils by TEM; thus, this mechanism can not apply to this study.

Our results suggest that the break may be due to the difference in frequency of occurrence and to the intensity of slip bands at low and high strain amplitudes. This interpretation is supported by optical observations of the surfaces of the fatigue samples. The density of slip bands and the slip step height increases as the magnitude of plastic strain is increased. Similar changes in slip features as a function of plastic strain amplitude (below and above the break point) were observed in TEM, as mentioned previously. The denser and more intensive slip bands are thought to be related to an early crack initiation and an easy crack propagation along these bands. Both crack initiation and propagation are found predominantly at these bands, regardless of

magnitude of plastic strain, as shown in Fig. 1.12. Based on the findings discussed above, the most logical mechanism for the break which occurred in these plots at $\frac{\Delta\varepsilon_p}{2} > 1.2\%$ is due to the changes from a brittle-like fatigue crack propagation fracture to a ductile (monotonic type) fracture and/or an increase in the density and intensity of slip bands at high plastic strain amplitudes, and/or the considerably smaller values of tensile ductility of the alloy than its fatigue ductility coefficient.

The Cyclic Hardening and Softening Curves

The cyclic hardening and softening curves exhibited significant hardening in the first few cycles, and then reached a saturated condition, afterwards, cyclic softening occurred for most samples especially for tests conducted in dry air. For instance, specimens of 0.01, 1.0 and 1.6% Cu alloys displayed cyclic softening in dry air, but only a few samples displayed cyclic softening in distilled water or in a 3.5% NaCl solution (see Figs. 1.17 to 1.20). However, cyclic softening was exhibited by samples of the 2.1% Cu alloy for all test environments (see Figs. 1.21 and 1.22). It is very important to note that if a sample exhibits cyclic softening, the softening is clearly identified by a gradual decrease of both tensile and compressive stress during cyclic-straining.

When samples of the low copper content alloys (< 1.6% Cu) were tested in distilled water or in a 3.5% NaCl solution, cyclic softening was observed in only a few samples. This is not due to the environmental effect on the cyclic softening processes, but

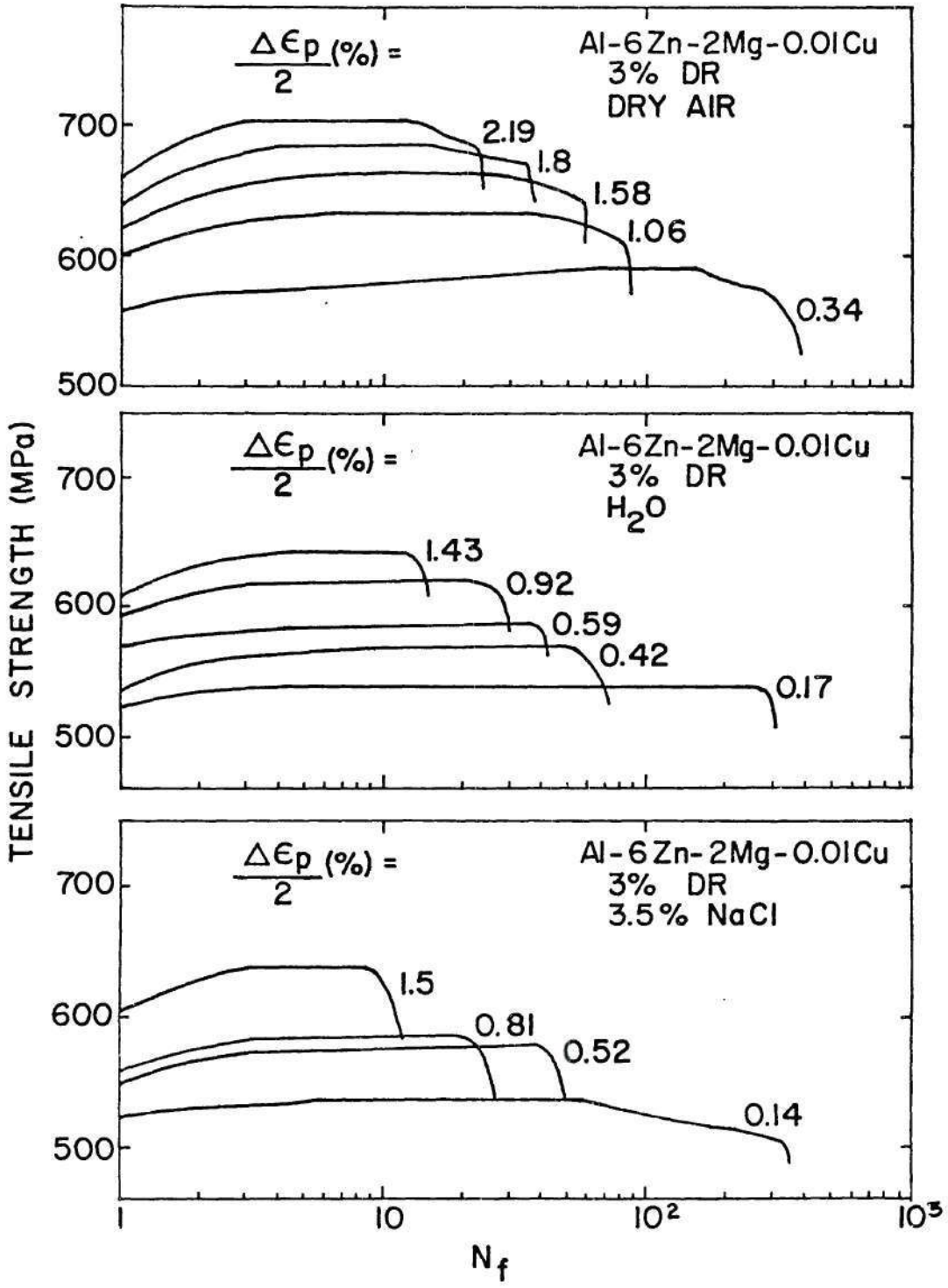

Figure 1.17. Cyclic hardening and softening curves for the 0.01% Cu alloy tested in various environments.

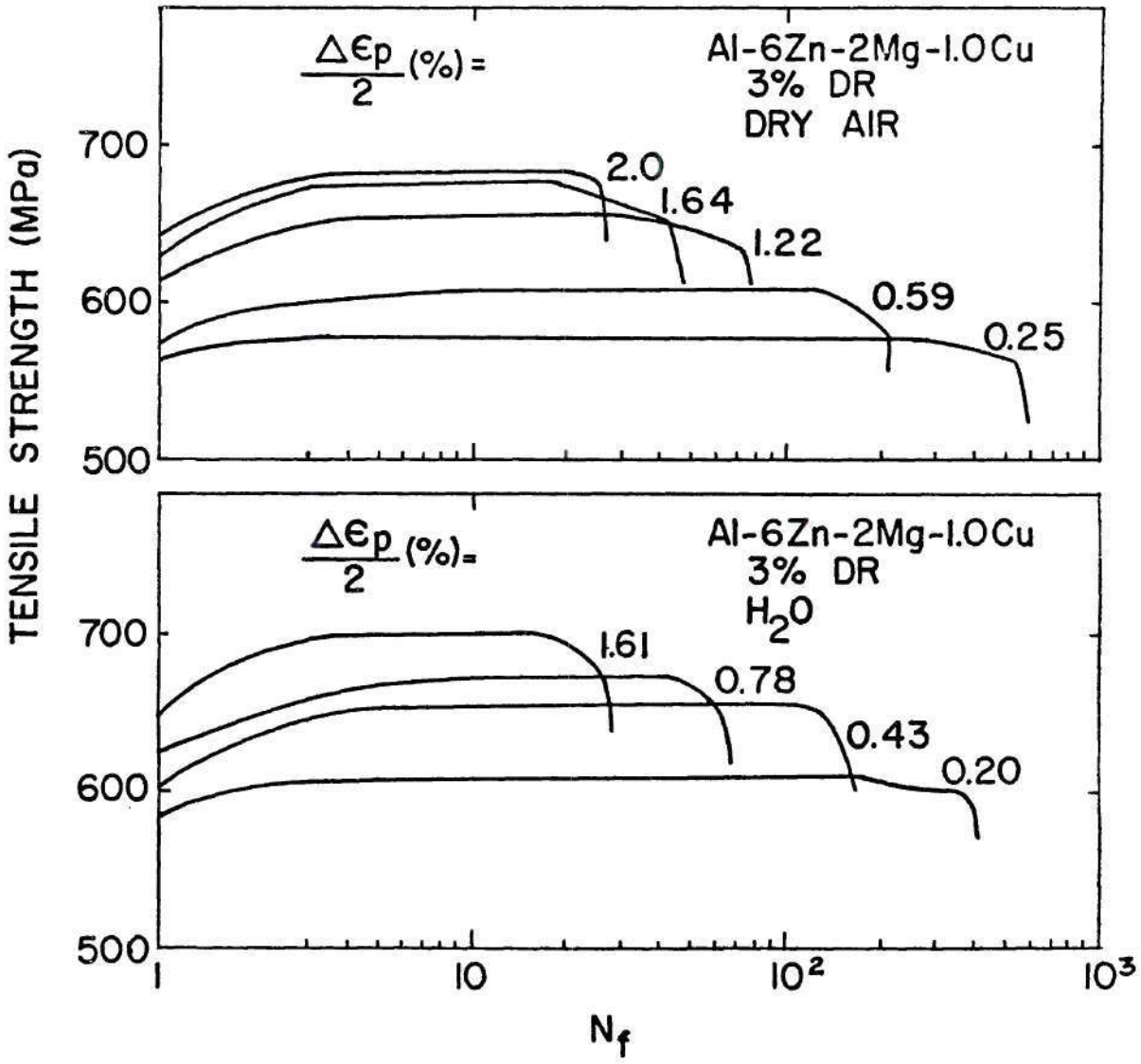

Figure 1.18. Cyclic hardening and softening curves for the 1.0% Cu alloy tested in dry air and distilled water.

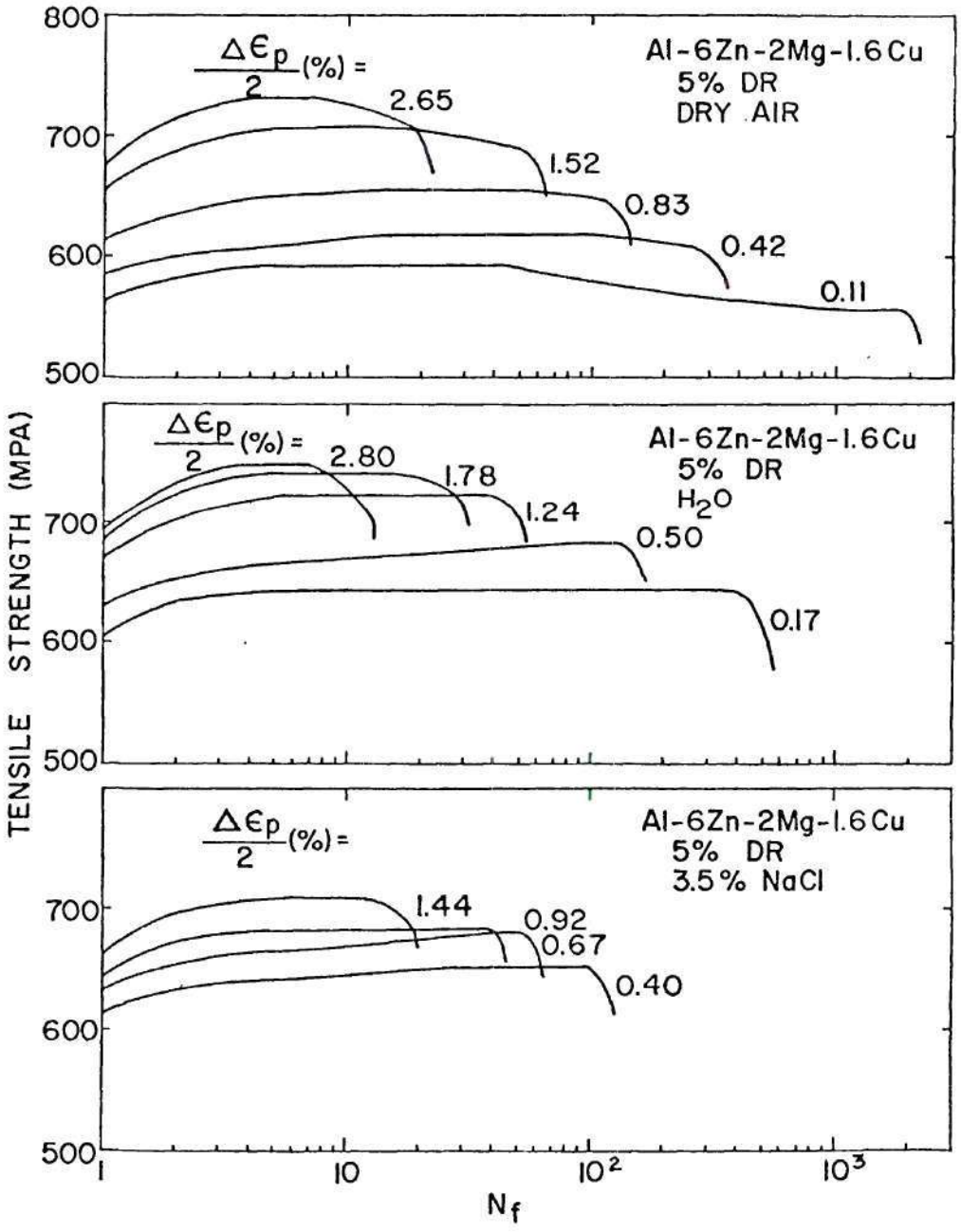

Figure 1.19. Cyclic hardening and softening curves for the 1.6% Cu alloy with 5% DR tested in various environments.

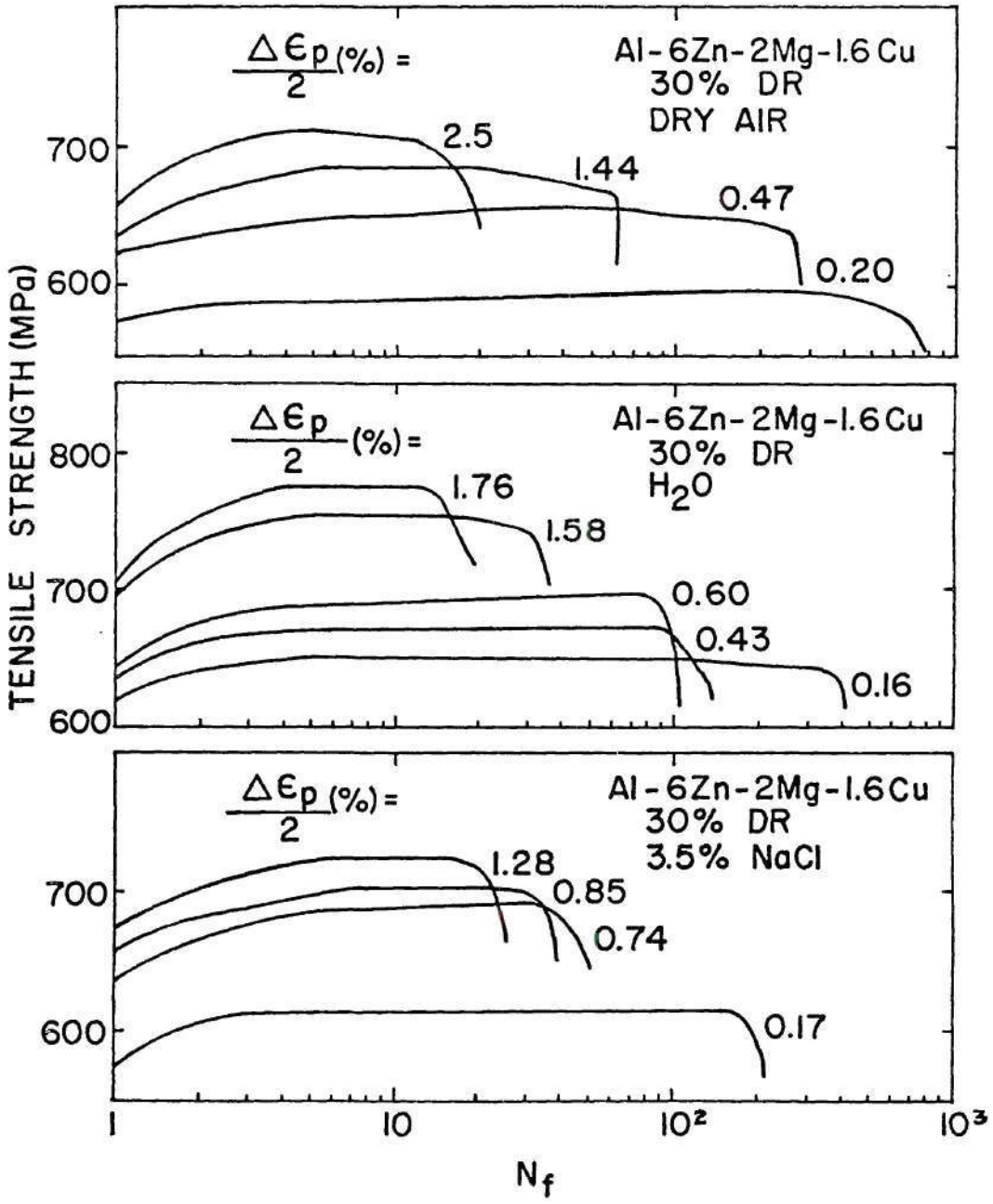

Figure 1.20. Cyclic hardening and softening curves for the 1.6% Cu alloy with 30% DR tested in various environments.

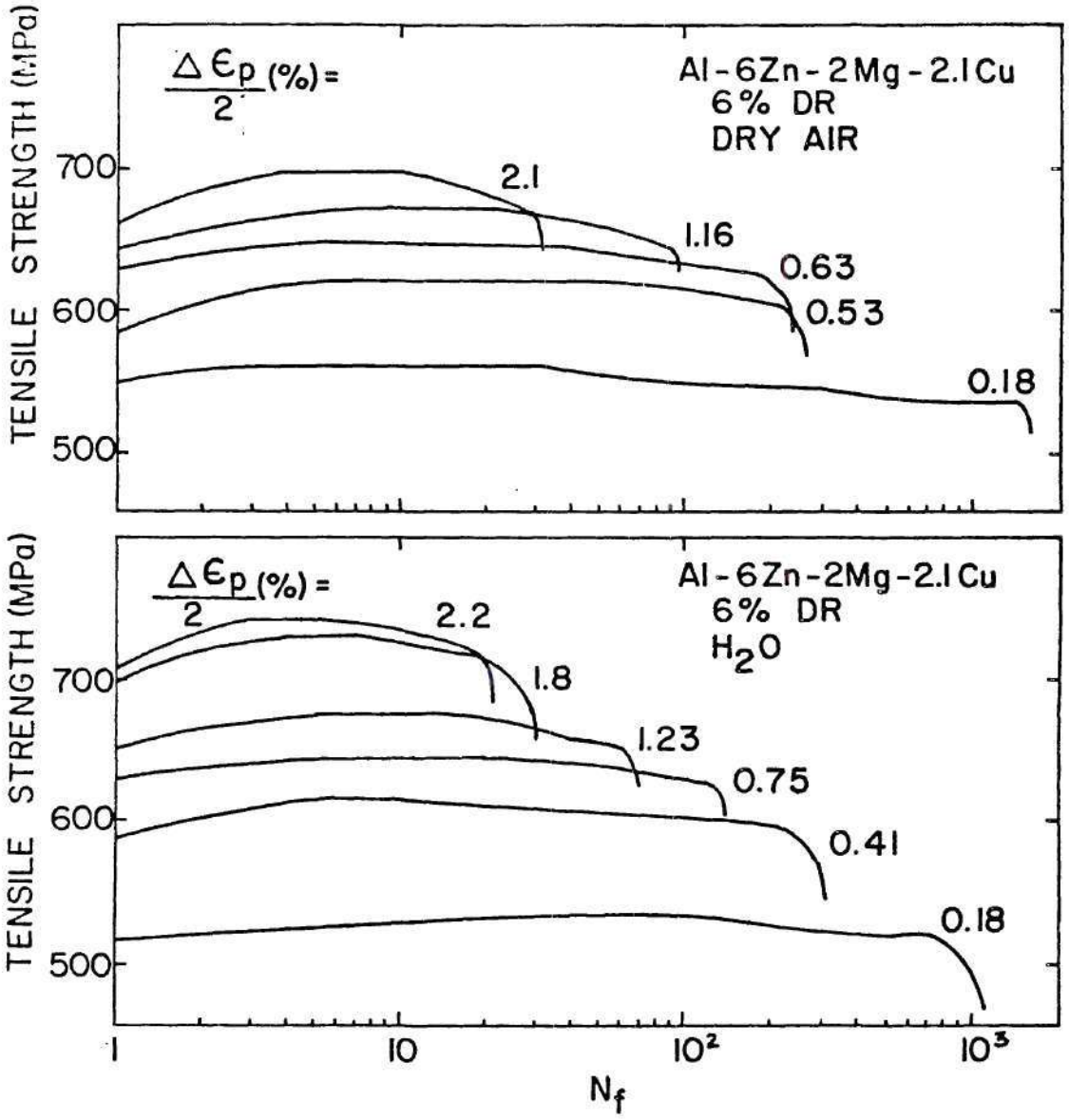

Figure 1.21. Cyclic hardening and softening curves for the 2.1% Cu alloy with 6% DR tested in dry air and distilled water.

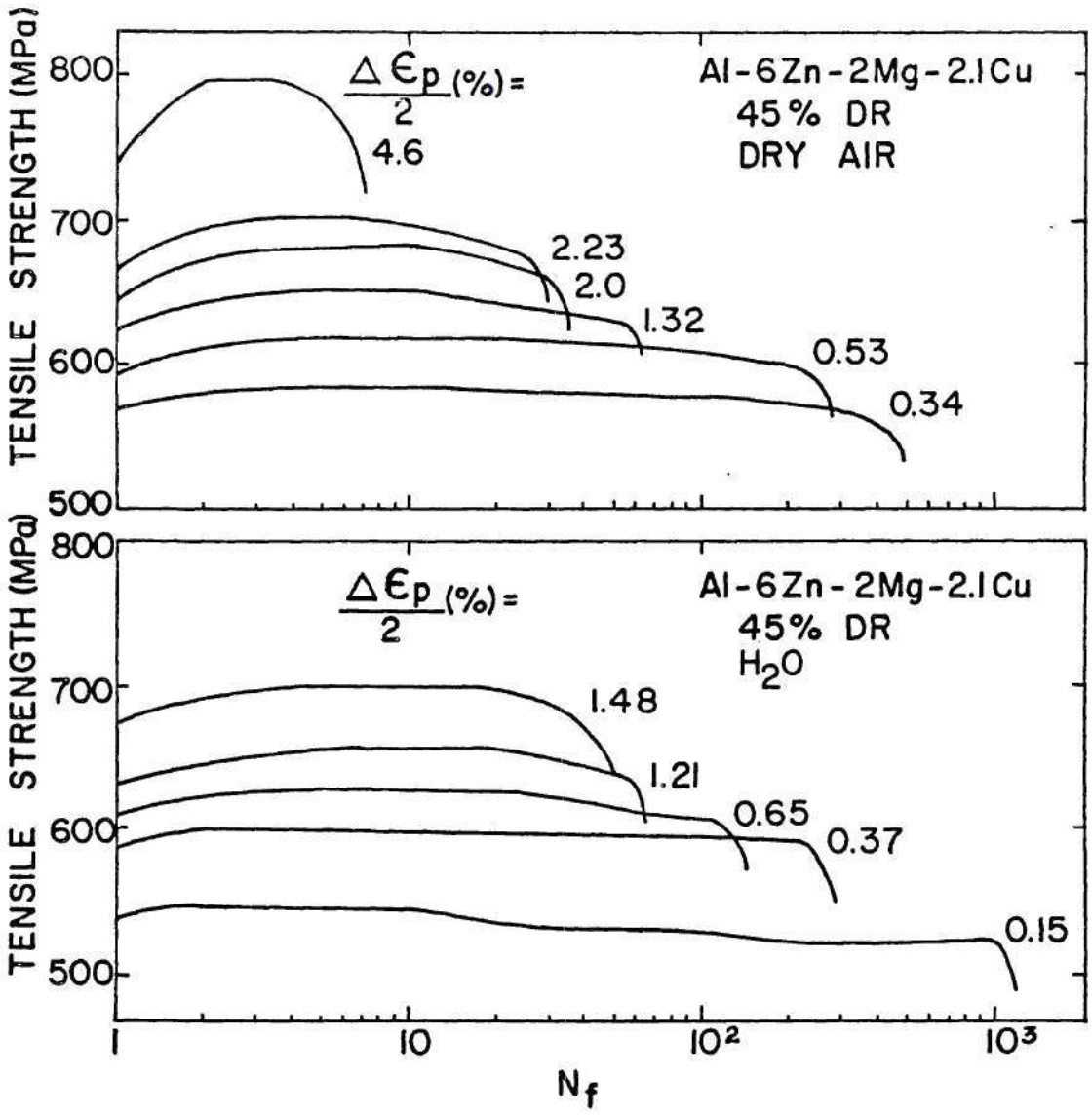

Figure 1.22. Cyclic hardening and softening curves for the 2.1% Cu alloy with 45% DR tested in dry air and distilled water.

due to environment induced cracking prior to softening. This can be seen by comparing the number of cycles for softening in dry air with that for failure in distilled water or in a 3.5% NaCl solution. For example, for the 0.01% Cu alloy, the number of cycles for softening is 25 cycles ($\frac{\Delta\varepsilon_p}{2}$ = 1.58%) in dry air (see Fig. 1.17), but a sample of the same alloy failed at 15 cycles ($\frac{\Delta\varepsilon_p}{2}$ = 1.43%) in distilled water. Thus, cyclic softening was not found in the latter environment. On the other hand, for the 2.1% Cu alloy, fatigue lives of samples were not significantly affected by distilled water, and hence, cyclic softening was observed for the samples tested in both dry air and distilled water, Figs. 1.21 and 1.22. Consequently, cyclic softening observed in this study is a mechanical and not an environmental effect.

Cyclic softening has been observed in a high purity ITMT 7075 alloy[63]. This was attributed to the rearrangement of dislocations introduced by the final deformation. Formally, cyclic softening was always thought to be associated with precipitate resolution during cyclic-loading and/or aging inhomogeneities[27,28]. If assumptions are based on these mechanisms, the magnitude of difficulty for cyclic softening should logically increase with increasing copper content since the extent of homogeneity of deformation and the degree of homogeneity of precipitate distribution are increased as copper content increases. Unfortunately, the test results showed that the number of cycles for softening does not systematically increase with increasing copper content. For instance, samples for the 0.01 and 1.6% Cu alloys were cyclic-

strained in dry air at $\frac{\Delta\varepsilon_p}{2}$ = 1.58 and 1.52% respectively, the 0.01% Cu alloy needed 20 cycles for softening while the 1.6% Cu alloy required 10 cycles (see Figs. 1.17 and 1.19). The other example is that for tests conducted in dry air, a sample of the 1.0% Cu alloy needed 130 cycles ($\frac{\Delta\varepsilon_p}{2}$ = 0.59%) for softening which was more than 50 cycles required for the 2.1% Cu alloy ($\frac{\Delta\varepsilon_p}{2}$ = 0.53%), Figs. 1.19 and 1.22. Presumably, in addition to softening on the localized slip bands[27,64], other factors may be involved in the cyclic softening processes, at least in this study. The occurrence of intensive grain boundary cracking (see Fig. 1.12) in all alloys may play some part in the softening processes since the cracked boundaries will reduce the strength of materials and may also induce dislocation egression. Thus, a large number of dislocations will move through slip bands during the tensile and compressive stroke, resulting in an acceleration of slip band softening. The mutual actions will lead to crack initiation on slip bands and that crack propagation just links up these bands. This explanation is consistent with the findings mentioned previously that crack initiation and propagation predominantly occurred on these slip bands.

The Cyclic Stress-Strain Curves

An important piece of information to be derived from the low cycle fatigue tests is called the cyclic strain hardening exponent, n'. The values of n' for different copper content alloys are shown in Fig. 1.23. One should note that the values of n' increase

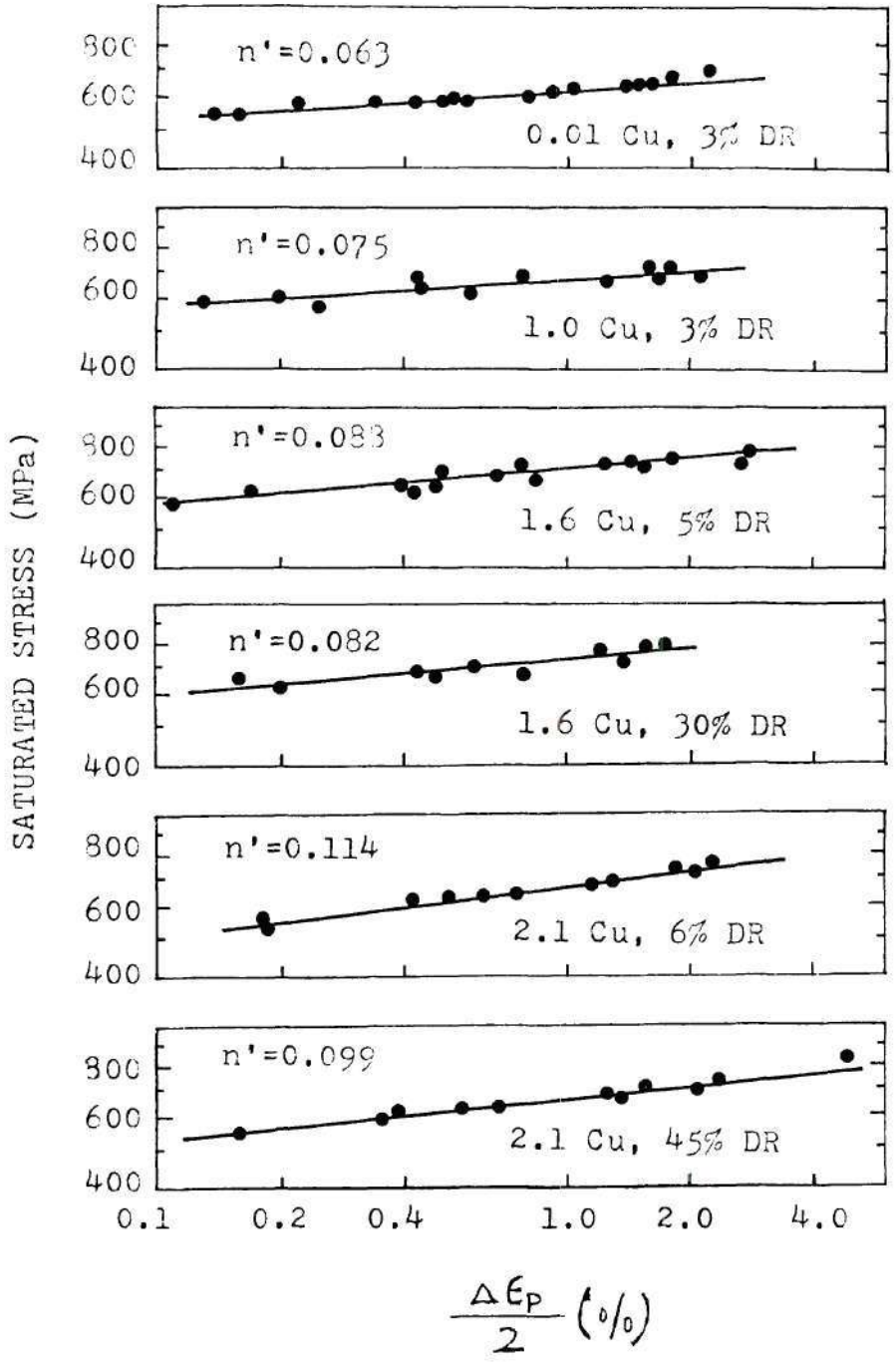

Figure 1.23. Cyclic stress-strain curves for various Al-6Zn-2Mg-xCu aluminum alloys.

with increasing copper content. The finding is in general agreement with the mechanism of work hardening for the precipitation hardenable alloys[19]. The lower copper content alloys contain more easily shearable precipitates resulting in lower values of n' than found for the high copper content alloys. The latter contain more partially coherent and incoherent precipitates which are looped by dislocations, resulting in higher values of n'. Note that for the 1.6 and 2.1% Cu alloys, the lower DR exhibits a higher value of n' than found for the same alloy with high DR. This suggests that the subgrains in the unrecrystallized grains must likely increase the cyclic hardening behavior by increasing the number of slip interactions. In addition, the values of n' can be correlated with the cyclic strain resistance. The cyclic strain resistance for various alloys is found to be directly related to the values of n', i.e., increasing values of n' for these alloys reduces systematically the values of -C. This result is consistent with the conclusion made previously that the improvement of the cyclic strain resistance is due to increased homogeneity of deformation since the higher values of n' reflects an increase in the degree of homogeneous deformation. This finding is also confirmed by Feltner and Beardmore[38] who state that for high cyclic strain resistance, a high value of n' should generally be sought.

The parameter C has been related to n'. Morrow[29] has shown through an energy analysis that this relation can be expressed as

$$C = - \frac{1}{1 + 5n'} \qquad (1.3)$$

Tompkins[65], using a crack growth model based by the crack tip opening displacement obtains the following relation

$$C = -\frac{1}{1 + 2n'} \tag{1.4}$$

The values for C calculated from the test data are given in Table 1.4. The values obtained from the relation given by Morrow are in better agreement with the experimental data than the values obtained from the relation from Tumpkins. It is of interest to note that for the 2.1% Cu alloy, the experimental values and the theoretical predictions from Morrow's equation are almost identical.

Environmental Effect on the LCF Behavior

The LCF resistance of aluminum alloys was considerably affected by the presence of distilled water or a 3.5% NaCl solution as shown in Figs. 1.6 and 1.7. It is very important to note that this trend becomes much more noticeable as copper content decreases. For example, the ratio of the fatigue life for the aluminum alloy in dry air to that in distilled water for $\frac{\Delta\epsilon_p}{2}$ = 1.0% is 4.0, 2.0, 1.7 and 1.2 for 0.01, 1.0, 1.6 and 2.1% Cu alloys, respectively. It is obvious that the environmental sensitivity of these alloys is considerably decreased as the copper content increases from 0.01 to 2.1%. The fatigue life of all aluminum alloys was further decreased when tests were conducted in a 3.5% NaCl solution as can be seen from diagram A of Figs. 1.6 and 1.7.

The environmental effect on the appearance of the fatigue fracture surfaces are shown in Figs. 1.24 and 1.25 for the low and

Table 1.4. Comparison of Experimental Data of C with Various Theoretical Predictions.

Alloy	$-C^*$	n'	$-C = \frac{1}{1 + 5n'}$	$-C = \frac{1}{1 + 2n'}$
0.01 Cu 3% DR	0.82	0.063	0.76	0.89
1.0 Cu 3% DR	0.78	0.075	0.73	0.87
1.6 Cu 30% DR	0.79	0.082	0.71	0.86
1.6 Cu 5% DR	0.77	0.088	0.69	0.85
2.1 Cu 45% DR	0.67	0.099	0.67	0.84
2.1 Cu 6% DR	0.63	0.114	0.64	0.81

*Experimental values before the break point.

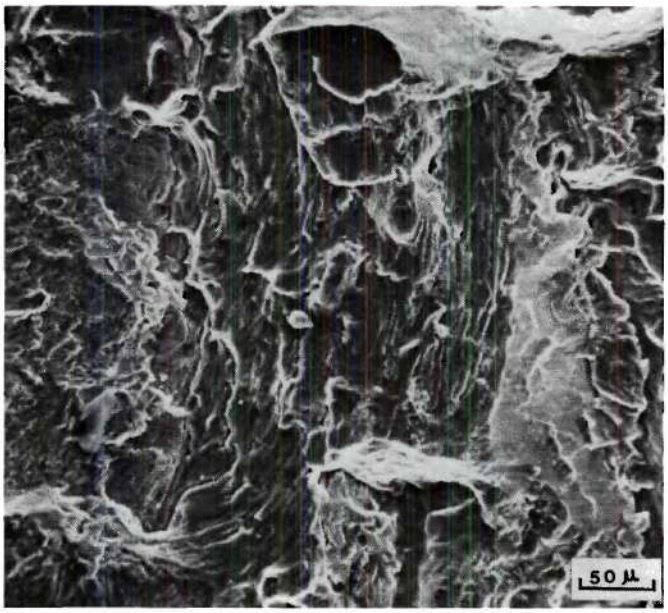

(A) ⟶

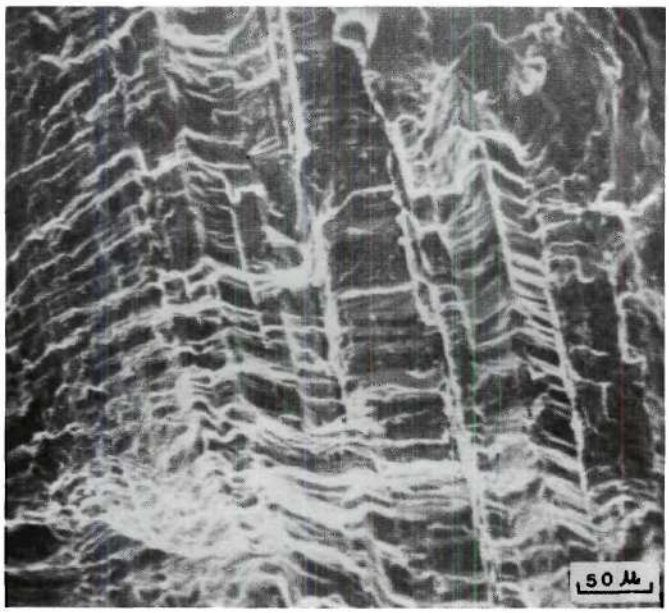

(B) ⟶

Figure 1.24. Scanning electron fractographs of the fatigue fracture surfaces for the 0.01% Cu alloy tested in various environments, (A) in dry air, $\Delta\varepsilon_p/2 = 0.34\%$, $N_f = 384$ cycles, (B) in distilled water, $\Delta\varepsilon_p/2 = 0.18\%$, $N_f = 342$ cycles. Arrow indicates direction of the crack propagation.

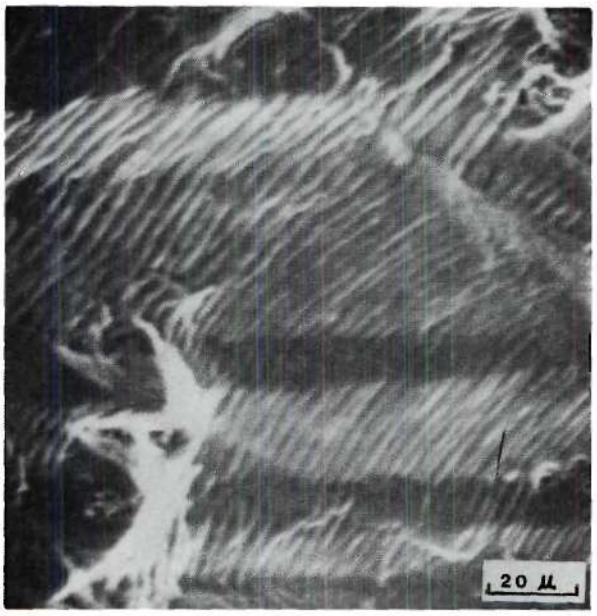

(A)

(B)

Figure 1.25. Scanning electron fractographs of the fatigue fracture surfaces for the 2.1% Cu alloy with 6% DR tested in various environments, (A) and (B) in dry air, $\Delta\varepsilon_p/2$ = 0.18%, N_f = 1562 cycles, (C) in distilled water, $\Delta\varepsilon_p/2$ = 0.18%, N_f = 1054 cycles, (D) in a 3.5% NaCl solution, $\Delta\varepsilon_p/2$ = 0.19%, N_f = 721 cycles.

Continued

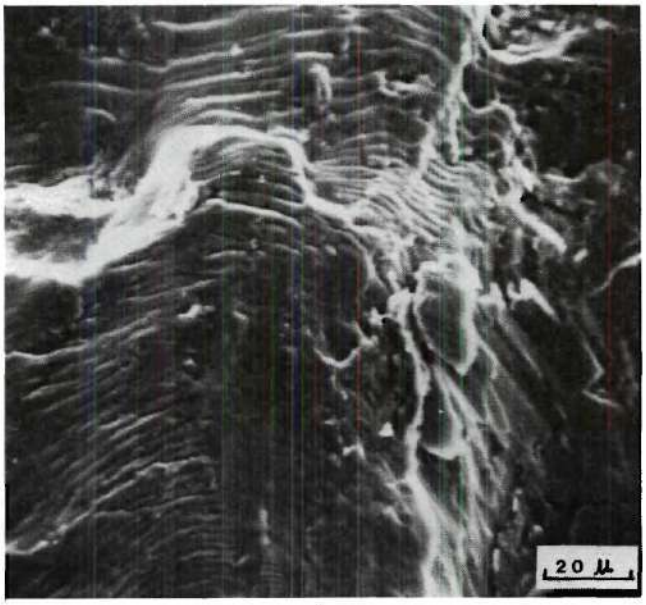

(C)

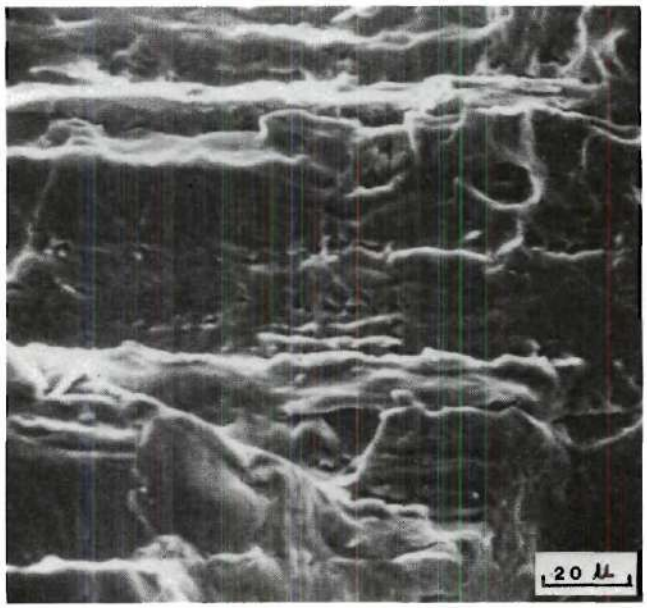

(D)

high copper content alloys. For the 0.01% Cu alloy, a few ductile striations were developed on the fracture surface within the stable fracture region as shown in micrograph A of Fig. 1.24, but a considerable amount of area was featureless in nature. This is likely an indication of only a few slip systems involved in the crack propagation. On the other hand, for tests conducted in distilled water, wide steps and straight cleavage-like markings running normal to the steps were observed, micrograph B. It also indicated that the direction of crack propagation was changed for each step, and the cleavage-like markings are indicative of a brittle fracture. The fracture surface appearance in the overload fracture region exhibited dimple patterns combined with some secondary cracking along the grain boundaries for all samples tested in the three environments. The fracture surface features of the samples tested in a 3.5% NaCl solution were analogous to those tested in distilled water as was the LCF life (small difference in fatigue life between these two environments), diagram A of Fig. 1.6. For samples of the 2.1% Cu alloy tested in dry air, the fracture surface in the stable fracture region exhibited the regular ductile striations, and numerous plateaus and ridges as shown in micrograph A and B of Fig. 1.25. Some clustered S-phase particles were also shown in micrograph B. These features are indicative of ductile fatigue fracture and many slip systems are involved in the crack propagation. In contrast to the 0.01% Cu alloy, the fracture surface features for the 2.1% Cu alloy tested in distilled water, still exhibited the ductile striations combined with local areas of featureless

patterns as shown in micrograph C. The amount of featureless area was larger than that observed in dry air. Micrograph D shows the fracture surface appearance of a sample tested in a 3.5% NaCl solution. The amount of featureless areas was further increased and some straight markings associated with the crack propagation were also developed. The fracture features in the overload fracture region displayed dimple patterns regardless of the test environment. These observations support the previous conclusion that an increase of copper content in 7000-type aluminum alloys decreases environmental sensitivity.

Several mechanisms[40-54] of corrosion fatigue have been proposed to explain the decrease of fatigue resistance in the presence of corrosive environments. These included an anodic dissolution, adsorption process, oxide film effect and hydrogen embrittlement. When the LCF sample is tested in distilled water, the major electrochemical reactions are hydrogen evolution and oxide formation. However oxide formation also occurs in dry air and lowering of the elastic property of oxide layer by water adsorption is considered unlikely to be a large detrimental effect[45]. The observed results of considerable decrease of cyclic strain resistance of aluminum alloys tested in distilled water are suggested that corrosion fatigue of aluminum alloys tested in this environment is primarily due to hydrogen embrittlement. Recent results obtained by other investigators[68] support this interpretation. They suggested that the low diffusivity of hydrogen is counterbalanced by the fact that hydrogen need only be present in the alloy free surface for crack initiation

and in the plastic zone of growing cracks for propagation. The mechanism possibly involves the production of hydrogen atoms at clean surfaces exposed by slip or at the crack tip, during cyclic-loading and the diffusion of hydrogen atoms into the metal. The exact function of hydrogen for embrittlement in aluminum alloys is still unknown, but it may be due to the combined action of high pressure of hydrogen, a decrease of plasticity and a reduction the cohesive strength of the lattice by adsorbed hydrogen. In a 3.5% NaCl solution, the cyclic strain resistance was further decreased. For this case, hydrogen embrittlement still plays an important role as is in distilled water, but anodic dissolution at the slip bands accelerates crack initiation[51-54]. Also, crack propagation is further accelerated by preferential dissolution at the base of the growing crack. Another possible contribution to corrosion fatigue in a 3.5% NaCl solution may be an adsorption process[54,55] which lowers surface energy and changes the fracture processes.

Although the mechanism of corrosion fatigue is not understood exactly, it has been well known that the change of mechanical properties can affect the susceptibility to corrosion fatigue. The present study clearly shows that the environmental sensitivity of 7000-type aluminum alloys can be suppressed by additions of copper. Ample results of the cyclic deformation characteristics for the various alloys discussed previously combined with the recent suggestions of the mechanism of hydrogen embrittlement[66,67] can be used to interpret this phenomenon. An increase in copper content also increases the homogeneity of deformation, resulting in the

decrease of the metal-environment interactions. For the low copper content alloys, especially for the 0.01% Cu alloy for the aging treatment studied, dislocation shearing of coherent precipitates results in planar slip. More hydrogen atoms would be transported by the denser dislocations moving in the localized slip bands, leading to the localized region of high hydrogen concentration than for higher copper alloys. These localized regions of high hydrogen concentration interacting with localized strain at slip bands may lead to an early crack initiation and crack propagation along these slip bands. Therefore, the low copper content alloys are more susceptible to corrosion fatigue.

CHAPTER V

CONCLUSIONS

1. The cyclic strain resistance of 7000-type aluminum alloys generally increases with increasing copper content from 0.01 to 2.1%, regardless of the test environment. Furthermore, this trend is more pronounced for tests conducted in distilled water or in a 3.5% NaCl solution. This improvement is attributed to the increased homogeneity of slip as the copper content increases.
2. For the 1.6 and 2.1% Cu alloys, the cyclic strain resistance is inversely related to the magnitude of the degree of recrystallization (DR) regardless of the test environment. This is attributed to a more uniform cyclic deformation of an alloy with low DR than with high DR.
3. The 2.1% Cu alloy exhibited less sensitivity to the changes in DR. This is due to a smaller difference in the homogeneity of deformation between the alloy with low DR and with high DR.
4. The distinct break point observed in the Coffin-Manson plots at the high plastic strain amplitude (> 1.2%) is interpreted as a change in fracture mode from a brittle-like fatigue fracture at low plastic strain amplitude to a ductile fracture at high plastic strain amplitude and/or an increase of the density and intensity of slip bands at high plastic strain amplitude, and/or the considerably smaller values of tensile ductility of the alloy than its fatigue ductility coefficient.

5. The mechanisms for cyclic softening are possibly associated with the combined actions of slip-band softening and the grain boundary cracking.
6. The cyclic strain hardening exponents increase with increasing copper content as does the cyclic strain resistance of the alloys.
7. The environmental sensitivity of 7000-type alloys decreases with increasing copper content. The higher environmental sensitivity of the low copper content alloys is attributed to the fact that the localized slip bands considerably intensify the metal-environment interactions.
8. Low cycle corrosion fatigue of these alloys tested in distilled water is primarily due to hydrogen embrittlement phenomenon; in a 3.5% NaCl solution, hydrogen embrittlement still plays an important role but the preferential dissolution and/or an adsorption process may also have a detrimental effect.

PART II

CORROSION FATIGUE CRACK PROPAGATION OF HIGH STRENGTH 7000-TYPE ALUMINUM ALLOYS

CHAPTER I

INTRODUCTION

In PART I, the effect of copper content and DR on the low cycle corrosion fatigue behavior in dry air, distilled water and a 3.5% NaCl solution was investigated. Experimental results clearly demonstrated that the cyclic strain resistance of the four different copper content alloys increased with increasing copper content, regardless of the test environment, and this trend became most noticeable when the tests were conducted in distilled or in a 3.5% NaCl solution. On the other hand, the cyclic strain resistance of the 1.6 and 2.1% Cu content alloys was inversely related to the magnitude of DR. In PART II, the same alloys are used to study the effect of these two parameters on the corrosion fatigue crack propagation in dry air, distilled water and a 3.5% NaCl solution.

Recent investigations have been directed towards corrosion fatigue crack growth rate studies, since materials may contain inherent flaws associated with their metallurgy or processing. The useful life of structures containing such defects is thus controlled mostly by the corrosion fatigue crack growth rates because most of these structures are exposed to a corrosive environment and undergo cyclic loading. Corrosion fatigue crack propagation behavior is very important to design philosophy and a large amount of research has been performed to improve the resistance of materials to FCP.

However, considerable inconsistencies still exist since the material parameters controlling FCP behavior are not well understood. Some workers suggest that the FCGR of many commercial aluminum alloys with different aging treatments are almost identical[2,69] and conclude that the FCP behavior is independent of the microstructure and composition of alloys. On the other hand, others indicate that the crack growth rates are affected by the microstructure[7], chemical composition and aging treatments[1,3] only if these parameters markedly influence the slip character. The purpose of this study is to determine which parameters are important to the FCP resistance when the tests are conducted in dry air, distilled water and a 3.5% NaCl solution. This will be achieved by systematically investigating the effect of copper content and microstructural features such as DR on the FCGR of Al-6Zn-2Mg-xCu type aluminum alloys.

CHAPTER II

REVIEW OF THE LITERATURE

Fatigue Crack Propagation Behavior

The most significant features of stage II crack propagation are twofold: (1) it takes place in an overall direction perpendicular to that of the tensile stress, and (2) the crack-tip deformation leaves characteristic striations on the fracture surface. Each striation is thought to be associated with one stress cycle. Laird[32] has conducted an extensive study of the profiles of striations on the fracture surfaces by means of replicating the fracture surfaces and then examining the replicas by TEM. The mechanism of crack propagation deduced from this study is now called "the repetitive blunting and re-sharpening processes." Meyn[70] was the first to show that fatigue striations were not formed when the FCP test was performed in a vacuum. Hence, Pelloux[71] proposed that the mechanism of crack extension was an alternating shear process. He explained that the absence of striations in vacuum was due to a completely reversed slip process. On the other hand, the slip decohesion mechanism has been proposed by Tomkins and Biggs[72], and then supported and modified by Wanhill[73]. Wanhill examined the fracture surface by means of a fractographic method and also observed, by TEM, dislocation features on thin foils cut just below the fracture surface. He concluded that, under a small tensile load, plastic flow occurs on the 45° planes and a new crack surface is formed by "flow-off" (combination of

shear and tensile decohesion) to produce a blunted crack tip with ears. Further straining in tension caused "flow-off" to stop at the edges of the initial flow planes due to considerable strain hardening. Fracture occurs at the center of the blunted crack, followed by further relaxation and crack growth on new flow bands. This procedure is repeated until the maximum tensile strain is reached. Load reversal causes the flow bands to operate in the opposite direction, more efficiently nearer the crack tip. Repetition of the entire process results in striations. In this model, when the FCP test is performed in a vacuum, considerable crack blunting and efficient slip reversal results in very small crack extension and cyclic crack growth markings with very shallow trenches.

Bowles and Broek[74] observed dislocation features from the thin foils containing the fracture surface by means of TEM, and then suggested that the mechanism of striation formation is that cyclic-loading results in the dense dislocation structures in the peaks and leading edges of the striations. Alternatively, Neumann[75] proposed that crack propagation is a coarse slip process, i.e., the interaction of coarse slip bands on the different planes (making an angle of 45° with respect to the crack propagation direction) during the tensile and compressive stroke leads to the formation of the crack surface.

The fatigue striations can be divided into ductile striations and brittle striations for Al-Zn-Mg alloys[44]. The ductile striations appear as smooth, almost featureless rumplings of the surface, while the brittle striations are wider, flatter than the ductile type, with

long tongue-like features and a river pattern normal to the crack front. A plane strain condition, low frequency of cycling and a low stress intensity range, combined with the most important parameter - a corrosive environment, favor the formation of brittle striations. The mechanism for the occurrence of brittle striations in the presence of a corrosive environment may be due to dislocation pinning[44,68], adsorption processes[54,55], anodic dissolution[52] and/or hydrogen embrittlement[46,47,68].

Effect of Microstructure on FCP

Although many studies have been done to determine the effect of microstructure on the fatigue properties, its influence on FCP is still uncertain. In order to study the effect of inclusions, El-Soudani and Pelloux[8] used aluminum alloys with markedly different inclusion contents. Their results showed that the effect of the particles depended on the size of the plastic zone at the crack tip. Large values of ΔK (stress intensity range) will create voids around the particles, and thus the inclusion content increases the FCGR only when $\Delta K > 20$ MPam$^{\frac{1}{2}}$. However, when $\Delta K < 10$ MPam$^{\frac{1}{2}}$, the FCGR of alloys with higher inclusion content were reduced. The results of Truckner, et al.[76] at Alcoa support this finding. However, Albrecht, et. al[78] have indicated that if the alloy contains hard, second phase particles, voids are formed at the particles during plastic deformation and the crack propagates by void coalescence. Thus, the FCGR is accelerated by the presence of second phase particles when $\Delta K > 12$ MPam$^{\frac{1}{2}}$ rather than 20 MPam$^{\frac{1}{2}}$. Some disagreement with the above

results is found in the work of Glassman and McEvily[77] who observed that a large number of inclusions may, in fact, slow down the FCGR by causing it to follow a more devious path. It is obvious from these results that the effect of inclusions depends on the magnitude of ΔK, interparticle spacing, volume fraction of inclusions, individual or clustered particles, particle distribution and the character of the matrix.

The influence of grain size is still a source of disagreement. Thompson and Backofen[39] showed that for stage I FCP, the FCGR of alloys with low SFE was dependent upon the grain size; while the FCGR of alloys with high SFE was independent of the grain size since cross slip is easy and a dislocation cell structure is formed during cyclic-loading. However, other investigators[80,81] found that grain size and prefered orientation had a minor effect on the FCGR in spite of the magnitude of the SFE. For the case of commercial aluminum alloys, considerable evidence[1,2,76] indicated that the FCGR is insensitive to grain size. On the other hand, Rosenfield, et al.[7] claim that grain size, DR and grain shape of 7000-type aluminum alloys do affect crack propagation, agreeing with the results of another investigator[82] who showed that the microcrack growth rate around the grain boundaries is about three times smaller than that in the interior of grains. The implication is that grain boundaries represent bigger obstacles to crack growth than the grain interior and that a sufficiently large number of boundaries in the path of the crack will reduce the growth rates. It is apparent, then, that the effect of grain size on the FCGR is not only dependent upon the type

of deformation mode and character of metal matrix, but also upon the mode of crack propagation (intergranular or transgranular).

There has been a considerable amount of discussion in the literature on the relative effect of alloy composition and heat treatment of aluminum alloys on the FCGR[1,3,50,78]. These data revealed that the chemical composition or aging treatment had a significant effect on the crack growth rates. The lower copper content alloys of the 7000-type aluminum alloys or alloys aged below peak hardness seem to be more environmentally sensitive. Recently, several investigators[2,67] have measured the FCGR of many aluminum alloys with different chemical compositions and some of them with different aging treatments. Their results implied that the FCGR was not significantly different for the alloys investigated, and thus crack propagation was insensitive to alloy chemistry and microstructure. The influence of environment on fatigue properties has been described in Part I, therefore will not be discussed further here.

Dislocation Structures Near the Fatigue Crack Tip

It has been considered that substructure formation around the crack tip may play some role in FCP. This suggestion has been supported by the following results which were obtained through TEM and X-ray microbeam techniques[84-87] to analyze the change of microstructure around the crack tip. It was found that in pure aluminum and its alloys, there existed a plastic zone in which a well-defined substructure was formed. The cell size was about 1 to 4 μm and the average misorientation between cells was approximately 1 to 4°,

but both values were dependent upon the distance from the crack tip. Therefore, it is suggested that cell walls may be a preferred path for FCP or that FCP is simply the linking of many fine microcracks formed along the cell walls. Several workers[88,89] showed that FCP along cell walls were observed directly from thin foils containing the crack tip by means of TEM. Gardner, et al.[90] also provided some direct evidence that microcracks initiated at cell walls in beryllium and iron single crystals in the monotonic tests. This direct evidence can be used to explain the crack propagation along cell walls proposed previously. These observations suggest that the formation of voids along cell walls is easier than within subgrains. The coalescence of these voids would result in FCP along the cell walls. However, Wilkins and Smith[85] did not find voids along the cell walls, nor fatigue crack propagation along the cell walls in an Al-0.5 Mg alloy. On the other hand, some conflict with the above results is shown by Awatani, et al. for iron[91] and for stainless steel[92]. These two alloys represent the high and the low SFE materials. However, both alloys showed that a high density of tangle dislocations was formed in the immediate vicinity of the crack tip and following this are cell structures, i.e. cell structures were not found in the immediate vicinity of the crack-tip. It was then suggested that cell walls may not play a role in the FCP behavior.

Equations of the FCGR

Numerous FCP equations have been derived theoretically and experimentally. A recent review of these equations has been given

by Stoloff and Duquette[93]. The most popular equation, for comparing the FCP resistance of various materials, is the Paris equation[94]

$$\frac{da}{dN} = A(\Delta K)^m \tag{2.1}$$

where da/dN is the FCGR per cycle, A and m are material constants. ΔK is the stress intensity range ($K_{max.}-K_{min.}$), where K is the stress intensity factor. Equations used to calculate K for various specimen configurations have been documented[95]. The stress intensity factor equation for the wedge opening loading (WOL) type specimens can be presented in the form

$$K_I = \frac{P}{BW^{\frac{1}{2}}} f\left(\frac{a}{W}\right) \tag{2.2}$$

where P is the applied load, B is the specimen thickness, W is the specimen width and a is the crack length. For a given ratio of specimen height H, to specimen width W, the function f(a/W) can be expressed in a polynomial form. For a specimen having H/W = 1.2, f(a/W) can be represented as

$$f\left(\frac{a}{W}\right) = 29.6\left(\frac{a}{W}\right)^{0.5} - 185.5\left(\frac{a}{W}\right)^{1.5} + 655.7\left(\frac{a}{W}\right)^{2.5} - 1017\left(\frac{a}{W}\right)^{3.5} + 638.9\left(\frac{a}{W}\right)^{4.5} \tag{2.3}$$

The polynomial is valid for a/W between 0.3 and 0.7.

When the experimental data for the FCP are plotted as da/dN vs ΔK, the FCP behavior for metals can be divided into three regions, as shown in Fig. 2.1[96]. The behavior in region I exhibits a "fatigue-

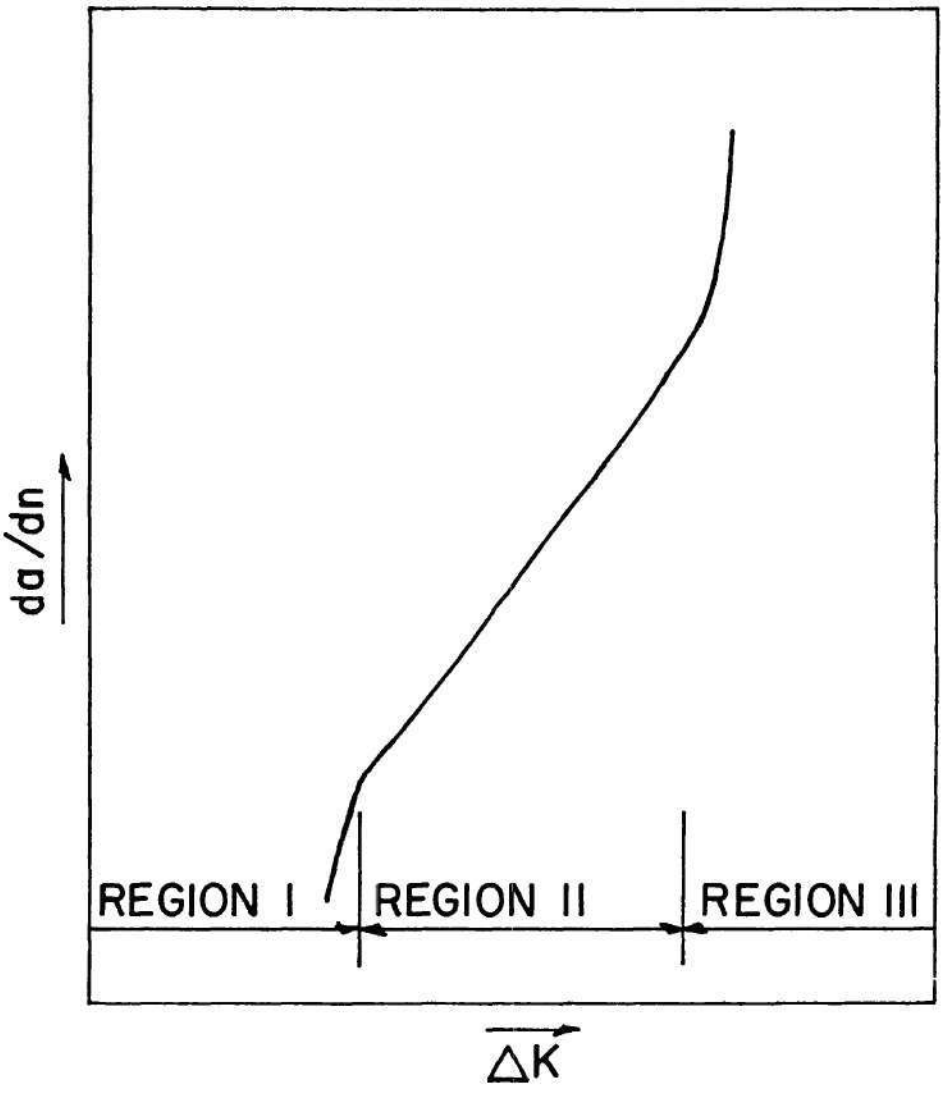

Figure 2.1. Schematic representation of fatigue crack growth of metals.

threshold" cyclic stress intensity factor fluctuation, ΔK_{th}, below which cracks do not propagate under cyclic loading. Region II represents the FCP behavior above ΔK_{th} which can be represented by the Paris equation. In region III the FCGR per cycle is higher than predicted for region II. The region II-III transition has been attributed to a change from plane strain to the plane stress condition.

Tompkins[65] has considered the stage II crack propagation process as a form of plastic decohesion at the crack tip. He has taken into account the cyclic strain hardening characteristics of materials and derived a crack propagation equation for a constant stress amplitude condition which is represented as

$$\frac{da}{dN} = \frac{\pi^2}{32} \frac{\Delta\sigma^{\frac{2n'+1}{n'}}}{k'^{\frac{1}{n'}} \sigma_y'^2} \cdot a \qquad (2.4)$$

where σ_y' is a cyclic flow stress, n' and K' are the cyclic strain hardening exponent and coefficient respectively, $\Delta\sigma$ is the applied stress range, and a is the crack length. The most interesting parameter in this equation is n'. If other parameters, such as σ_y' and K' are constant, a decrease of n' will reduce the FCGR, da/dN. Clearly, n, if this equation is true, emerges as an important parameter which could be used to control FCP resistance.

Majumder and Morrow[97] have derived a crack propagation equation on the assumption that the crack tip radius is blunted to the value of the crack tip opening displacement. This results in the exponent m in the Paris equation being equal to two. The

coefficient, A, is defined as a function of the LCF properties of the materials only. If the additional assumption is made that each metal has a microstructure size, ρ', below which continuum mechanics solutions are not applicable, the coefficient, A, is also found to be a function of ΔK. Chakrabortty[98] has modified the equation of Majumdar and Morrow by considering the entire strain field and using the ρ' parameter to represent the average distance between barriers to slip. His equation is presented as

$$\frac{da}{dN} = 4\rho' \, (2\varepsilon'_f)^{\frac{1}{c}} \sum_{n=1}^{\infty} \left[\int_{x=r+(n-1)\rho'}^{x=r+n\rho'} x^q \Delta\varepsilon_p(x)\,dx \Big/ \int_{x=r+(n-1)\rho'}^{x=r+n\rho'} x^q \, dx \right]^{-\frac{1}{c}} \tag{2.5}$$

where $\Delta\varepsilon_p(x)$ and X are related as

$$X = \frac{\Delta K^2}{(1+n')\pi K' E} \cdot \frac{1}{[\Delta\varepsilon_p(x)]^{n'+1} + \frac{k'}{E}\,[\Delta\varepsilon_p(x)]^{2n'}}$$

and $\Delta\sigma = k'(\Delta\varepsilon_p)^{n'}$

and $r = \frac{COD}{2}$, and $q = 0.5$

where C and ε'_f are the fatigue ductility exponent and coefficient respectively, and COD is the crack opening displacement, q is parabolic averaging exponent. Other symbols have been defined previously.

CHAPTER III

EXPERIMENTAL PROCEDURES

The chemical composition of the four 7000-type alloys, their manufacturing processes for producing different DR, the methods for determining the DR and the subgrain size measurement have been described in PART I. Each alloy has been prepared to show four different DR, but only the minimum and the maximum DR were chosen to study the effect of DR on the FCP resistance. Alloys with four different copper contents, but with almost identical grain structures, were chosen to study the effect of copper content on the FCGR. The FCP tests were conducted in dry air, distilled water and a 3.5% NaCl solution. A plexiglass tube with dimensions of 1.0 inch diameter and 5.5 inch long was sealed to the sample as an environment chamber. The solution was not circulated in this study.

A wedge-opening-loading (WOL)-type compact specimen was employed to measure the FCGR. The configuration of the test sample is illustrated in Fig. 2.2. The samples were approximately 7.4 mm thick and had an H/W ratio of 1.2. The direction of crack propagation was parallel to the longitudinal orientation, i.e., T-L orientation, where L = longitudinal and T = long transverse. (The first letter indicates the direction of applied stress, and the second letter indicates the direction of crack propagation.) A MTS system was employed for the FCP tests, cycling at a frequency of 10 Hz. All

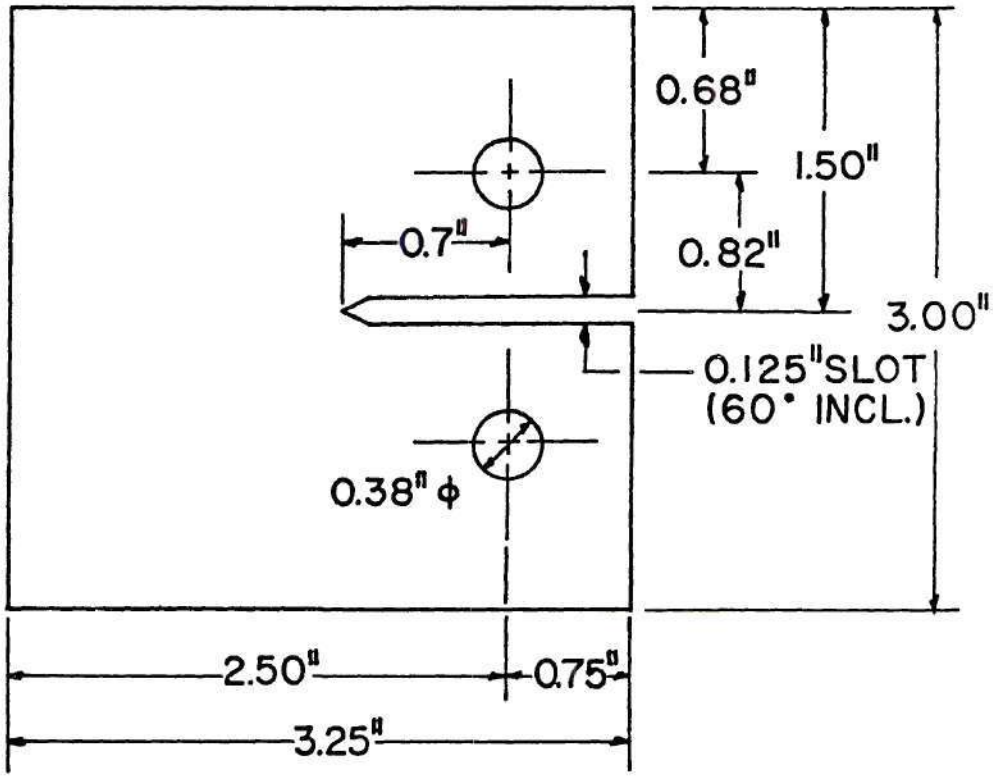

(A)

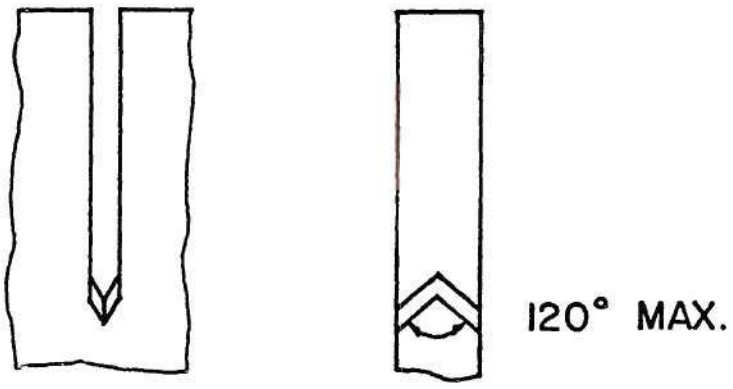

(B)

Figure 2.2. (A) The WOL-type compact specimen, and (B) chevron notch crack starter.

tests were conducted with a stress ratio of R = 0.1. The loading wave form for all tests was sinusoidal. The crack length was measured with a travelling microscope at 10x magnification to an accuracy of 0.1 mm. The secant method[99] was used to calculate the crack growth rate.

The specimen was first pre-cracked at a high stress intensity range (ΔK = 15 $MPam^{\frac{1}{2}}$) to produce an initial crack, and then the ΔK level was gradually reduced step by step until it was close to the intended ΔK level for starting the FCP measurement. The ΔK range chosen in this study was 5 to 15 $MPam^{\frac{1}{2}}$ and a a/W ratio between 3.2 and 6.5 was chosen for the FCP measurement. Data obtained from the tests were presented on log-log coordinates in terms of crack growth rate (da/dN) as a function of the stress intensity range (ΔK). The fracture surfaces of selected FCP specimens were examined by SEM. In an attempt to characterize the fatigue damage that occurred in the plastic zone, thin foils were sectioned from positions adjacent to the fracture surface containing the reversed plastic zone and were examined by TEM. The preparation of thin foils has been described in PART I.

CHAPTER IV

EXPERIMENTAL RESULTS AND DISCUSSION

Microstructural Examination

The size of subgrains in the unrecrystallized grains, precipitation features and the unrecrystallized grain size, for each alloy, have been described in PART I. Four different DR of each alloy (0.01, 1.0 1.6 and 2.1% Cu) have been determined and shown in Table 2.1, along with the fracture toughness of materials. As is apparent from the table, for each alloy only the minimum and the maximum DR showed a large difference, and hence were chosen for investigating the effect of DR on the FCP resistance. Four different copper content alloys with the minimum DR were selected for studying the effect of the copper content on the FCGR since they showed almost identical microstructures, as discussed in PART I. It is also obvious from this table that the DR of various alloys increases with increasing copper content at the same treatment, and the fracture toughness also increases with increasing copper content up to 1.6%, but only a slight difference exists between the 1.0 and 1.6% Cu alloys. However, the 2.1% Cu alloy exhibits a lower toughness which is attributed to the presence of the S-phase (Al_2CuMg) particles in this alloy. This explanation is strongly supported by the results of examining the overload fracture surfaces with SEM which show that voids are created around the clustered particles, as seen in

Table 2.1 Degree of Recrystallization and Fracture Toughness of Aluminum Alloys.

Alloy		DR (%)		Fracture Toughness ($MPam^{\frac{1}{2}}$)* T-L Orientation	
		L-T Section	T-S Section	Pop-in	Maximum
0.01Cu	1-1	5	5	-	49.8
	1-2	10	9		
	1-3	10	11		
	1-4	18	16	-	48.7
1.0Cu	2-1	7	8	50.8	57.6
	2-2	8	10		
	2-3	11	10		
	2-4	31	33	55.7	58.2
1.6Cu	3-1	9	9	51.7	57.6
	3-2	12	10		
	3-3	25	21		
	3-4	49	50	50.8	58.6
2.1Cu	4-1	12	14	42.4	46.8
	4-2	24	26		
	4-3	28	26		
	4-4	69	65	43.9	47.4

*1. The magnitude of fracture toughness at pop-in is K_Q value (0.29 inch thick plate), K_Q values for the 0.01% Cu alloy are the maximum values of toughness.

2. These values obtained by testing samples after finishing crack growth measurements.

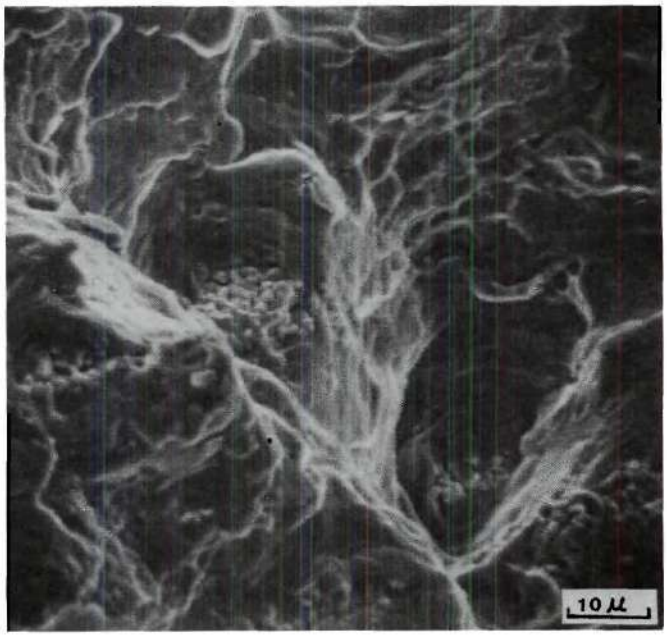

Figure 2.3. Scanning electron micrograph of the overload fracture surface for the 2.1% Cu alloy with 12% DR. Note the clustered particles and voids created around these particles.

Figure 2.3. The presence of S-phase particles for similar alloys also has been found by other investigators[8,76] and the volume fraction of these particles is about 1.0%. Over the range of DR prepared in this study, it appears that the DR of the alloy has a negligible effect on fracture toughness. This result seemingly contradicts those previously reported by Rosenfield, et al.[7] who indicated that aluminum alloys with high DR have lower toughness values. However, they controlled the DR of alloys by two different homogenization practices - a high temperature and long homogenization time, and a low temperature and short homogenization time. Different homogenization practices not only change DR but also change the particle features. The former practice increases both DR and particle size, and thus the lower values of fracture toughness of aluminum alloys with higher DR in their study are probably due to the presence of coarse particles.

Figure 2.4 illustrates that the DR varies significantly with the distance from the plate surfaces, and near the surfaces of the plate, a higher DR is obtained. Note that the DR is not symmetrical with respect to the center of the plate. High DR occurred in the area near the surfaces of the plate due to the fact that a larger amount of strain energy is introduced into the area close to the plate surfaces during the rolling process. This provides a larger driving force for recrystallization to occur during the subsequent solution treatment. Typical microstructural variations with distance from the surface are shown in Figure 2.5 for the 2.1% Cu alloy with 69% DR. Picture A is a optical micrograph near the plate surface,

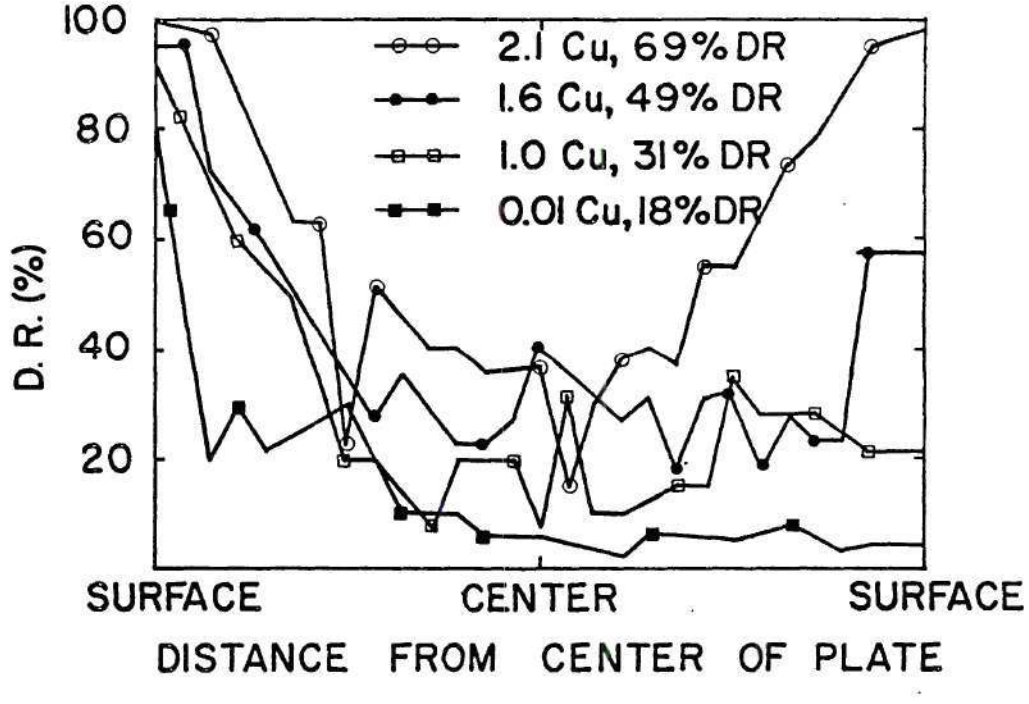

Figure 2.4. The variation of DR with respect to the distance from the center of plates (7.4 mm thick) for the four different copper content alloys with maximum DR.

showing almost complete recrystallization, but some small subgrains in several local areas are clearly observed. Picture B is a micrograph of an area 2.2 mm from the plate surface, showing a partially recrystallized grain structures with the dark areas representing the unrecrystallized grains. Subgrain features for an alloy with the minimum DR also vary with distance from the plate surface. Figure 2.6 is an example for the 2.1% Cu alloy with 12% DR. Picture A shows the subgrain structures near the plate surface, and that the subgrain boundaries are completely etched out by the HNO_3 solution. Picture B shows the microstructure of an area 3 mm from the plate surface. Some subgrain boundaries are also etched out and the straight line markings, shown in the picture, correspond to the unrecrystallized grain boundaries.

Observation of Crack Path and Fracture Surface Appearance

As described in the experimental procedures, the FCP direction was parallel to the rolling direction and the load was applied parallel to the long transvese direction (T-L orientation). During FCP measurements, much attention was paid to observe crack path features for correlation with the crack growth rate, $\frac{da}{dN}$. The relationship between these two parameters is presented in Figure 2.7. Type I crack path is a mixture of the relatively straight crack and a short zig-zag crack (a crack grows on a slip plane for a short distance and then jumps to another), and the crack growth rate of this type is the fastest one. Type II crack path is also a kind of zig-zag, but a crack grows on a slip plane for a longer distance than type I before

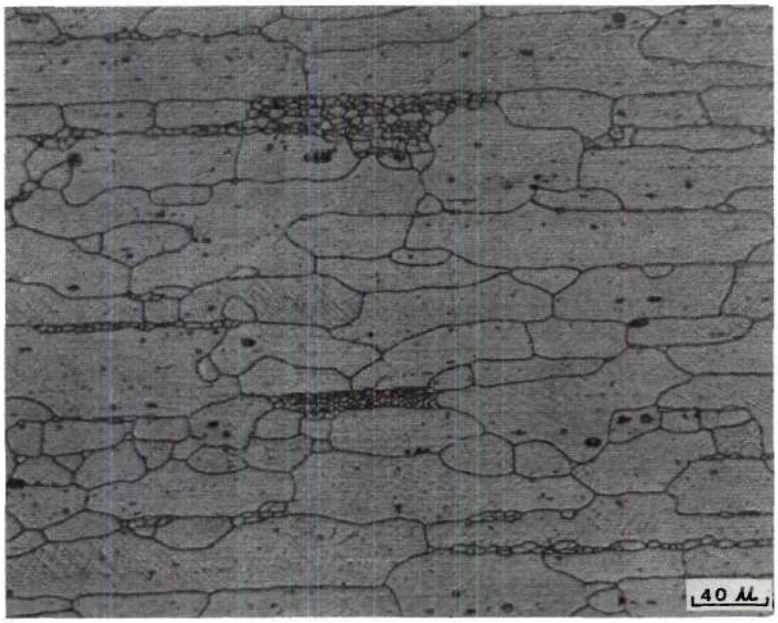

(A)

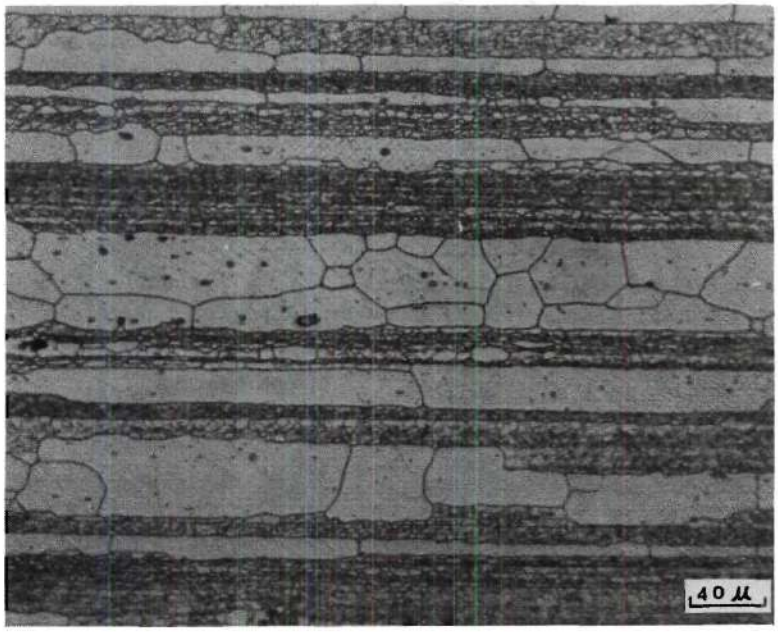

(B)

Figure 2.5. Microstructure of the 2.1% Cu alloy with 69% DR, (A) an area near the plate surface, (B) an area 2.2 mm from the plate surface, HNO_3 etch.

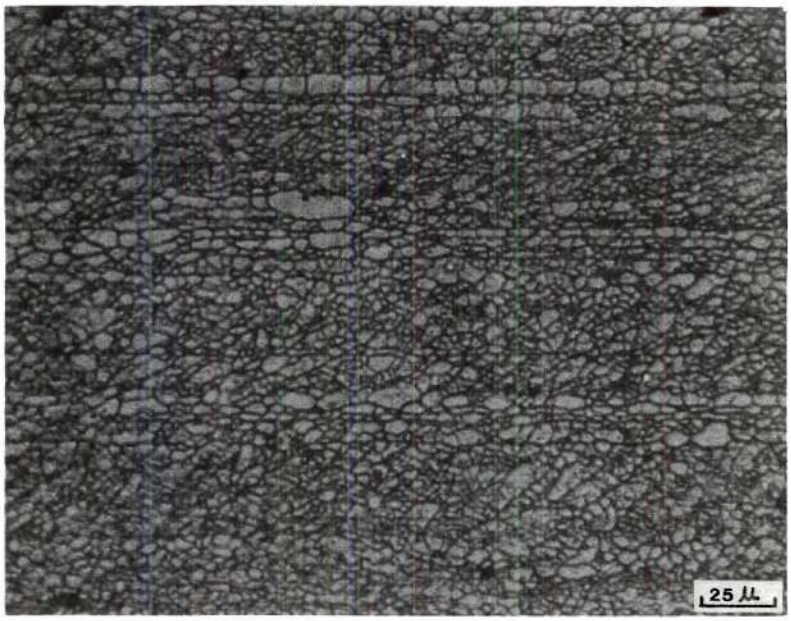

(A)

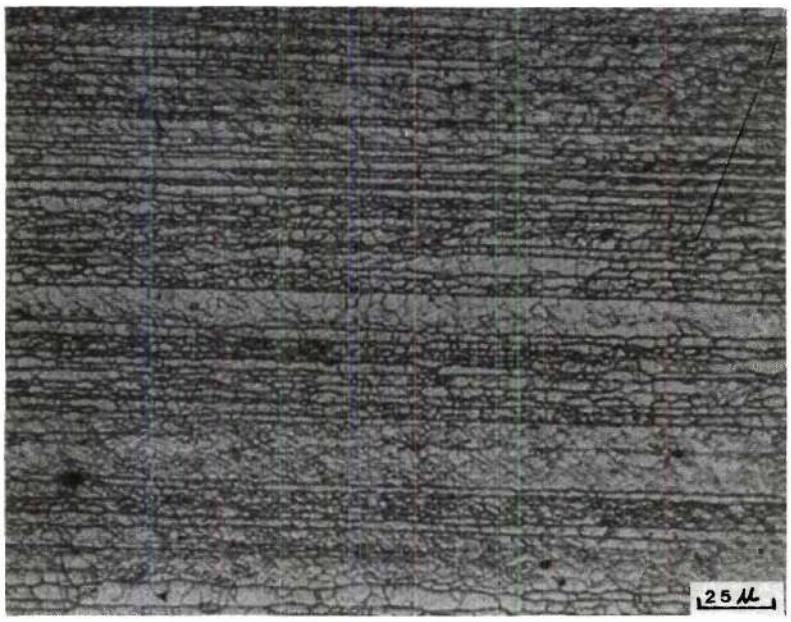

(B)

Figure 2.6. Microstructure of the 2.1% Cu alloy with 12% DR, (A) an area near the plate surface, (B) an area 3.0 mm from the plate surface, HNO_3 etch.

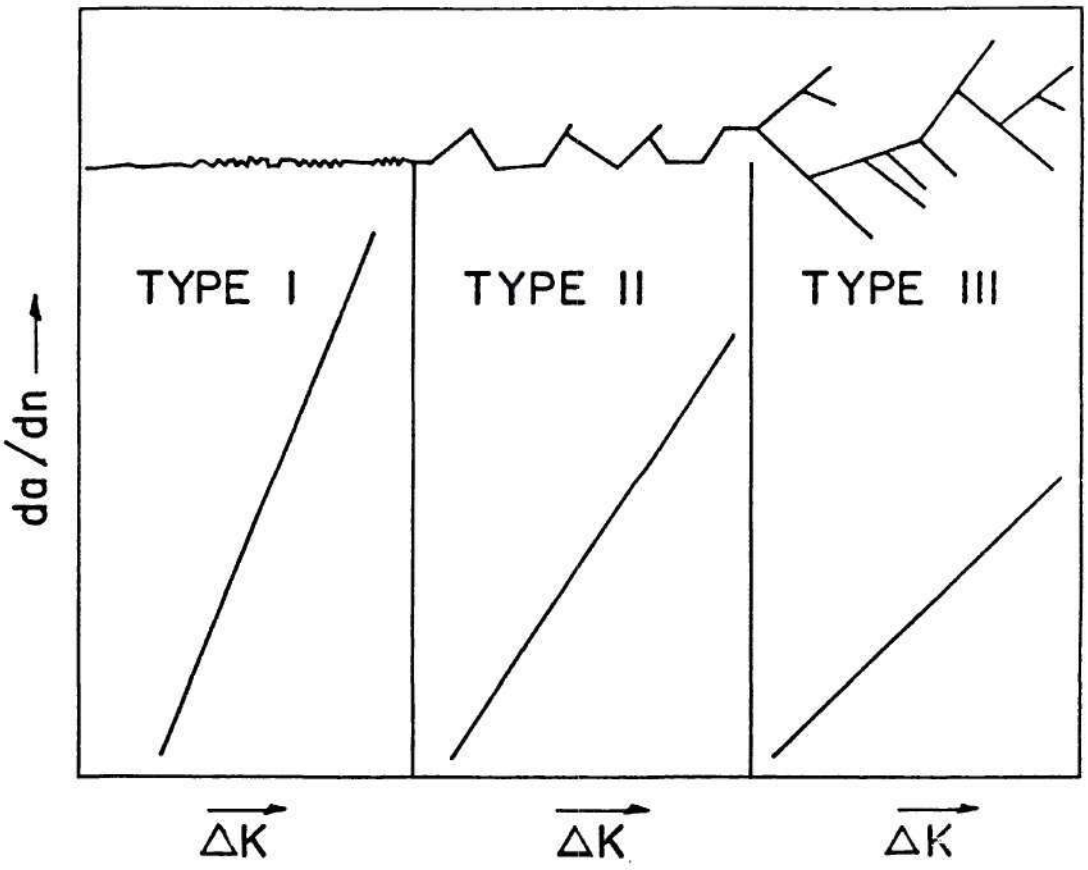

Figure 2.7. Schematic diagram of the FCGR as a function of the crack path features, $(da/dN)_{type\ I} > (da/dN)_{type\ II} > (da/dN)_{type\ III}$.

jumping to another slip plane. The crack growth rate of this type is slower than that of type I. Type III is a kind of branching with one crack branched into two forks. One fork became dominant, but the other continued growing at a much slower rate. The crack growth rate of this type is the slowest one since branching probably reduces the local stress intensity at the crack tip. The crack length measured was the projected length rather than the real length. The three types of crack features discussed here, with their corresponding microstructural appearance, are illustrated in Figure 2.8, for the 1.6% Cu alloy with 49% DR. Picture A shows a relatively straight crack with transgranular cracking. Picture B exhibits a zig-zag crack (slip band cracking). Note that the direction of slip band cracking changed its direction at high grain boundaries but remained unchanged at subgrain boundaries. Picture C shows crack branching, with cracks passing through both recrystallized and unrecrystallized grains. These crack path features are generally characteristic for all the alloys studied here regardless of the test environment. However, the frequency of occurrence of each type is dependent upon alloy chemistry, the test environment and the magnitude of ΔK. For example, the occurrence of types II and III for the 0.01 and 1.0% Cu alloys is about three times larger than in the 1.6 and 2.1% Cu alloys, Figure 2.9. This is attributed to a larger number of more easily shearable precipitates in the low copper content alloys, and thus dislocation shearing of precipitates in a few slip systems will be favorable for the occurrence of types II and III crack features. One the other hand, the frequency of occurrence of types II and III

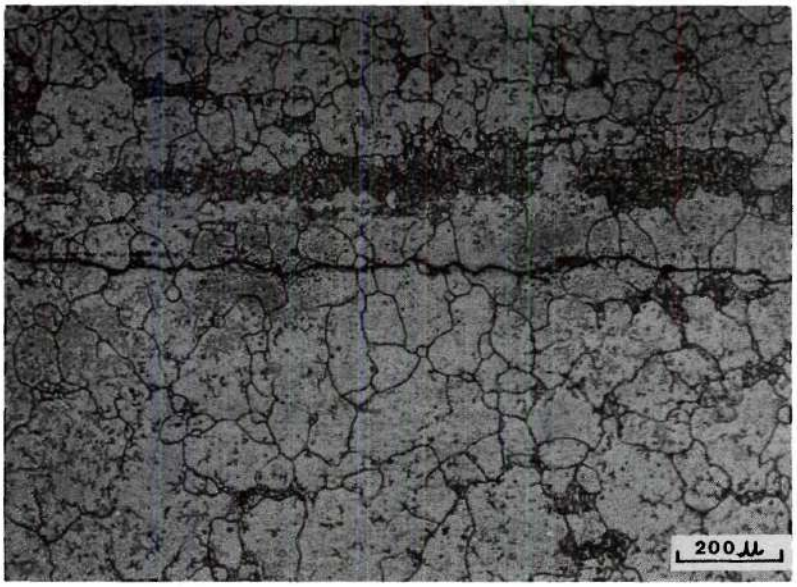

(A)

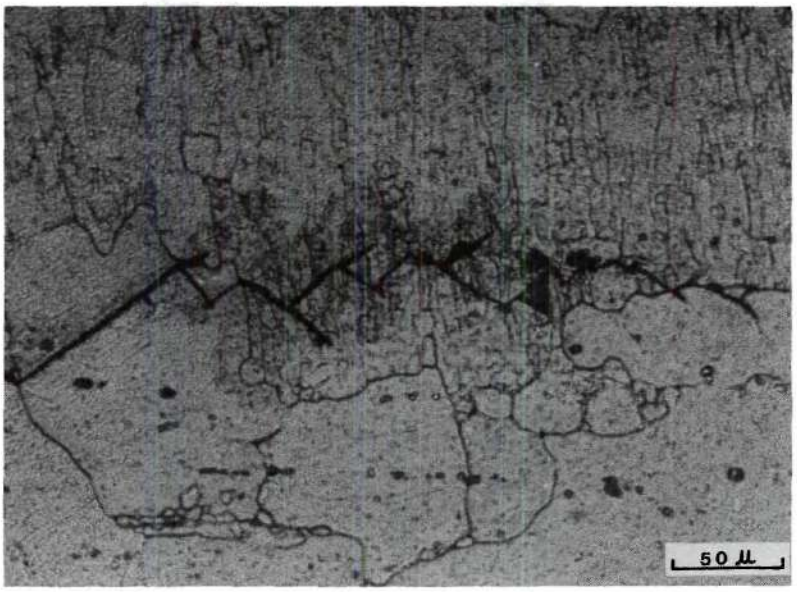

(B)

Figure 2.8. Fatigue crack path features of the 1.6% Cu alloy with 49% DR tested in H_2O, (A) ΔK = 7.0 $MPam^{\frac{1}{2}}$, (B) ΔK = 7.5 $MPam^{\frac{1}{2}}$, (C) ΔK = 8.5 $MPam^{\frac{1}{2}}$, HNO_3 etch.

Continued

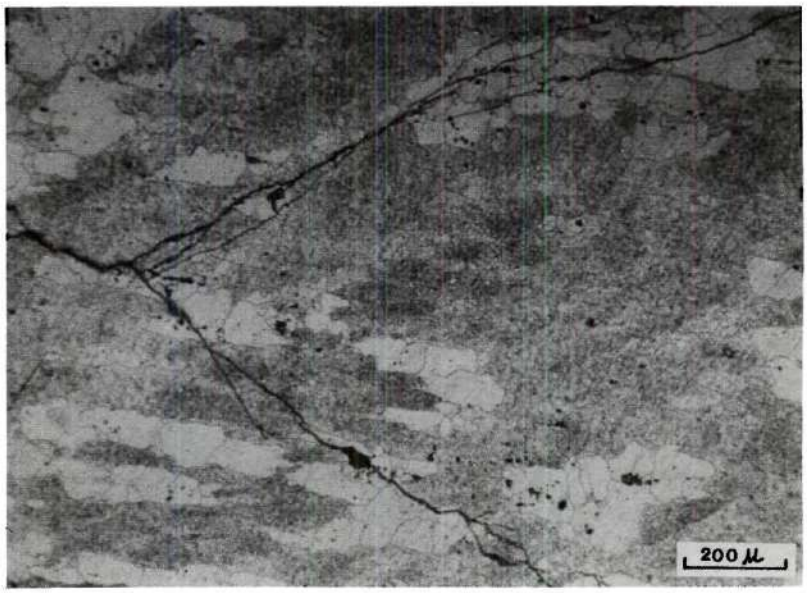

(C)

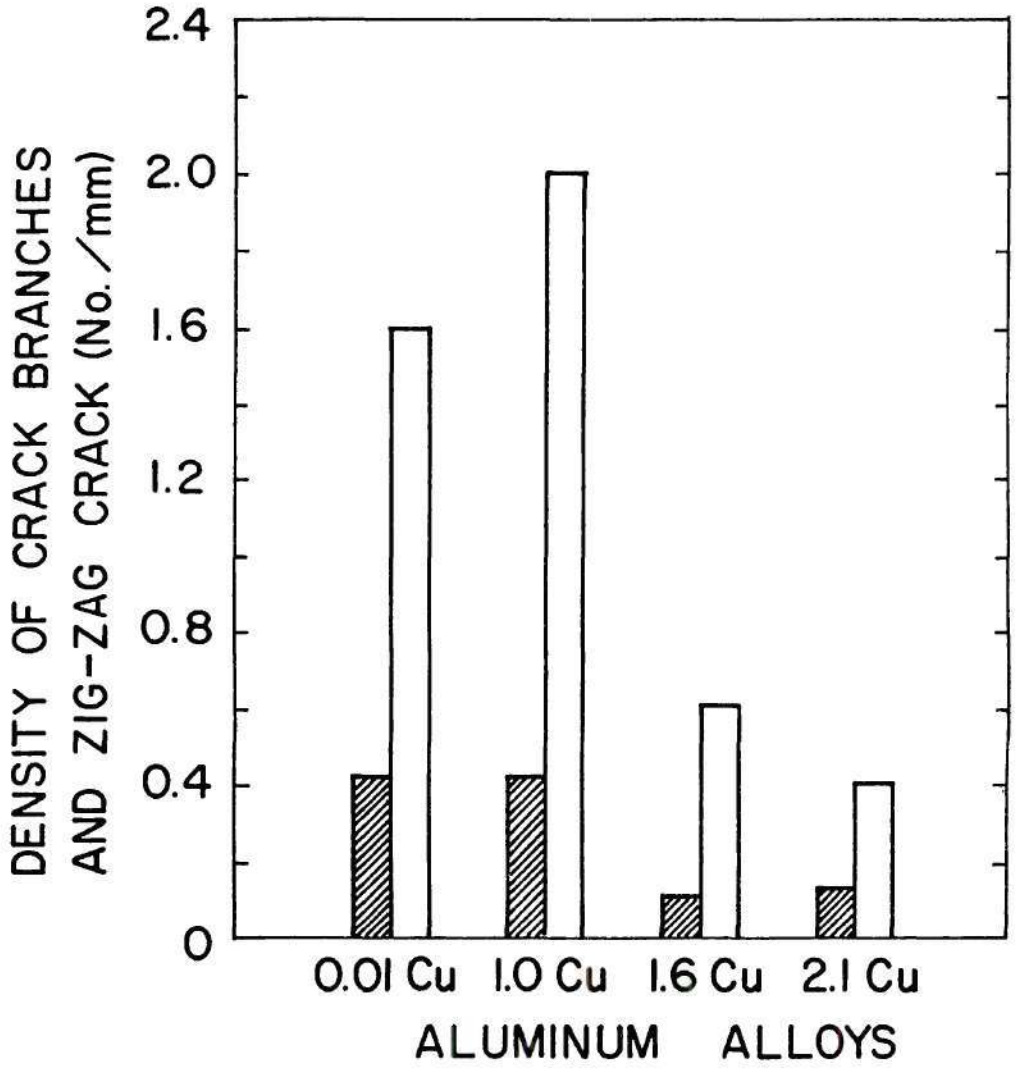

Figure 2.9. Crack path features as a function of the copper contents of 7000-type alloys tested in dry air, and the measurement of the crack path features made only from ΔK = 7.0 to 10.0 MPam$^{1/2}$. □ : zig-zag crack (type II), ▨ : crack branching (type III).

was considerably reduced when tests were conducted in distilled water or in a 3.5% NaCl solution. They were also reduced by increasing the magnitude of ΔK, especially for the type III crack path. The formation of type II and III cracking is probably restrained by the introduction of hydrogen atoms which are produced by the interaction of distilled water with the fresh aluminum surfaces created at the crack tip[46,83]. At higher ΔK values, the probability of triggering more slip systems increases, resulting in a decrease of the occurrence of types II and III cracking.

The function of subgrains in the unrecrystallized grains involved in the FCP process at low ΔK values ($\leq$ 7 $MPam^{\frac{1}{2}}$) appears to be dependent upon the test environment. It can be seen from Figure 2.10 that the fatigue crack path mainly followed subgrain boundaries when the tests were conducted in distilled water (picture A), while in dry air the crack path was predominantly trans-subgrains (picture B). For the 2.1% Cu alloy, a quantitative determination of the percentage of crack path along subgrain boundaries or trans-subgrain in the unrecrystallized regions was performed. The results showed that the percentage of the fracture path covered by subgrain boundaries was about 80% for tests conducted in distilled water, but only 30% in dry air. The small subgrains and the equilibrium precipitates along subgrain boundaries (Figure 1.4, PART I) provide favorable condition for cracking along subgrain boundaries. The increase in tendency for cracking along high grain boundaries when the tests were conducted in moist air has also been reported by other investigators[100] who indicated that for a high purity Al-Zn-Mg alloy

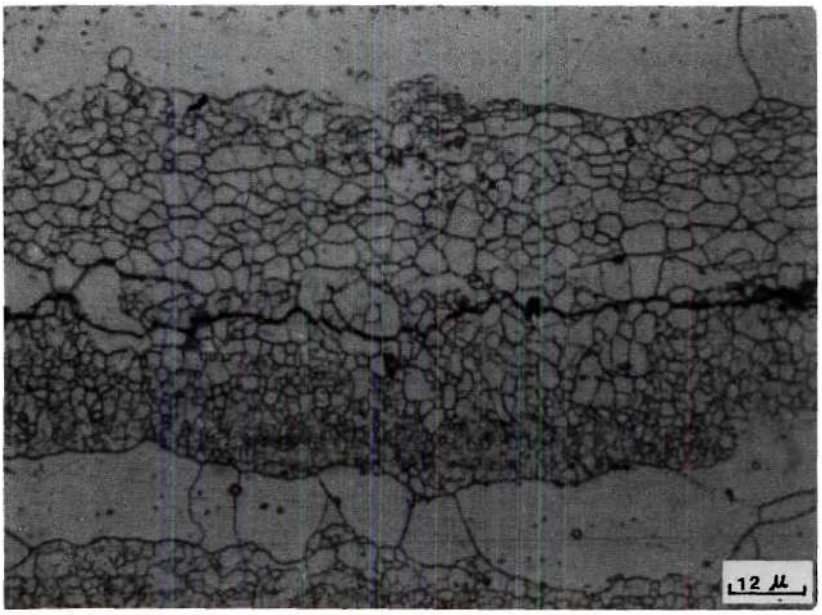

(A)

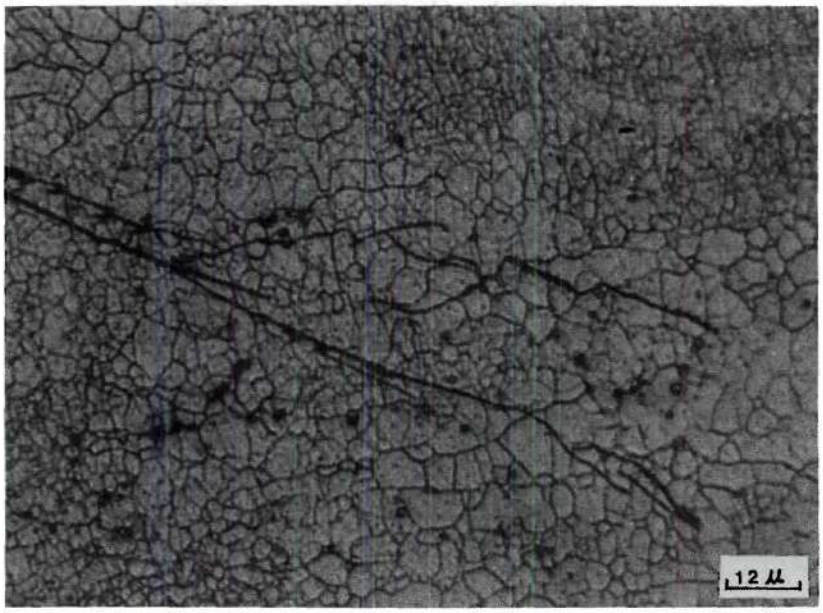

(B)

Figure 2.10. Fatigue crack path characteristics in unrecrystallized grains of the 2.1% Cu alloy with 12% DR. Test conducted (A) in distilled water, subgrain boundary cracking predominantly, (B) in dry air, trans-subgrain cracking predominantly, $\Delta K = 7.0$ MPam$^{\frac{1}{2}}$, HNO_3 etch.

aged to peak hardness, the fatigue crack path was about 50% intergranular cracking when the tests were conducted in moist air, while in dry argon transgranular cracking was predominant. The 2.1% Cu alloy was chosen for investigating crack path features in the unrecrystallized regions since its subgrain boundaries were very easily revealed by an HNO_3 etch. For the low copper content alloys, the planar slip mode is more prevalent, thus it is plausible to predict that the percentage of crack path along subgrain boundaries may be less than that observed for the higher copper content alloys.

Scanning electron fractographic studies were performed to investigate the effect of microstructural features on the FCP behavior. Figure 2.11 shows a typical fracture appearance for the 0.01, 1.0 and 1.6% Cu alloys with minimum DR when the tests were conducted in distilled water. The fracture surface consists of stepwise crack growth markings and irregular plateaus and ridges. The straight strips shown in micrograph A represent the unrecrystallized grains, and it is clear from this micrograph that the direction of crack propagation does change from one unrecrystallized grain to another. Note that the fracture patterns in each unrecrystallized grain are quite different from one grain to another, and suggests that the propagation of the crack is dependent upon local crystallography. Clustered particles were not found on the fracture surfaces of the FCP samples in these three alloys. The fracture features of samples with high DR were different from those of samples with low DR. Figure 2.12 shows the fracture surface of the 1.6% Cu alloy with 49% DR, but this micrograph was taken from an area near the

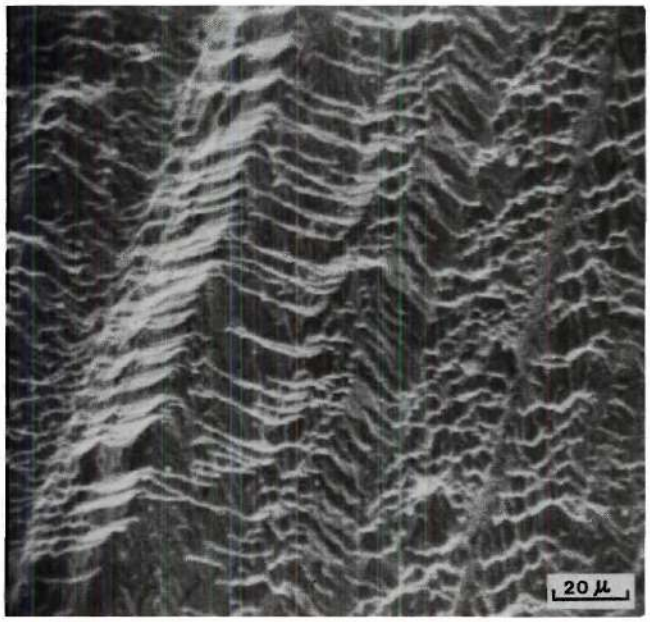

(A) ↑

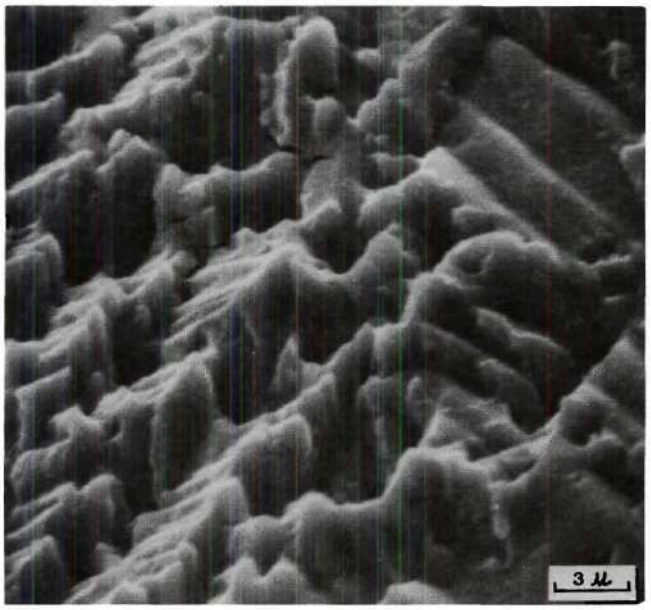

(B) ↑

Figure 2.11. Scanning electron fractographs of the fatigue fracture surfaces for the 1.6% Cu alloy with 9% DR tested in distilled water, (A) illustrating the step-wise crack growth and the irregular plateaus and ridges, (B) at high mag. Arrow: the crack propagation direction, $\Delta K = 7.0$ MPam$^{\frac{1}{2}}$.

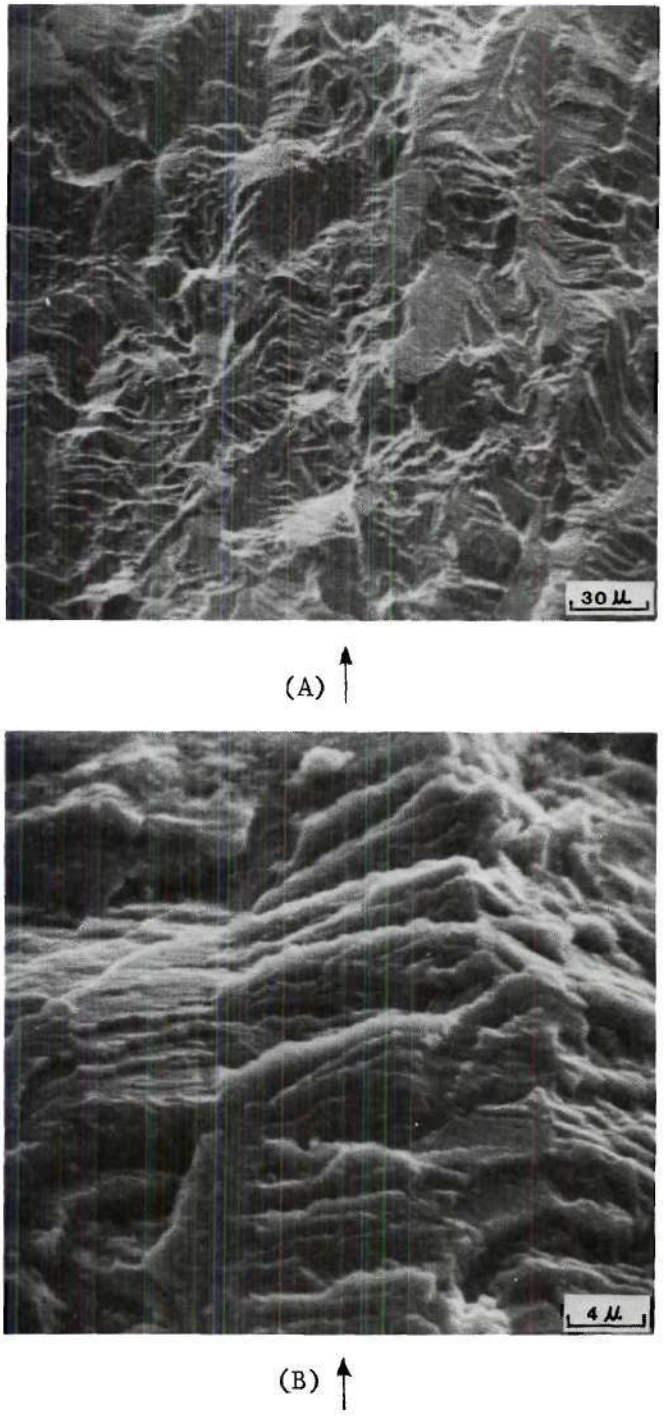

Figure 2.12. Scanning electron fractographs of the fatigue fracture surfaces for the 1.6% Cu alloy with 49% DR tested in distilled water, (A) showing how the crack propagation orientation varies from grain to grain, (B) at high mag., $\Delta K = 7.5$ MPam$^{\frac{1}{2}}$.

plate surface, i.e., almost completely recrystallized. Markings of individual grain structures (micrograph A) imply that the fatigue fracture surface changed orientation from grain to grain. The slip-mode markings were terminated at grain boundaries. This finding combined with the results of examining the fracture features in the unrecrystallized regions described previously reflects the fact that high angle grain boundaries appear to play some role in the FCP behavior. A comparison of the fracture features was made between Figure 2.11 and Figure 2.12 which represented the fracture surfaces in unrecrystallized grains and in recrystallized grains respectively. Figure 2.12 illustrates more regular slip-markings and more feature-less patterns developed in many recrystallized grains. Figure 2.11, on the other hand, shows more irregular plateaus and ridges which may be associated with the presence of subgrains. In general, the scanning electron fractographic studies show that the recrystallized grains exhibit more featureless patterns. However, an alloy with a higher DR did not display a significant difference in the FCGR (will be shown later). This may be due to the fact that alloys studied here were not completely recrystallized, thus the presence of the unrecrystallized regions in an alloy may reduce the influence of the recrystallized regions on the FCP behavior.

The fracture appearance of the fatigue samples tested in a 3.5% NaCl solution was very similar to that in distilled water as was the FCGR measured in these two environments (will be shown later). The main difference in the fatigue fracture appearance between 2.1% Cu alloy and the others is that the clustered particles of the

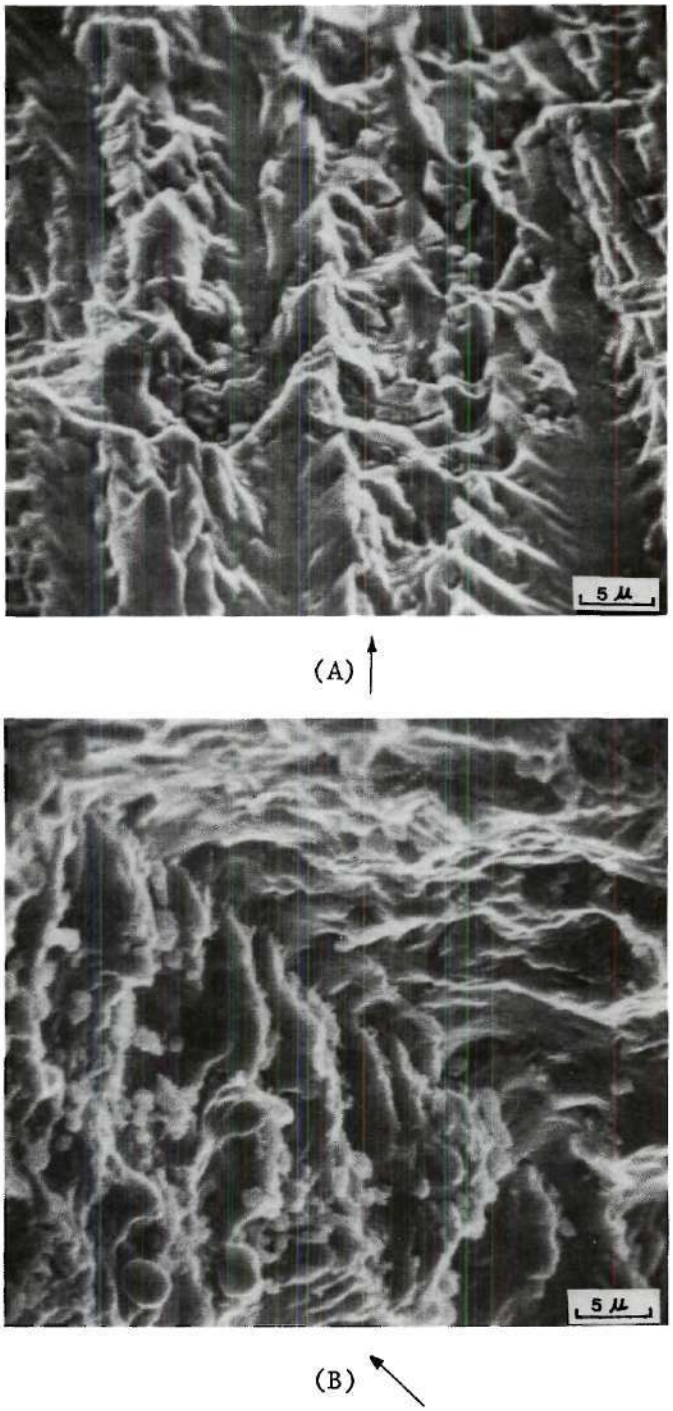

Figure 2.13. Scanning electron fractographs of the fatigue fracture surfaces for the 2.1% Cu alloy with 12% DR, (A) the test conducted in distilled water, showing a large amount of flat area, (B) in dry air showing more irregular plateaus and ridges. Note the clustered particles on the fracture surfaces, $\Delta K = 8.5$ MPam$^{\frac{1}{2}}$.

S-phase were found on the fracture surface of the 2.1% Cu alloy as illustrated in Figure 2.13. Void formation around the clustered particles was not observed in the present study over the range of ΔK studied. However, voids have been found on the overload fracture surface, Figure 2.3, or on the fatigue fracture surface at a higher ΔK values as found by El-Soudani and Pelloux[8]. Therefore, the effect of clustered particles of S-phase on the FCGR at low ΔK values may be different from that at high ΔK values[8,76] or for fracture toughness. The significant difference between fracture surfaces of samples tested in dry air and in distilled water can be identified from Figure 2.13. For distilled water, micrograph A displays a larger amount of area with flat features, which are indicative of more brittle fracture; whereas in dry air, micrograph B shows a larger number of plateaus and ridges, which are indicative of more ductile fracture.

Effect of Copper Content on the FCP Behavior

The fatigue crack growth data for the experimental materials, plotted as $\frac{da}{dN}$ vs ΔK, are shown in Figures 2.14 to 2.17. It is of interest to note that a knee (transition from region I to II) always occurs in each curve of these plots for all alloys tested in all three environments. This suggests that its occurrence is not associated with environmental effects. The result is consistent with the findings of Feeney, et al.[50] However, environment can slightly change the ΔK values required for its occurrence. For each alloy tested in dry air the knee occurred at $\Delta K = 5.6 \sim 6.5$

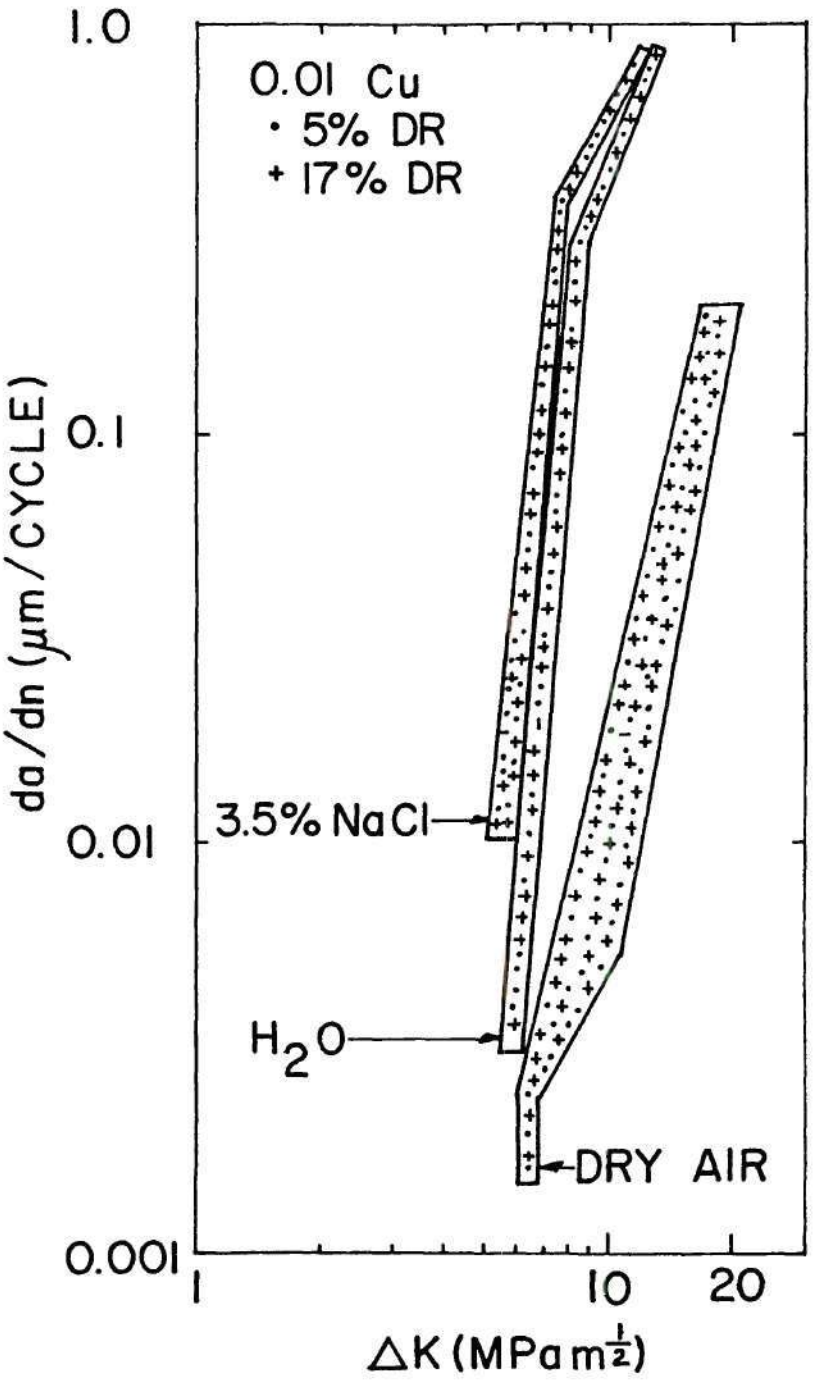

Figure 2.14. Effect of DR on the FCGR for Al-6Zn-2Mg-0.01 Cu alloys tested in dry air, distilled water and a 3.5% NaCl solution.

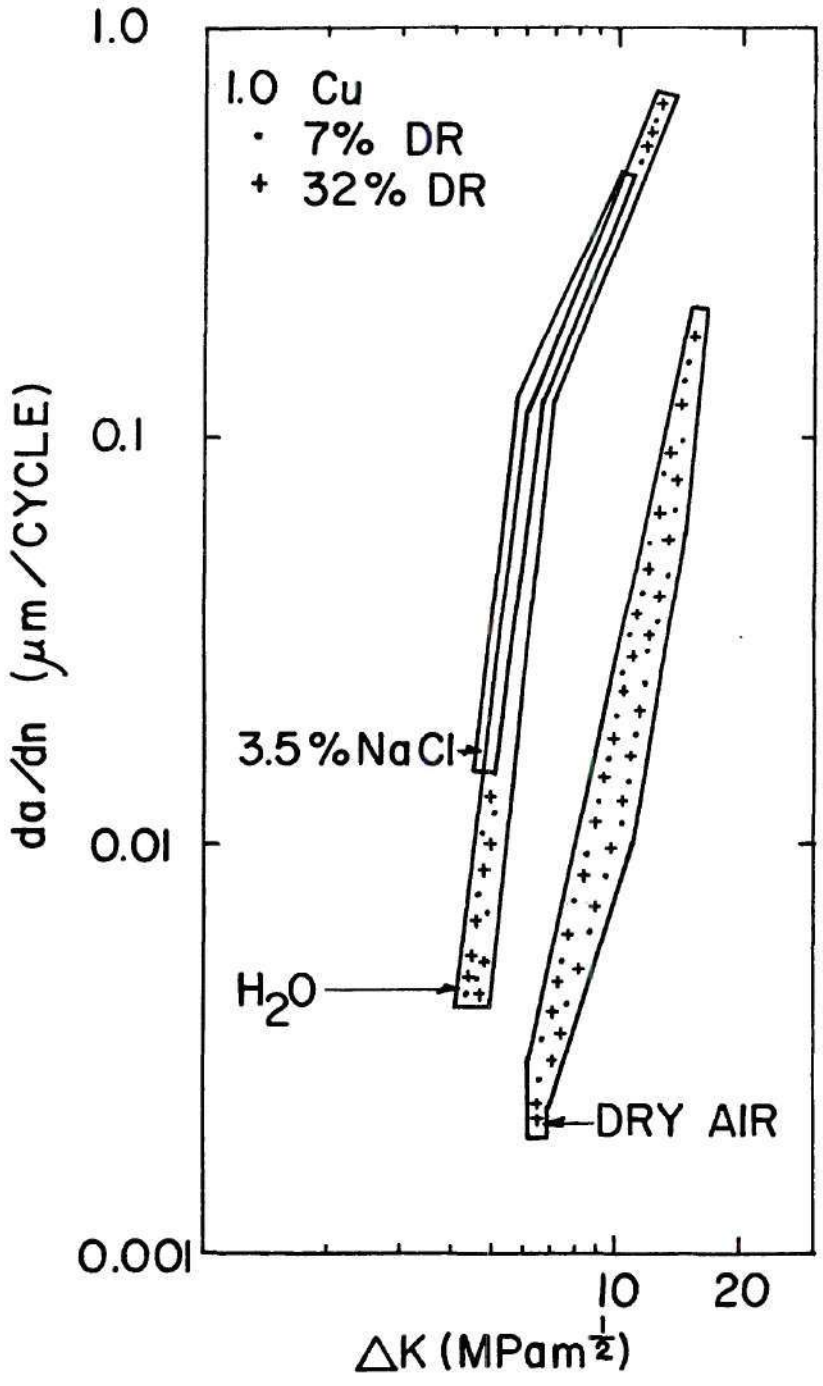

Figure 2.15. Effect of DR on the FCGR for Al-6Zn-2Mg-1.0 Cu alloys tested in dry air, distilled water and a 3.5% NaCl solution.

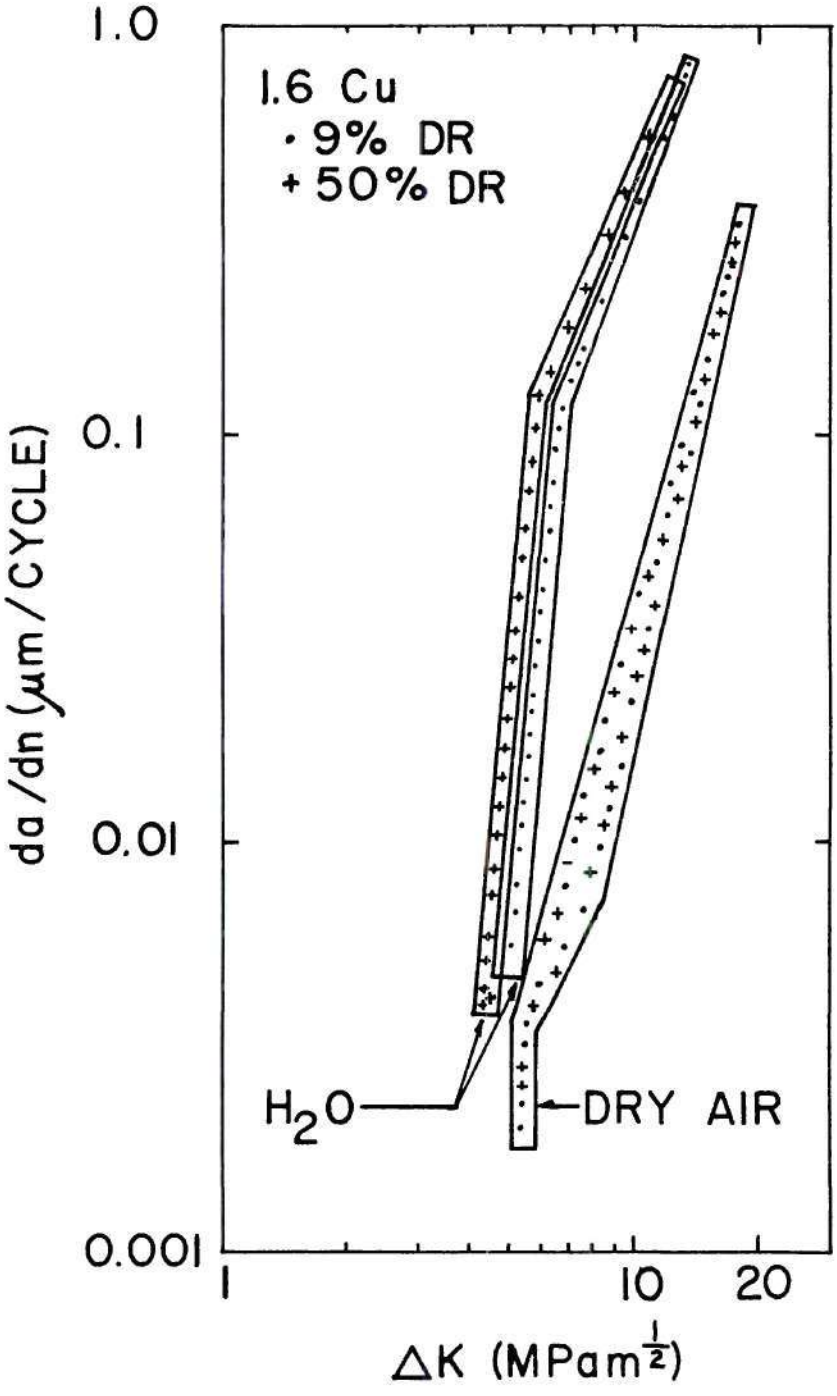

Figure 2.16. Effect of DR on the FCGR for Al-6Zn-2Mg-1.6 Cu alloys tested in dry air and distilled water.

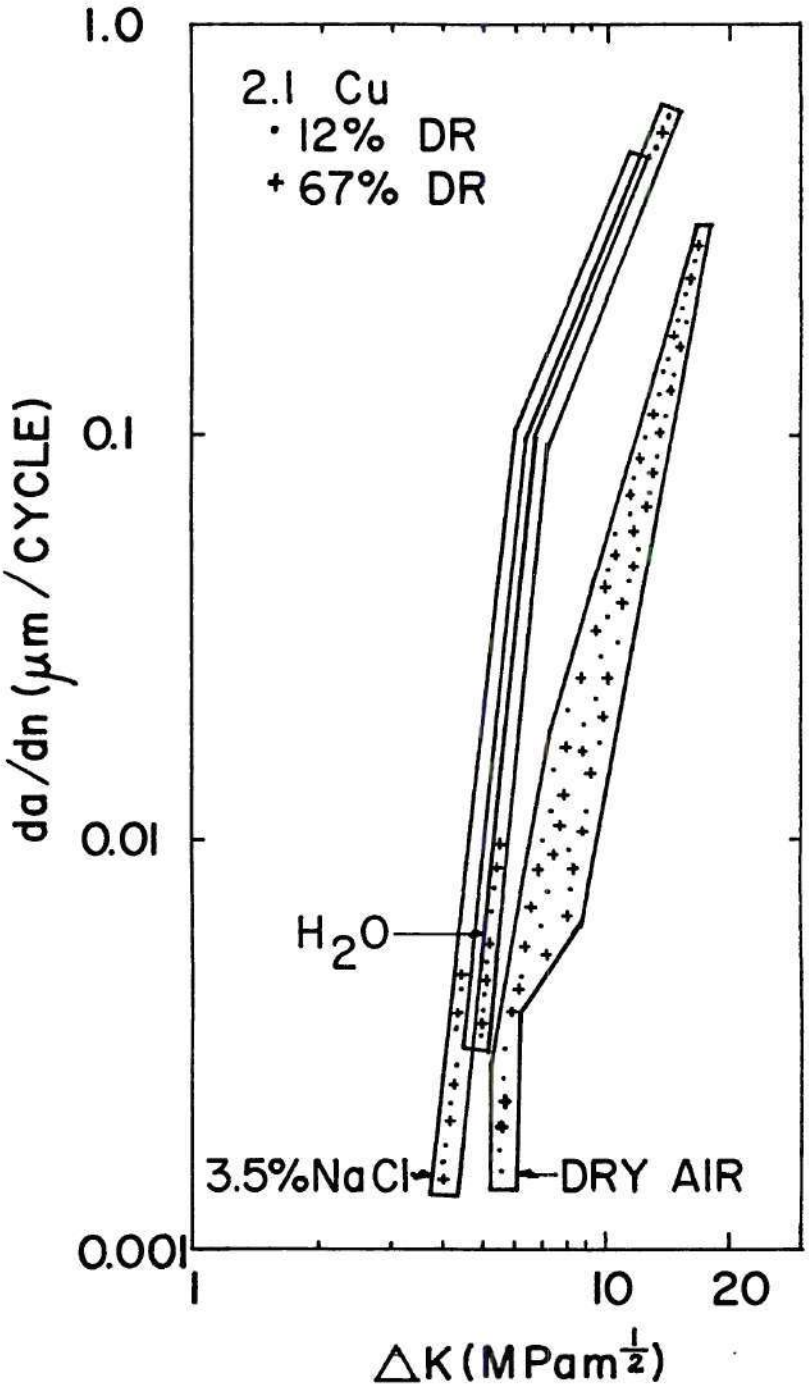

Figure 2.17. Effect of DR on the FCGR for Al-6Zn-2Mg-2.1 Cu alloys tested in dry air, distilled water and a 3.5% NaCl solution.

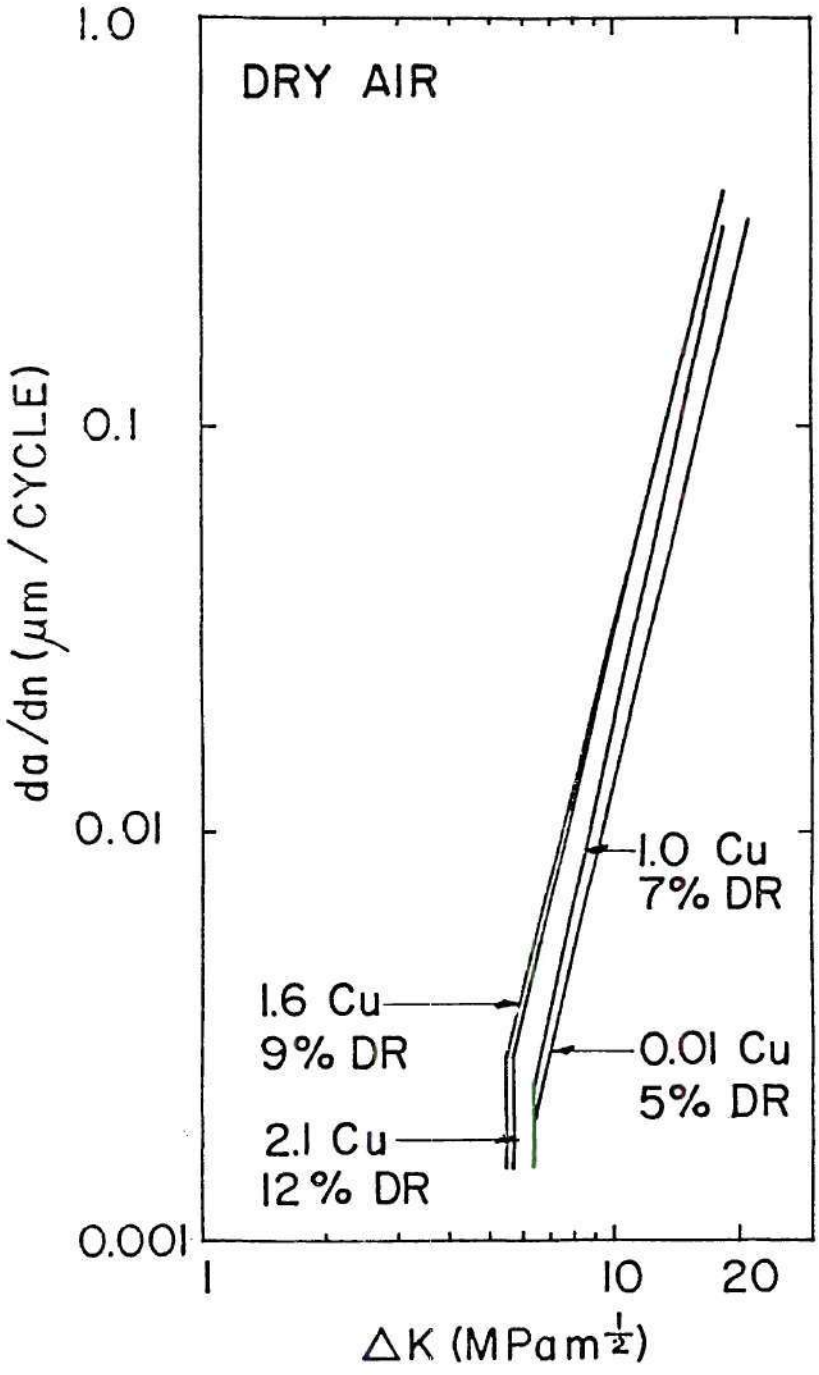

Figure 2.18. Effect of the copper content of Al-6Zn-2Mg-xCu alloys on the FCGR tested in dry air.

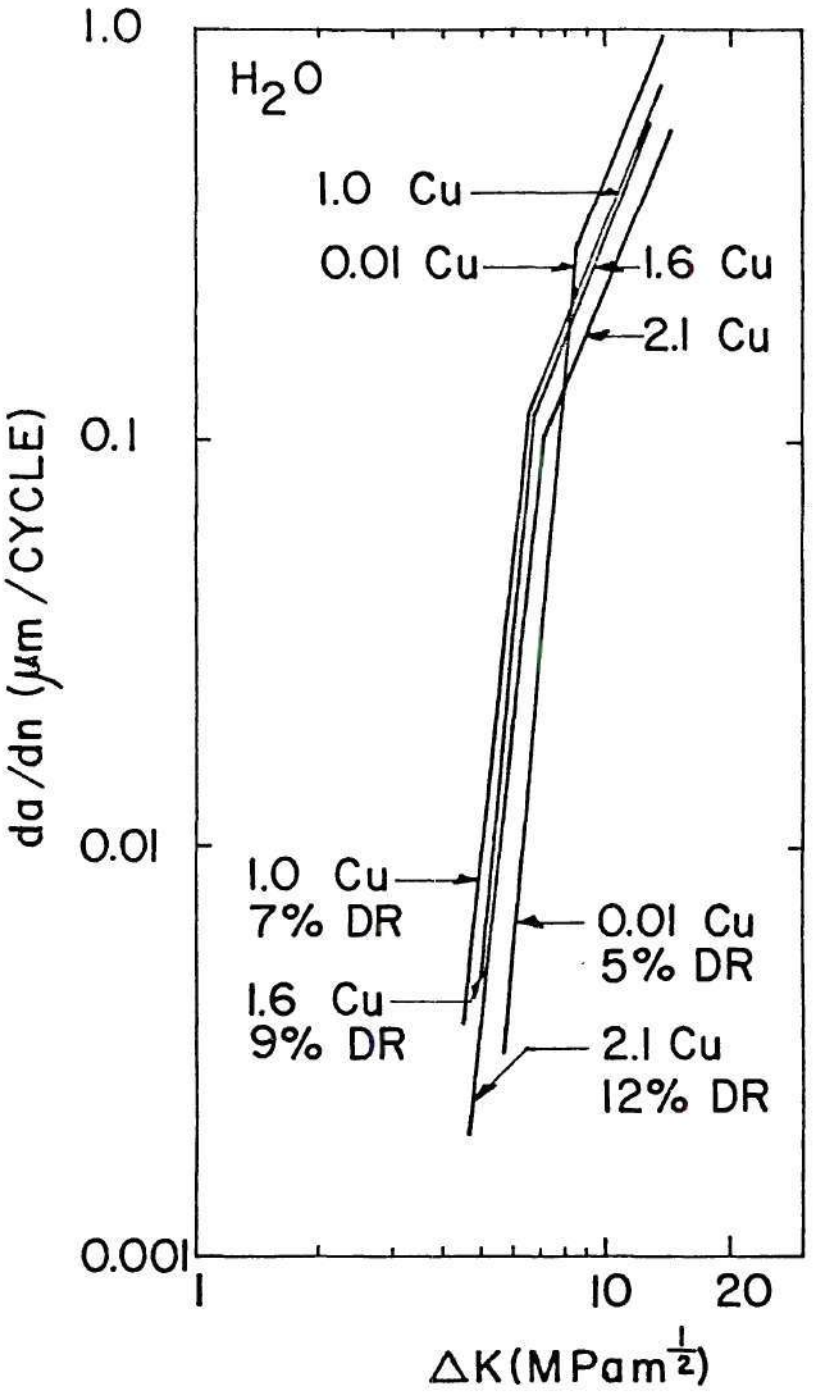

Figure 2.19. Effect of the copper content of Al-6Zn-2Mg-xCu Alloy on the FCGR tested in distilled water.

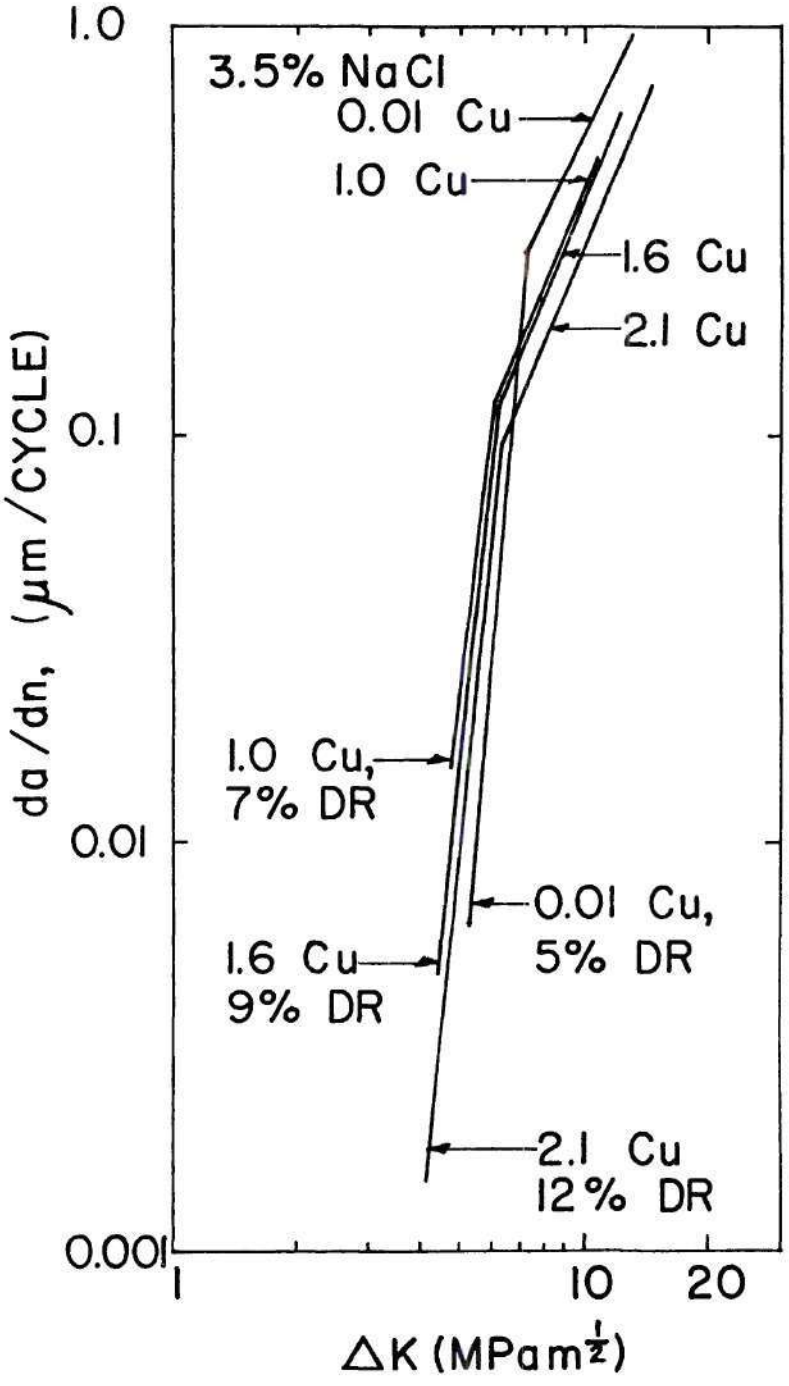

Figure 2.20. Effect of the copper content of Al-6Zn-2Mg-xCu alloys on the FCGR tested in a 3.5% NaCl solution.

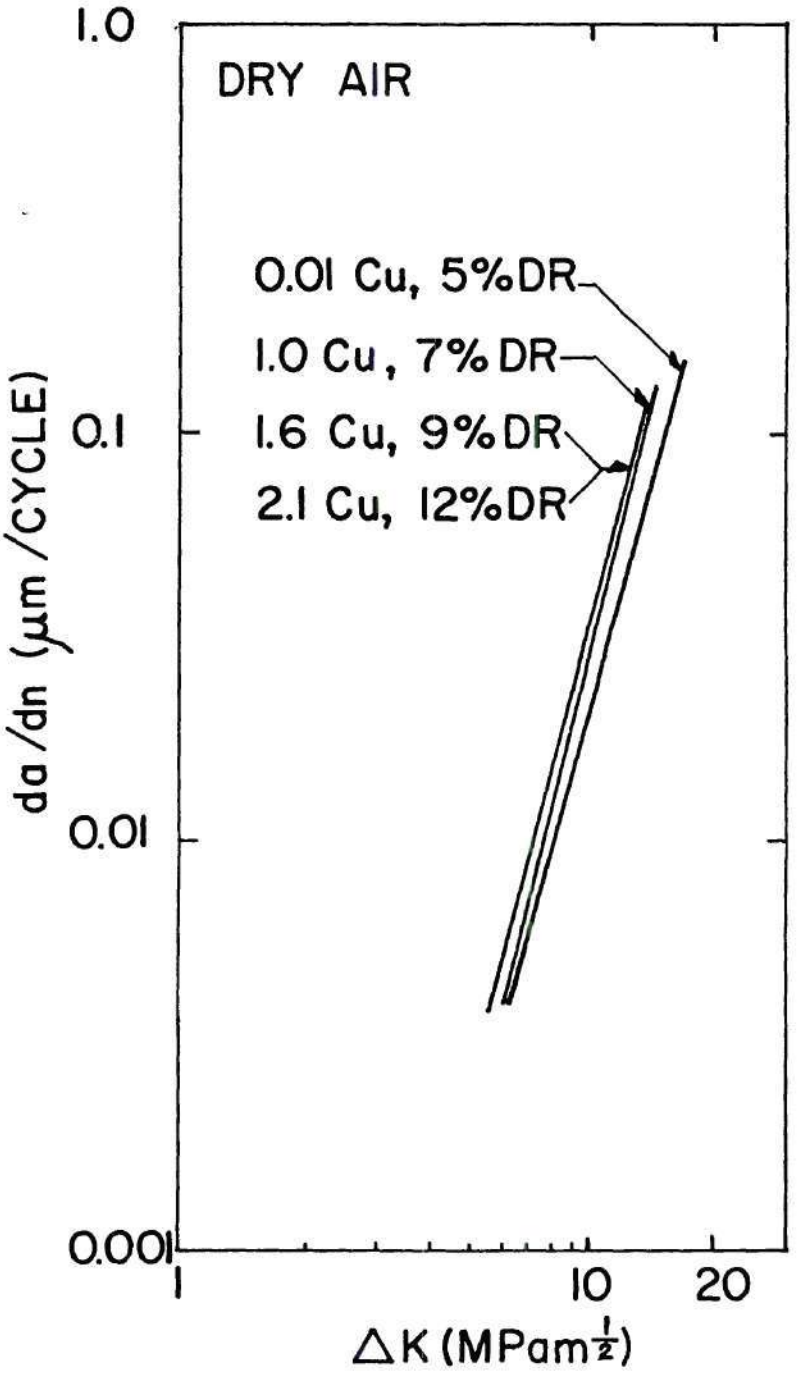

Figure 2.21. Effect of the copper content of Al-6Zn-2Mg-xCu alloys on the FCGR tested in dry air, da/dN was calculated by measuring the real crack length on the surfaces of the FCP samples.

$MPam^{\frac{1}{2}}$, which was slightly lower than the value obtained in distilled water or in a 3.5% NaCl solution. The mechanism of occurrence of a knee at low ΔK values has been discussed by Feeney, et al.[50] who indicated that this may be rationalized with some intrinsic property of the material, i.e. the property of the matrix and the hardenable precipitates associated with the plastic zone size.

For a clear comparison of the effect of copper content on the FCGR, the data were replotted, grouping similar microstructures and test environment together, and are shown in Figures 2.18 to 2.20. Figure 2.18 reveals that, in dry air, the slowest FCGR was exhibited by samples with the 0.01% Cu alloy, followed by 1.0, 2.1 and 1.6% Cu alloys respectively. However, the latter two alloys showed almost identical rates. Since there was a large amount of experimental scatter in dry air (see Figures 2.14 to 2.17), the small difference in the FCGR may not be commercially significant, but the relative FCGR is still valid. As discussed in PART I, the four different copper content alloys designed for this specific study had almost identical microstructures. Therefore, the significant parameter involved in the FCP behavior must be due to the copper content. The copper atoms participate in the precipitation process resulting in a different precipitate type, i.e., degree of coherence. Ample evidence was presented in PART I showing that, for this aging condition, the low copper content alloys contain mostly easily shearable precipitates while the high copper content alloys contain more partially coherent (η'), and some incoherent precipitates (η) and Cu rich S-phase particles. These results indicate why the low

copper content alloys displayed lower FCGR when tests were conducted in dry air. Dislocation shearing of coherent precipitates results in planar slip, thus numerous dislocations will move back and forth on the same slip plane within the plastic zone ahead of a growing crack during cyclic-loading, i.e., increasing the slip reversibility. However, in age-hardenable alloys, this may cause softening on slip bands[27,83] and lead to an early slip band decohesion and the occurrence of a larger amount of a zig-zag crack and the crack branching. This explanation is consistent with observations of crack path features in these four alloys. The frequency for occurrence of a zig-zag crack (type II) and the crack branching (type III), as shown in Figure 2.7, is increased considerably as the copper content decreases. The low copper content alloys exhibited type II and III crack path approximately three times more often than those of the high copper content alloys, Figure 2.9. The type II and III crack path features will reduce the FCGR, as shown in Figure 2.7. For the high copper content alloys, the presence of more incoherent precipitates will create many prismatic loops as dislocations move in the matrix and catalyse numerous slip systems[19]. These involve more slip systems in the FCP process, resulting in a large amount of straight crack path (Figure 2.9). The straight crack path, type I in Figure 2.7, exhibited the faster FCGR in the present study.

The low copper content alloys display planar slip in the reversed plastic zone resulting in an early slip band decohesion, and presumably, they should show lower FCP resistance in the same manner as they exhibited in the LCF tests, i.e., the decrease of

copper content in 7000-type alloys also reduces the cyclic strain resistance. This explanation is attributed to the fact that the plastic deformation behavior in the reversed plastic zone for the FCP samples is similar to that of LCF samples[102,103]. The observed difference in the sequence between the FCP and LCF resistance is thus considered to be due to the difference of the projected length and the real length of crack path since the low copper content alloys exhibited a larger amount of a zig-zag crack and the crack branching when the FCP tests were conducted in dry air. The FCGR, therefore, was calculated by measuring the real length of the crack on the surfaces of samples, and then the real $\frac{da}{dN}$ vs ΔK was plotted as shown in Figure 2.21. It is apparent that the low copper content alloys still exhibited lower FCGR, but the difference in the FCGR for the low and the high copper content alloys was reduced, as compared in Figures 2.18 and 2.21. The primary reason why the low copper content alloys did not display higher FCGR even when the real $\frac{da}{dN}$ was measured is that a reduction of the effective ΔK values in the presence of a zig-zag crack and/or a crack with branches can not be expressed simply in terms of the real length of the crack. The effective ΔK values for a zig-zag crack, deviating an angle of about 32 degrees from the plane perpendicular to the loading axis, would be only 85% of the applied ΔK values; furthermore, the effective ΔK values for a crack with branches must be less than that since the applied ΔK values would be distributed over the number of branches. The other reason is that the features of a crack path vary from one region to another through the sample thickness, and it is very difficult to

measure the real crack length. The faster FCGR of the high copper content alloys tested in dry air is not due to the presence of the clustered S-phase particles (see Figure 2.13 for the 2.1% Cu alloy) for the range of ΔK values studied here, as discussed previously, or to the lower fracture toughness (See Table 2.1). This can be further confirmed by the FCP behavior of the 1.6% Cu alloy. The clustered particles were not observed on the FCP fracture surfaces of this alloy and its fracture toughness is the highest for all alloys, but its FCGR is almost identical to that of the 2.1% Cu alloy.

In order to observe any difference in the cyclic deformation behavior within the plastic zone of the FCP sample for each alloy, since this can affect the measured FCGR as discussed above, thin foils were taken from positions adjacent to the fracture surface and examined by TEM. It appears that the probability of developing cell structures is increased with increasing copper content. For example, in the low copper content alloys, uniform plastic deformation was prevalent in the plastic zone, with local areas of slip bands and cell structures. The slip band features are shown in Figure 2.22, picture A. However, for the high copper content alloys, (1.6 and 2.1% Cu) the cell structures were more prevalent. A typical example of this structure is presented in picture B, showing that numerous dislocations were decorated within an individual cell. These observations suggest that for the high copper content alloys, cross slip is triggered in the reversed plastic zone resulting in the formation of cell structures. This leads to a decrease in the

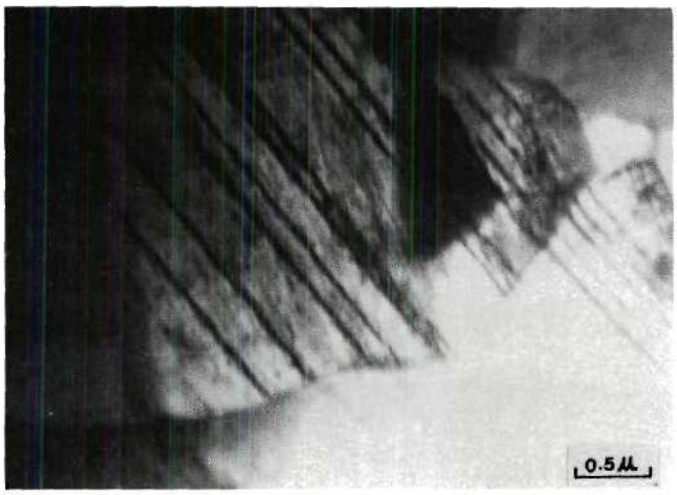

(A)

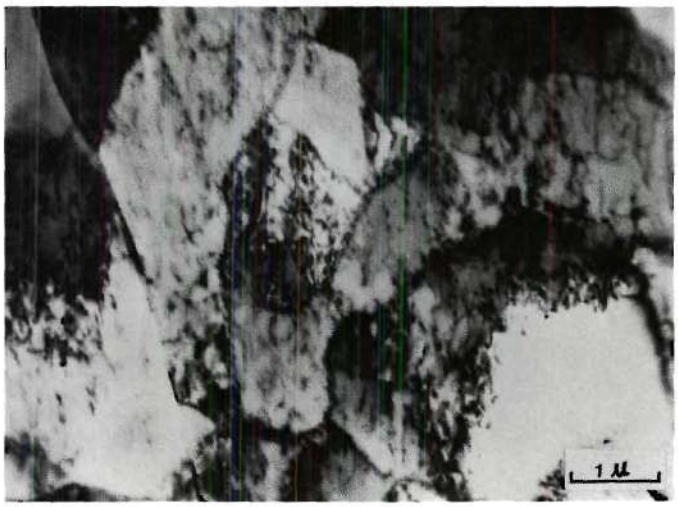

(B)

Figure 2.22. Transmission electron micrographs taken at an area adjacent to the fatigue fracture surface, (A) showing slip bands in a 1.0% Cu alloy, $\Delta K = 9.5$ MPam$^{\frac{1}{2}}$, and (B) showing cell structures in a 2.1% Cu alloy, $\Delta K = 10.5$ MPam$^{\frac{1}{2}}$.

reversibility of slip, but an increase in the degree of homogeneity of deformation, and thus results in the occurrence of the relatively straight crack path. These observations are consistent with the findings described previously that the amount of a zig-zag crack and the crack branching decreases with increasing copper contents in the 7000-type aluminum alloys.

The FCP behavior for the four different copper content alloys that were tested in distilled water or in a 3.5% NaCl solution was quite similar, except that in the latter environment, a slightly higher FCGR was observed (see Figures 2.19 to 2.20). A comparison of Figures 2.19 and 2.20 with 2.18 reveals that FCP behavior in dry air was considerably different from that in distilled water or in a 3.5% NaCl solution. Not only were the rates different but also the sequence of the FCP resistance. Note that when $\Delta K > 7.5$ MPam$^{\frac{1}{2}}$, the sequence of the FCGR for the four different copper content alloys was 2.1, 1.6, 1.0 and 0.01% Cu, i.e., increasing in FCGR with decreasing copper content. However it is of interest to note that when $\Delta K < 7.5$ MPam$^{\frac{1}{2}}$, the 0.01% Cu alloy markedly increased its FCP resistance and showed the lowest FCGR, and the sequence for the other three alloys was the same as that for $\Delta K > 7.5$ MPam$^{\frac{1}{2}}$. As discussed previously, the slower FCGR for the low copper content alloys tested in dry air is attributed to the formation of a larger amount of a zig-zag crack and the crack branching, i.e., depends on a mechanical parameter only. However, when the FCP tests were conducted in corrosive environments such as distilled water and a 3.5% NaCl solution, two important parameters must be considered

simultaneously, i.e., a mechanical and a metal-environment interaction. At intermediate ΔK values (> 7.5 $MPam^{\frac{1}{2}}$), the influence of the metal-environment interactions becomes important[101], and the effect of this parameter is considerably intensified when dislocation shearing of coherent precipitates results in planar slip, as in the low copper content alloys discussed in PART I and shown in micrograph A, Figure 2.22. Therefore, the metal-environment interaction parameter becomes dominant and has a dramatic detrimental effect on FCP. The low copper content alloys now lose their larger advantage in the FCP resistance over the high copper content alloys since they did not exhibit a larger amount of a zig-zag crack and the crack branching as they did in dry air. The effect of environment on the features of crack path has been discussed previously. On the other hand, the high copper content alloys exhibited a larger degree of homogeneous deformation, such as formation of cell structures in the plastic zone (micrograph B in Fig. 2.22), leading to a significant decrease of the metal-environmental interactions, and thus this results in a lower FCGR for these alloys. However, for lower ΔK values (< 7.5 $MPam^{\frac{1}{2}}$), the intensity of the metal-environment interactions is not so strong as it is if ΔK > 7.5 $MPam^{\frac{1}{2}}$, thus the 0.01% Cu alloy still exhibited a larger amount of a zig-zag crack and the crack branching than other alloys since it contained the largest amount of easily shearable precipitates.

Experimental results in this study revealed that the alloy chemistry can change FCP resistance. This is consistent with the findings of other investigators[7,8,55] who indicate that any change

in alloy chemistry will have a marked effect on the FCGR only if it will markedly influence the slip character. The conclusion drawn from these results is that in dry air, the lower FCGR for the low copper content alloys is attributed to the occurrence of a larger amount of a zig-zag crack and the crack branching; while in corrosive environments, the lower FCGR for the high copper content alloys is due to a larger degree of homogeneous deformation, resulting in a significant decrease of the metal-environment interactions, especially for $\Delta K > 7.5$ MPam$^{\frac{1}{2}}$.

The fatigue crack growth law (Paris equation) constants for region II crack propagation are presented in Table 2.2. The m values for the four alloys tested in distilled water are identical ($m = 2.6$). It means that four curves are parallel to each other in region II, and log A values of these four curves are inversely related to the copper content of the four alloys. Also note that m values for all alloys are inversely related to the corrosivity of environment whereas log A values are directly related to the corrosivity. Note that both m and log A values for all alloys are very sensitive to the corrosivity of the test environment, i.e., a considerable difference between dry air and distilled water, but only a slight difference between distilled water and a 3.5% NaCl solution. This relationship is in agreement with that of the FCGR measured in these three environments. Most m values ranged between 2 and 4 except that the values of 0.01 and 1.0% Cu alloys, tested in dry air, are larger than 4. However, if the real length of the crack was measured and then real $\frac{da}{dN}$ vs ΔK was plotted and shown in Figure 2.21,

Table 2.2 Fatigue Crack Growth Law (Paris Equation) Constants for Region II Crack Propagation

Alloy	Environment	$\frac{da}{dN}$ Measured by Projected Length		$\frac{da}{dN}$ Measured by Real Length	
		Log A	m	Log A	m
0.01%Cu	Dry Air	1.6×10^{-6}	4.3	5×10^{-6}	3.9
	H_2O	2.0×10^{-3}	2.6	-	-
	NaCl	1.0×10^{-2}	2.1	-	-
1.0%Cu	Dry Air	5.5×10^{-7}	4.7	4×10^{-6}	4.0
	H_2O	1.6×10^{-3}	2.6	-	-
	NaCl	2.0×10^{-3}	2.5	-	-
1.6%Cu	Dry Air	3.8×10^{-6}	4.0	5.6×10^{-6}	3.8
	H_2O	1.1×10^{-3}	2.6	-	-
	NaCl	2.0×10^{-3}	2.4	-	-
2.1%Cu	Dry Air	2.0×10^{-6}	4.0	5.6×10^{-6}	3.8
	H_2O	7.8×10^{-4}	2.6	-	-
	NaCl	1.2×10^{-3}	2.5	-	-

the m values for all alloys, tested in these three environments, range between 2 and 4. This is in agreement with experimental values for most materials[96]. A much higher value of m for the dry air tests is attributed to the occurrence of a large amount of a zig-zag crack and the crack branching as described previously. This explanation is further confirmed by the finding that m values for the 0.01 and 1.0% Cu alloys are larger than those for the 1.6 and 2.1% Cu alloys since the amount of a zig-zag crack and the crack branching for the former alloys is approximately three times of that for the latter alloys. This interpretation is consistent with the relationship between crack path features, the test environment, alloy chemistry, and the magnitude of ΔK values, as discussed previously.

Effect of DR on the FCP Behavior

The FCGR data for the four alloys with different DR, tested in three environments, are presented in Figures 2.14 to 2.17. It is apparent that the FCGR data for each alloy, with different DR, fall in the same scatter band for all test environments except for the 1.6% Cu alloy tested in the corrosive environment. For the 0.01 and 1.0% Cu alloys, no difference in FCGR was found between the low and the high DR. This is probably due to the small difference in DR, i.e., only 12 and 25% difference for the 0.01 and 1.0% Cu alloys, respectively. Therefore, a further study with a large difference in DR is needed to clarify this point. However, for the 2.1% Cu alloy, there was a large difference in DR (55%),

but no difference in FCGR was observed. Two important microstructural features can be used to explain this phenomenon. One is that the presence of the clustered S-phase particles in this alloy (see Figure 2.13) would affect the FCGR to a certain extent[8,76]. The other is that the development of cell structures in the reversed plastic zone (Figure 2.22, micrograph B), and cell walls may play some role in the FCP behavior[1,81,88,89]. For the case of the 1.6% Cu alloy, there was a slight difference in FCGR due to the difference in DR when tests were conducted in a corrosive environment (see Figure 2.16), but in dry air no difference was found. The slightly higher FCGR in the 1.6% Cu alloy with a high DR, tested in a corrosive environment, is possibly due to the fact that the large recrystallized grains were involved in FCP process and a large amount of these grains displayed slip band features (see Figure 2.23, micrograph A). These slip bands in the reversed plastic zone will intensively interact with the corrosive environment, resulting in an acceleration of the FCGR. However, the unrecrystallized grains in the reversed plastic zone consisted of cell structures (Figure 2.23, micrograph B) which may suppress the metal-environment interaction parameter. In dry air, the absence of the metal-environment interactions decreases the effect of DR on the FCGR, and a big scatter band may mask its difference.

For the high copper content alloys, 80% and 30% of the crack length were covered by subgrain boundaries when tests were conducted in distilled water and in dry air respectively. An intensive SEM study of fracture features revealed that the orientation of the

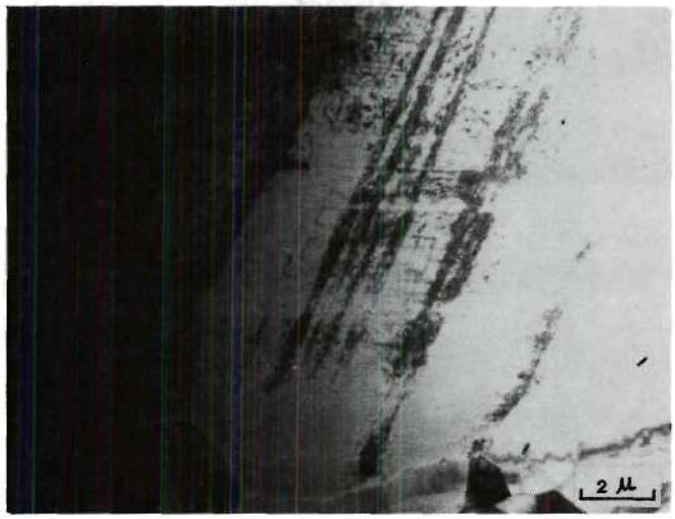

(A)

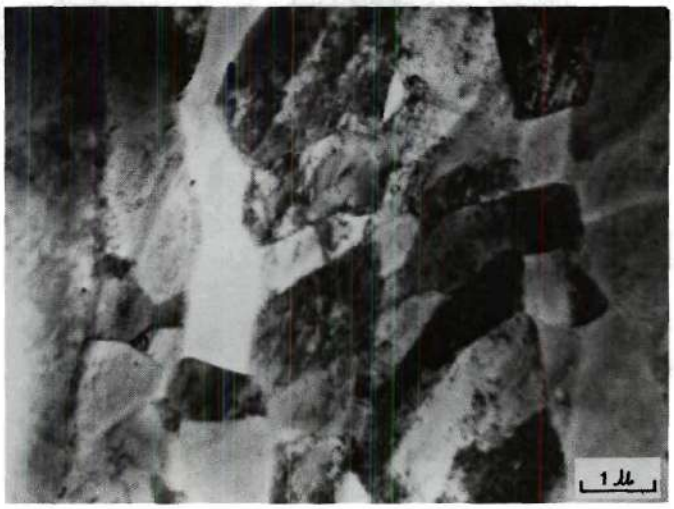

(B)

Figure 2.23. Transmission electron micrographs taken at an area adjacent to the fatigue fracture surface, (A) the 1.6% Cu alloy with 50% DR, ΔK = 9.0 MPam$^{\frac{1}{2}}$, showing slip bands in a large recrystallized grain, (B) the same alloy with 9% DR, ΔK = 9.5 MPam$^{\frac{1}{2}}$, showing cell structures in the unrecrystallized grain.

fracture surface changed at grain boundaries, as discussed previously. However, the experimental results showed that the FCGR was insensitive to the change of DR. These results, however, do imply that the low angle subgrain boundaries in the unrecrystallized grains and the high angle grain boundaries of the recrystallized grains play some role in FCP. The results of this section suggest that the effect of DR on the FCP behavior is dependent upon the slip mode, the magnitude of DR, the recrystallized grain size, the presence of insoluble particles, subgrain size and the test environment. A further study is needed to clarify the effect of DR on the FCGR by controlling these parameters.

Effect of Environment on the FCP Behavior

The crack growth curves for various alloys tested in the three environments (see Figures 2.14 to 2.17) converge either at low or at high ΔK values. These phenomena revealed that the environmental effect on the FCGR was dependent upon the magnitude of ΔK values. Both distilled water and 3.5% NaCl solution had a smaller effect on the FCGR at lower ΔK levels when compared with the reference environment - dry air, but markedly increased their effects when the ΔK values were increased, and then reduced their effects as the ΔK values were further increased. The aggressive effects became maximum when the magnitude of the ΔK values reached approximately 9 $MPam^{\frac{1}{2}}$ for all alloys studied here. The ratio of FCGR in distilled water and in dry air at this maximum stage was 56, 31, 14, and 13, corresponding to 0.01, 1.0, 1.6 and 2.1% Cu alloys. The environ-

mental sensitivity to FCGR does decrease with increasing copper content in these 7000-type aluminum alloys. A comparison of these ratio values reveals that a considerable change in environmental sensitivity is found as the copper content increases from 0.01 to 1.6%, and only a slight change as the copper content further increases from 1.6 to 2.1%. This phenomenon is, in general, consistent with the results obtained from the LCF tests in PART I, and also in agreement with Hyatt and Quist[1] who indicated that the environmental sensitivity was suppressed by increasing the copper content in 7000-type alloys.

As mentioned previously, a considerable difference in FCGR was observed when tests were conducted in dry air and in distilled water, whereas only a slight difference was found between distilled water and a 3.5% NaCl solution. On the basis of these results, the controlling factors in corrosion fatigue, i.e., an adsorption process such as adsorption of specific chloride ions to the crack tip suggested by several investigators[3,51-55], and/or an anodic dissolution favored by the presence of chloride ions in solution proposed by other workers[51-53], may not be critical factors in the present study. Another possibility, that of an oxide film blocking the reversal of slip offset as offered by Stoltz and Pelloux[51,54], may not be the case either since oxide formation also occurs in dry air. Another mechanism, proposed by several investigators[56-59], based on the lowering of the elastic property of oxide layer by water adsorption, is considered unlikely. Since the fresh surfaces are continuously created at the crack tip due to the high plastic

strain deformation within the plastic zone during cyclic loading; and because the thickness of the oxide layer near the crack tip may be of the order of a few monolayers, the resulting change in the "image force" on the dislocation in the metal matrix would not be sufficient to cause a considerable change in FCGR[45]. Therefore, it is suggested that the cause of the considerable increase in FCGR when measured in distilled water or in a 3.5% NaCl solution is essentially a hydrogen embrittlement phenomenon. Hydrogen atoms will be liberated by the interaction of water with the freshly created crack surfaces at the crack tip and some of them will diffuse into the plastic zone. This proposal is supported by Jacko and Duquette[43] who suggest that hydrogen may diffuse in the vicinity of the plastic zone since dislocations associated with the plastic zone may act as high diffusivity paths for hydrogen. Hydrogen embrittlement in corrosion fatigue is further confirmed by the finding of Wei[46] who stated that crack propagation in water is controlled by a thermally activated processes with apparent activation energies that depend strongly on the crack-tip stress-intensity parameter. Thus, the rate controlling process is the mechanical process of creating new crack surfaces, instead of either the transport of aggressive environment to the crack tip or diffusion of hydrogen ions into the material ahead of the crack tip. In addition, the greater environmental sensitivity of low copper content alloys to distilled water may also give some indication that hydrogen embrittlement plays an important role in corrosion fatigue. For the low copper content alloys, planar dislocations move only on a few slip planes in the plastic zone due to

dislocation shearing of coherent precipitates. Therefore, the density of mobile dislocations on those slip planes is considerably greater and this leads to localized regions of high hydrogen concentrations which result in accelerating FCGR. On the other hand, for the high copper content alloys, the formation of cell structures in the plastic zone reduces the mobility of dislocations, and homogeneous deformation also reduces localized regions of high hydrogen concentrations. Both lead to a decrease in susceptibility to hydrogen embrittlement. These explanations are fully supported by the recent reports of hydrogen embrittlement phenomena[65,66] which conclude that the movement of hydrogen atoms with mobile dislocations is an essential requirement for embrittlement and the amount of hydrogen atoms diffusing into the bulk of metal is proportional to the density of mobile dislocations. These results strongly suggest that corrosion fatigue of aluminum alloys in distilled water or in a 3.5% NaCl solution for the present study at a frequency of 10 Hz is primarily due to a hydrogen embrittlement phenomenon.

Monotonic, Cyclic Properties and FCP

A comparison of the monotonic and LCF test data shows that the cyclic strain resistance of the four alloys tested in each environment can be directly related to the yield strength and ductility, especially for $\frac{\Delta\varepsilon_p}{2} < 1.2\%$. This relationship is probably coincidental since it is well-known that the yield strength of 7000-type alloys is systematically increased with increasing copper content for the same aging treatment. Other parameters being

constant, the yield strength of materials has been, in general, considered to correlate with the cyclic stress resistance, but the ductility is, of course, related to the cyclic strain resistance[38]. For the FCP, there is no direct relationship between fracture toughness and FCGR found in this study. However, it has been found previously[7,78] that an increase in fracture toughness did reduce the FCGR. Except for the cyclic strain hardening exponent, the monotonic and LCF data are difficult to correlate with FCP resistance for the three environments since the sequence of FCP resistance for the four different copper content alloys was almost inversely related when tests were conducted in dry air and in distilled water. For example, the FCGR for the four different copper content alloys, tested in distilled water or a 3.5% NaCl solution, was directly related to both yield strength and ductility, especially for $\Delta K > 7.5$ MPam$^{\frac{1}{2}}$; whereas there is no physical meaning in the converse statement that the FCGR for the four alloys tested in dry air is inversely related to the yield strength or ductility. Recently, the cyclic straining hardening exponent, n', has emerged as the single parameter most related to the FCP and LCF resistance of materials[38,79]. This parameter, n', can also be correlated with the FCP and LCF behavior for this study since n' displays the best relationship with the slip mode found in these materials, as discussed in PART I. Lower values of n' are associated with planar slip mode materials, such as the low copper content alloys, while higher values of n' are associated with homogeneous deformation mode materials, like the higher copper content alloys. Experimental results of this study revealed that

materials with higher values of n' exhibit better LCF resistance, regardless of the test environment. Explanations of this phenomenon has been discussed in PART I. On the other hand, n' can also be related to the FCGR of materials. In dry air, the alloys with lower values of n' appeared to have the lower FCGR because the planar slip caused the occurrence of a larger amount of a zig-zag crack and the crack branching. Thus, the effective ΔK values for a zig-zag crack or for a crack with branches is smaller than the applied ΔK values. However, in distilled water or a 3.5% NaCl solution the low copper content alloys with lower values of n' appeared to increase their FCGR over the high copper content alloys since planar slip within the plastic zone resulted in a significant increase of the metal-environment interactions, especially for $\Delta K > 7.5$ MPam$^{\frac{1}{2}}$.

Recently, it has been suggested that the plastic deformation behavior in the plastic zone of FCP samples may be similar to that in LCF samples[102,103]. Consequently, to predict the FCP resistance of materials, the fatigue behavior of the small plastic zone can be simulated by testing smooth samples under strain-controlled condition. On the basis of this assumption, materials with better cyclic strain resistance in the LCF tests should exhibit the same behavior in the reversed plastic zone ahead of a growing crack, leading to a better FCP resistance. However, this theoretical prediction is not consistent with the experimental results in this study, i.e., the cyclic strain resistance in the LCF tests is directly related to the copper content regardless of the test environment while the sequence of FCP resistance is not the same as

that of the LCF tests, expecially for testing in dry air. The main reasons for this difference are related to the occurrence of a larger amount of a zig-zag crack and the crack branching for the low copper content alloys tested in dry air, and to the considerable difference in the amount of material involved in the reversed plastic deformation process between the LCF and FCP samples. The difference in frequency between the LCF and FCP tests may also have an influence on the plastic deformation behavior and on the metal-environment interactions. The alloys with minimum DR had the unrecrystallized grain size larger than 1,000 μm, which is about ten times larger than the reversed plastic zone size of the FCP samples for ΔK values up to 10 $MPam^{\frac{1}{2}}$. Consequently, the unrecrystallized grain boundaries only play a small role in plastic deformation within the plastic zone for the FCP samples, but they will play an important role in plastic deformation for the LCF samples, especially for the low copper content alloys that exhibit planar slip. The large grain size will cause an increase in the localized stress and/or strain concentration, resulting in some detrimental effects.

Several workers[97,98,103] derived the FCP equations on the basis of a combination of the monotonic and LCF parameters since the plastic deformation behavior within the plastic zone is similar to that in the LCF samples[102,103]. Chakrabortty[98] modified the model proposed by Majumder and Morrow[97] and considered the entire strain field as well as a ρ' parameter which represents the average distance between the major deformation barriers. Chakrabortty[98] and Coyne and Starke[104] used Chakabortty's equation (Equation 2.5)

to predict the FCGR of titanium alloys and an Al-Zn-Mg aluminum alloy. It was found that the predicted growth rates were close to the experimental data. Since the LCF data for the four different copper content alloys tested in these three environments were available, an attempt was made to calculate FCGR of these alloys based on Equation 2.5. When the FCP tests were conducted in dry air, the microstructural parameter, ρ', was the half grain diameter in the direction of the propagating crack since the grain boundaries were considered to be the major barriers for slip, especially for the low copper content alloys. In more corrosive environments, however, the subgrain size was chosen for ρ' because 80% of the crack paths were covered by subgrain boundaries, especially for the high copper content alloys. The values of all parameters in Equation 2.5 are given in Table 2.3. The calculated FCGR are shown in Figure 2.24, along with the experimental data. A comparison of the diagrams in Figure 2.24 reveals that the calculated curves are acceptably close to the experimental curves except for the 0.01% Cu alloy tested in corrosive environments. Although the calculated growth rates are close to the experimental data, the sequence of FCP resistance calculated from Equation 2.5 is not consistent with that obtained from the experimental results. For example, the experimental results showed that in dry air, the FCP resistance of materials was generally increased with decreasing copper content; whereas the calculated data failed to show the same results. Also, the experimental data indicated that the microstructure of the alloys does not affect FCGR, while the calculated results showed that it does.

Table 2.3 Optimum Values of all Parameters Required in Equation 2.5

Alloy	Environment	-C	ε'_f	n'	K'	E (MPa)	ρ' (μ)
0.01Cu,5%DR	Dry Air	0.82	125	0.063	1274	7000	550
	H_2O	0.68	23	0.063	1274	7000	5
	3.5%NaCl	0.68	20	0.063	1274	7000	5
1.0Cu,7%DR	Dry Air	0.78	115	0.075	1373	7000	550
	H_2O	0.77	63	0.075	1373	7000	3
1.6Cu,9%DR	Dry Air	0.77	110	0.088	1471	7000	500
	H_2O	0.85	125	0.088	1471	7000	5
	3.5%NaCl	0.85	100	0.088	1471	7000	5
1.6Cu,50%DR	Dry Air	0.79	118	0.082	1491	7000	256
	H_2O	0.93	180	0.082	1491	7000	16
	3.5%NaCl	0.85	90	0.082	1491	7000	16
2.1Cu,12%DR	Dry Air	0.63	46	0.114	1412	7000	490
	H_2O	0.68	54	0.114	1412	700	6
2.1Cu,67%DR	Dry Air	0.67	50	0.099	1373	7000	188
	H_2O	0.71	60	0.099	1373	7000	31

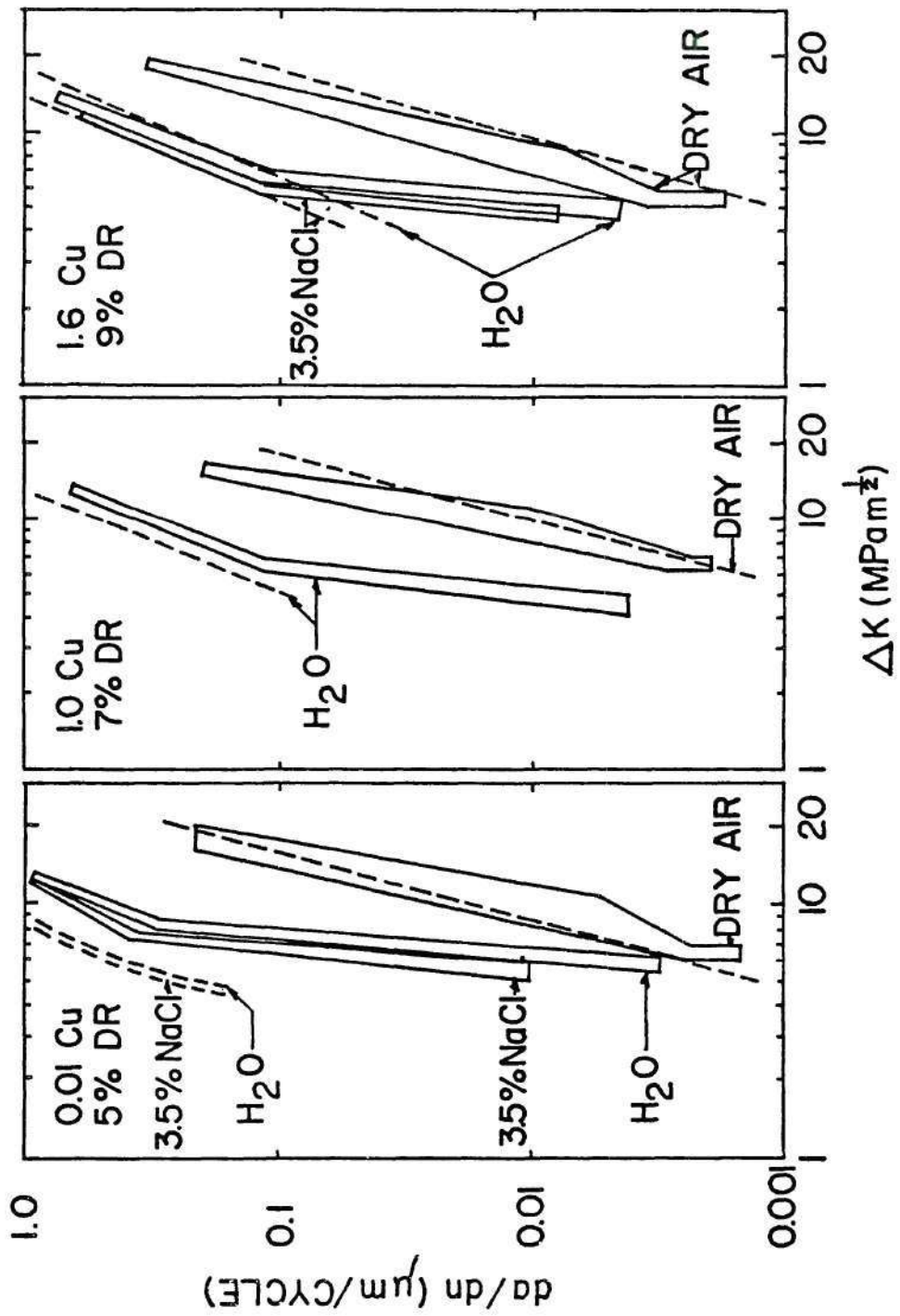

Figure 2.24. Experimental and calculated crack growth rates, using Chakrabortty equation, for different copper content alloys tested in various environments. Dashed line:predicted, solid line:experimental.

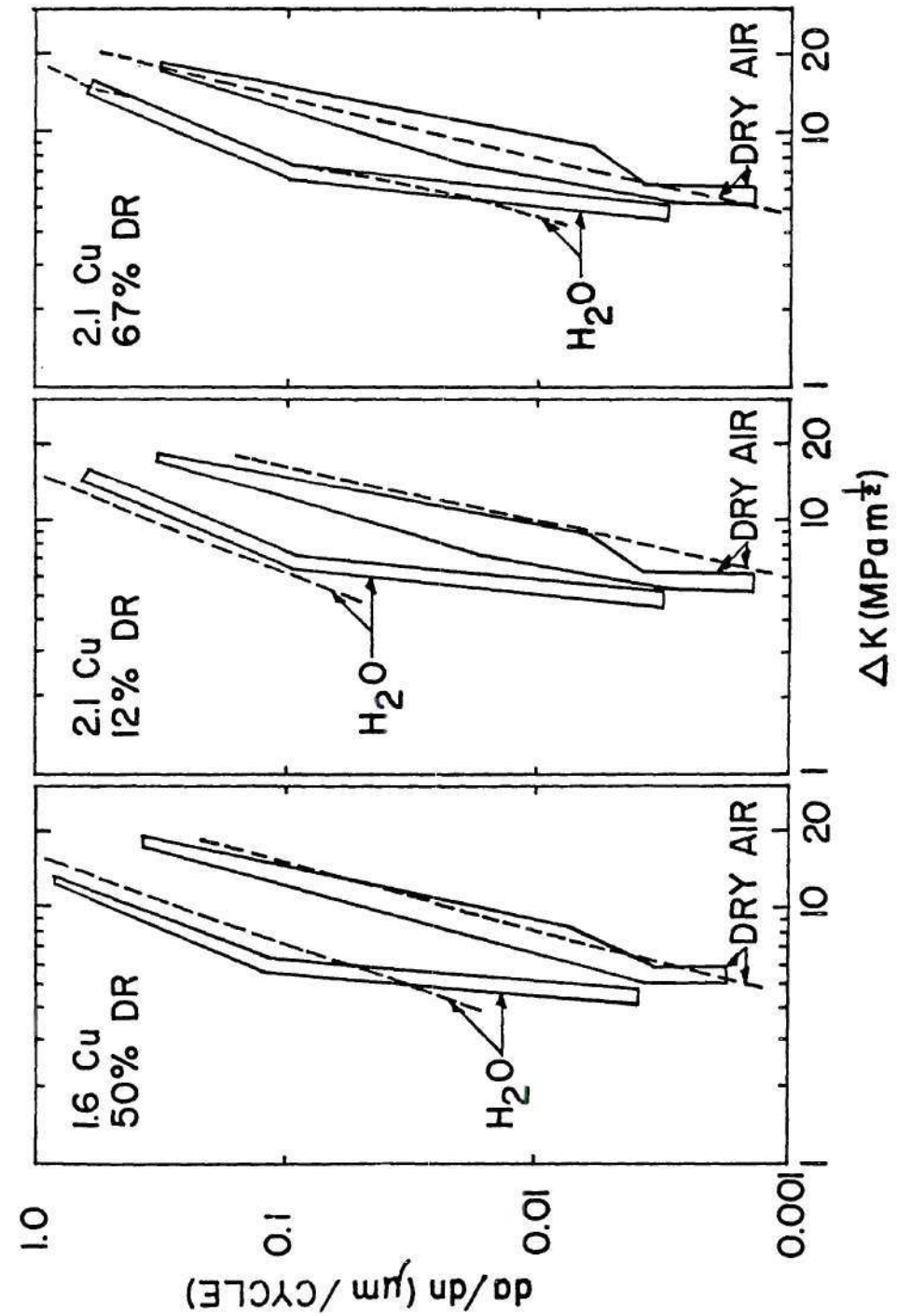
1.6 Cu
50% DR
2.1 Cu
12% DR
2.1 Cu
67% DR
H2O
DRY AIR
1.0
0.1
0.01
0.001
da/dn (μm/CYCLE)
1
10
20
ΔK (MPa m½)

Continued

This contradiction is probably due to the occurrence of a large amount of a zig-zag crack and the crack branching since the theoretical equation does not account for these crack path features. However, even when the real $\frac{da}{dN}$ was measured on the surfaces of samples, the inconsistency was still existed. This is very likely because a reduction of the effective ΔK values in the presence of a zig-zag crack and a crack with branches cannot be expressed simply in terms of the real crack length. Furthermore the crack path features vary from one region to another through the thickness of the sample and thus it is very difficult to measure the real length of the crack.

The results show that the Chakrabortty equation predicts the FCGR with acceptable accuracy for all alloys studied in the three environments. In addition, the best advantage of this equation is that only the LCF parameters and the microstructural parameter, ρ', (which can be determined from actual microstructural parameters) are needed for the prediction of the FCGR. However, since the real crack path in the FCP sample is more complex than that assumed in deriving the equation. This would limit the accuracy for the prediction of the FCGR. It was, then, felt that if the real crack features and the exact FCP mechanism could be considered for developing the equation, it could be more widely applied to predict the FCGR with more accuracy.

CHAPTER V

CONCLUSIONS

1. The DR of four alloys increases with increasing copper content at the same treatment, and it also varies significantly with the distance from the plate surfaces.
2. The 2.1% Cu alloy exhibited a lower fracture toughness, and this is attributed to the presence of the S-phase particles since voids are created around the clustered particles on the overload fracture surfaces; however, voids around the clustered particles were not observed on the fatigue fracture surfaces.
3. The frequency of occurrence of a zig-zag crack and the crack branching is dependent upon the alloy chemistry, which affected the slip mode, the magnitude of ΔK values and the test environment.
4. For the high copper content alloys, approximately 80% and 30% of the fracture path were covered by subgrain boundaries when tests were conducted in distilled water and in dry air respectively. The orientation of the fatigue fracture surface changed at grain boundaries. Thus, both subgrain and grain boundaries appear to play some role in the FCP behavior.
5. The DR of these alloys studied here only had a minor effect on the FCP resistance as tested in these three environments. However, the limited results indicated that the effect of DR

on the FCP resistance was dependent upon the slip mode, the magnitude of DR, the recrystallized grain size, the presence of insoluble particles, the subgrain size and the test environment.

6. When tests were conducted in dry air, the low copper content alloys exhibited a slower FCGR. This is attributed to the planar slip occurred in the plastic zone, resulting in the occurrence of a larger amount of a zig-zag crack and the crack branching.
7. When tests were conducted in corrosive environments, the high copper content alloys exhibited a slower FCGR, especially for $\Delta K > 7.5$ MPam$^{\frac{1}{2}}$. This is attributed to a larger degree of homogeneous deformation, resulting in a significant decrease of the metal-environment interactions.
8. The environmental sensitivity to the FCGR decreases with increasing copper content of these 7000-type aluminum alloys. A considerable change is found as the copper content increases from 0.01 to 1.6%, but only a slight change is observed as the copper content increases further.
9. A considerable difference in the FCGR was observed when tests were conducted in dry air and in distilled water, but an insignificant difference was found between distilled water and a 3.5% NaCl solution. On the basis of these results and discussion, it is suggested that the corrosion fatigue of aluminum alloys in distilled water or in a 3.5% NaCl solution for the present study at a frequency of 10 Hz is primarily due to a hydrogen embrittlement phenomenon.

10. Cell structures were observed at regions adjacent to the fatigue fracture surfaces, and the probability of their occurrence is greater with increasing copper content.
11. The fracture toughness of different copper content alloys could not be correlated with their FCGR.
12. The cyclic strain hardening exponent, n', emerged as a single index to be correlated with the LCF and FCP resistance for all test environments.
13. The higher values of m (the slope of curve for the region II crack propagation) for all alloys tested in dry air is due to the occurrence of a larger amount of a zig-zag crack and the crack branching.
14. The sequence of the LCF resistance (which increases with increasing copper content) is not consistent with that of the FCP resistance, especially for dry air. The main reasons for this difference are related to the occurrence of a larger amount of a zig-zag crack and the crack branching, and to the considerable difference in the amount of material involved in the reversed plastic deformation process between the LCF and FCP samples.
15. The predicted crack growth rates are acceptably close to the experimental data for all alloys tested in various environments.

BIBLIOGRAPHY

1. M. V. Hyatt and W. E. Quist, Technical Report AFML-TR-67-329, 1967, p. 827

2. M. O. Speidel, NATO Advanced Study Institute on SCC, Copenhagen, Denmark, July, 1975

3. R. M. N. Pelloux, Fracture, Proc. of the Second Int. Conf. on Fracture, Brighton, 1969, p. 731

4. T. H. Sanders, Jr. and E. A. Starke, Jr., Met. Trans. 7A, No. 9, 1976, p. 1407

5. R. E. Sanders, Jr. and E. A. Starke, Jr., Met. Sci. & Eng. Vol. 28, 1977, p. 53

6. F. S. Lin and E. A. Starke, Jr., ICF4, Waterloo, Canada, Vol. 2, 1977, p. 879

7. A. R. Rosenfield, C. W. Price and C. J. Martin, Research on Synthesis of High-Strength Al alloys, Part II, AFML-TR-74-129, 1972

8. S. M. El-Soudani and R. M. N. Pelloux, Met Trans. Vol. 4, 1973, p. 519

9. C. Q. Bowles and J. Schijve, Int. J. of Fracture, Vol. 9, No. 2 1973, p. 171

10. W. H. Reimann and A. W. Brisbane, Eng. Fra. Mech., Vol. 5, 1973, p. 67

11. F. Ostermann, Met. Trans., Vol. 2, 1971, p. 2897

12. E. D. Russo, M. Conserva, F. Gatto and H. Markus, Met. Trans., Vol. 4, 1973, p. 1133

13. P. A. Thackery, J. Inst. of Metals, Vol. 96, 1968, p. 228

14. A. J. Cornish and M. B. Day, ibid, Vol. 99, 1971, p. 377

15. H. Y. Hunsicker, Aluminum, Vol. 1, ASM, Metal Park, 1967, p 124

16. B. W. Lifka and D. O. Sprowls; Localized Corrosion, ASTM, STP 516, 1972, p 135

17. Y. Baba, Trans. Japan Inst. Metals, Vol. 7, 1966, p. 224

18. J. W. Martin, Precipitation Hardening, Pergamon Press, 1968

19. A. Kelly and R. B. Nicholson, Progr. Mater. Sci., Vol. 10, 1963, p. 151

20. E. Orowan, Symp. on Internal Stress in Metals and Alloys, Inst. Metals, London, 1948, p. 451

21. S. S. Manson, NACA Tech. Notes, 1954, p. 625

22. L. F. Coffin, Jr., Trans. ASME, Vol. 6, 1954, p. 931

23. R. W. Landgraf, ASTM STP 467, 1970, p. 3

24. L. F. Coffin, Jr., J. of Materials, Vol. 6, 1971, p 388

25. C. Laird, V. J. Langelo, M. Hollrah, N. C. Yang, and R. de la Veaux, Dept. of Met. and Mat. Sci., U. of Penn., Philadelphia, Pa., Nov. 15, 1976

26. C. E. Feltner and C. Laird, Acta Met., Vol. 15, 1967, p. 1621

27. G. A. Stubbington and P. J. E. Forsyth, Acta Met., Vol. 14, 1966, p. 5

28. C. Laird and G. Thomas, Intern. J. Fracture Mech. Vol. 3, 1967, p. 81

29. J. Morrow, ASTM STP 378, 1965, p. 45

30. P. J. E. Forsyth, Proceedings of the Crack-Propagation Symposium, Cranfield, 1961, p. 76

31. J. C. Grosskreutz, Phys. Stat. Sol. (b) Vol. 47, 1971, p. 11

32. C. Laird, ASTM STP 415, 1967, p. 137

33. W. J. Plumbridge and D. A. Ryder, Met. Reviews, 136

34. C. Calabrese and C. Laird, Met. Trans., Vol. 5, 1974, p. 1785

35. C. E. Feltner and C. Laird, Trans. AIME, Vol. 231, p. 1253, 1968

36. J. C. Grosskreutz, ASTM STP 485, 1971, p. 5

37. G. Lutjering, H. Doker, and D. Munz, "Microstructure and Fatigue Behavior of Al-Alloys," Int. Conf. on the Strength of Metals and Alloys, paper 87, 1970

38. C. E. Feltner and P. Beardmore, ASTM STP 467, 1970, p. 77

39. A. W. Thompson and W. A. Backofen, Acta Met., Vol. 19, 1971 p. 597

40. R. C. Boettner, C. Laird and A. J. McEvily, Jr., Trans. AIME, Vol. 233, p. 379, 1965

41. T. Broom and A. Nicholson, J. Inst. Metals, Vol. 89, 1960, p.183

42. J. A. Bennett, J. Res. of the National Bureau of Standards, Vol. 68C, 1964, p. 91

43. R. Jacko and D. J. Duquette, Met Trans., Vol. 8A, 1977, p. 1821

44. C. A. Stubbington, Metallurgia, Vol. 68, 1963, p. 109

45. R. P. Wei, Eng. Frac. Mech., Vol. 1, 1970, p. 633

46. R. P. Wei, Int. J. of Frac. Mech., Vol. 4, 1968, p. 159

47. E. J. Bradshaw, and C. Wheeler, Int. J. of Frac. Mech., Vol. 5, 1969, p. 255

48. A. Hartman, Int. J. of Frac. Mech., Vol. 1, 1965, p. 167

49. F. J. Bradshaw and C. Wheeler, Applied Mat. Res., 1966, p. 112

50. J. A. Feeney, J. C. McMillan and R. P. Wei, Met. Trans., Vol 1, 1970, p. 1741

51. R. E. Stoltz and R. M. Pelloux, Corrosion, Vol. 29, 1973, p. 13

52. D. J. Duquette, Corrosion Fatigue, NACE, Houston, Texas, 1972, p. 12

53. T. Pyle, V. Rollins and D. Howard, ibid, p. 312

54. R. E. Stoltz and R. M. Pelloux, Met. Trans., Vol. 3, 1972, p. 2433

55. R. M. Pelloux, ICF2, 1969, p. 731

56. A. K. Head, Phil. Mag., Vol. 44, 1953, p. 92

57. J. C. Grosskreutz, Surface Science, Vol. 8, 1967, p. 173

58. J. C. Grosskreutz, J. Electrochem. Soc., Vol. 7, 1970, p. 940

59. A. Hartman, F. J. Jacobs, A. Nederveen and R. DeRijk, NLR Tech. Note No. M 2182, 1967

60. J. E. Hilliard, "Recrystallization, Grain Growth and Texture" ASM, Metal Park, Ohio, 1965, p. 267

61. P. Cotterill and P. R. Mould, "Recrystallization and Grain Growth in Metals," A. Halsted Press Book, 1976

62. R. E. Stoltz and R. M. Pelloux, Met. Trans., Vol 7A, 1976, p. 1295

63. C. Laird, "The General Cyclic Stress-Strain Response of Aluminum Alloys" Department of Met. and Mat. Sci., U. of Pennsylvania, Philadelphia, Pa., 1976

64. C. Calabrese and C. Laird, Met. Sci. and Eng., Vol. 13, 1974, p. 159

65. B. Tompkins, Phil. Mag., Vol. 18, 1968, p. 1041

66. J. A. Donovan, Met. Trans., Vol. 7A, 1976, p. 1677

67. M. R. Louthan, Jr., G. R. Caskey, Jr., J. A. Donovan and D. E. Rawl, Jr., Mater. Sci. Eng., Vol. 10, 1972, p. 317

68. R. J. Jacko and D. J. Duquette, Met. Trans., Vol. 8A, 1977, p. 1821

69. T. W. Crooker, Trans. of ASME, Vol. 95, Series H, 1973, p. 150

70. D. A. Meyn, Trans. ASM, Vol. 61, 1968, p. 42

71. R. M. N. Pelloux, Trans. ASM, Vol. 62, 1969, p. 281

72. B. Tompkins and W. D. Biggs, J. Mater. Sci., Vol. 4, 1969, p. 544

73. R. J. H. Wanhill, Met. Trans., Vol. 6A, 1975, p. 1587

74. C. Q. Bowles and B. Broek, Int. J. of Frac. Mech., 8, 1972, p. 75

75. P. Neumann, Acta Met., Vol. 17, 1969, p. 1219

76. W. G. Truckner, J. T. Staley, R. J. Bucci and A. B. Thakker, Alcoa Laboratories, Alcoa Center, Pa. 1976

77. L. H. Glassman and A. J. McEvily, NASA TN D-928, 1962

78. J. Albrecht, J. W. R. Martin, G. Lutjering and J. W. Martin, Ruhr-University, Bochun, Germany, 1972

79. J. C. Grosskreutz, Met. Trans., Vol. 3, 1972, p. 1255

80. J. H. Weber and R. W. Hertzberg, Met. Trans., Vol. 4, 1973, p. 595

81. A. W. Thompson and R. J. Bucci, ibid, Vol. 4, 1973, p. 1174

82. C. Y. Kung, Ph.D. Thesis, Northwestern University, Evanston, Ill., 1978

83. M. Wilhelm, M. Negeswararao and R. Meyer, to be published

84. J. C. Grosskreutz, J. App. Physics, Vol. 34, 1963, p. 372

85. M. A. Wilkins and G. C. Smith, Acta Met., Vol. 18, 1970, p. 1035

86. J. C. Grosskreutz and G. G. Shaw, ibid, Vol. 20, 1972, p. 523

87. T. Ogura and S. Karashima, Trans. JIM, Vol. 13, 1972, p. 428

88. S. Karashima, H. Oikawa and T. Ogura, ibid, Vol. 9, 1968, p. 205

89. T. Ogura and S. Karashima, ibid, Vol. 15, 1974, p. 324

90. R. N. Grardner, T. C. Pollock and H. G. F. Wilsdorf, Mat. Sci. and Eng., Vol. 29, 1977, p. 167

91. J. Awatani, K. Katagiri and T. Shiraishi, Met. Trans., Vol. 7A, 1976, p. 807

92. J. Awatani and T. Shiraishi, ibid, Vol. 7A, 1976, p. 1599

93. N. S. Stoloff and D. J. Duquette, "Microstructural Effects in the Fatigue Behavior of Metals and Alloys" R.P.I. Troy, NY, 1974

94. P. C. Paris and F. Erdogan, J. Basic Eng., Vol. 85, 1963, p. 528

95. N. E. Frost, K. J. Marsh and L. P. Dook, "Metal Fatigue," Oxford, University Press, London, 1974

96. S. T. Rolfe and J. M. Barson, "Fatigue and Fatigue Control in Structures," Prentice-Hall, Inc. N.J., 1977

97. S. Majumder and J. Morrow, Depart. of Theoretical and Applied Mechanics, U. of Ill., Urbana, Ill., 1973

98. S. Chakrabortty, to be published, Georgia Institute of Technology

99. W. G. Clark, Jr., and S. J. Hudak, Jr., J. of Testing and Evaluation, Vol. 3, No. 6, 1975, p. 454

100. W. Nageswararao, V. Gerold and G. Kralik, J. Mat. Sci., Vol. 10 1975, p. 515

101. M. O. Speidel, Met. Trans., Vol. 6A, 1975, p. 631

102. H. P. Hickerson, Jr., and R. W. Hertzberg, Met. Trans., Vol. 3 1972, p. 179

103. A. Saxena and S. D. Antolovich, Met. Trans., Vol. 6A, 1975, p. 1809

104. E. J. Coyne, Jr., and E. A. Starke, Jr., to be published, Georgia Institute of Technology

VITA

Fu-Shiong Lin, the son of Mr. Chau-Kau Lin and Mrs. Ken-Chau Young Lin, was born in Char-Fu Li, Char-Li Jeng, Tainan, Taiwan, China, on July 8, 1942. After graduating from Pei-Men Agricultural Middle High School and Tainan Secondary High School, he entered the Department of Mining and Metallurgical Engineering, Cheng-Kung University, Tainan, Taiwan. In June, 1966 he received a Bachelor's degree. In September, 1968, he attended the Georgia Institute of Technology to pursue graduate studies in metallurgy and received a Master's degree in June, 1971. The topic of the thesis was "Stress Corrosion Cracking of Titanium Alloys," and his thesis advisor was Dr. R. F. Hochman.

After graduation from Georgia Tech, he joined the Metal Industrial Research Institute, located in Kaoshiung, Taiwan, as an assistant research engineer. He was in charge of the mechanical testing laboratory and was responsible for research on welding of metals. In 1973, he was promoted to an associate research engineer, following that year, he was awarded as an Outstanding Young Man by the government of his country for his achievements in research and for his contributions to the industry in his country. In 1975 he was named as the Head of the Physical Metallurgy Department of the Institute.

In January, 1976, he returned to Georgia Tech to pursue his Ph.D. degree. Under the nice guidance of his thesis advisor,

Dr. E. A. Starke, Jr., he got a Ph.D. degree in June, 1978. The topic of the thesis is "Low Cycle Corrosion Fatigue and Corrosion Fatigue Crack Propagation of High Strength 7000-Type Aluminum Alloys." He has many publications on stress corrosion cracking, corrosion, welding and corrosion fatigue of metals and alloys.